



Toxin-Antitoxin Battle in Bacteria

PhD Thesis

Author:

Ilaria Cataudella

Principal Supervisor:

Prof. Namiko Mitarai

PhD Thesis submitted to
The PhD School of Science
Faculty of Science
Niels Bohr Institute
Center for Models of Life
University of Copenhagen
Denmark

30th September 2013

a Titti

Aknowledgments

This work was performed at the Center for Models of Life (CMoL) at the Niels Bohr Institute, Copenhagen University from October 2010 to Septmber 2013. I Thank **Prof. Mogens Høgh Jensen** and **Prof. Kim Sneppen** for having given me the opportunity to join CMoL as a PhD student. Furthermore I thank Prof. Kim Sneppen for the continuative collaboration and the important role that his experience and ideas have played in the development of all the projects we worked on during these three years. A very special thanks goes to my supervisor **Prof. Namiko Mitarai** that has been always incredibly attentive and present every time I needed her advice, and has been the source of so many brilliant solutions to my scientific problems. I have learned a lot from her, and at the same time I always felt that my opinions were trusted and respected. She not only has been a great supervisor, but also a friend. The work presented in this thesis has been performed in collaboration with **Prof. Kenn Gerdes**, from The Centre for Bacterial Cell Biology, Newcastle University, UK. Prof. Kenn Gerdes has introduced us to the fascinating topic of Toxin-Antitoxin loci and guided us through the enormous amount of biological data available. I want to thank him for the fruitful collaboration that has continued throughout all my PhD and the several enlightening discussions.

In the first project I have worked on, I also collaborated with **Prof. Ala Trusina**, that I thank for the all the time and energy employed in my project, the interesting discussions and the technical advices she has given me.

On a more personal note, I want to thank my family and especially my parents, Enrica and Vittorio, for having taught me everything, especially the value of knowledge and deep understanding. But above all for supporting all of my choices, even the ones that might hurt a little, like moving 2000 km away from home. I want to say thank you to Lars and I don't even know where to start to explain how much we have been in this together and how much help, support and balance I have received from him. I also want to thank Lars' family, because they have all helped me so much feeling at home in Denmark. And last but not least, I want to thank all the amazing people on the B, C and nowadays also A floor, especially all the master and other PhD students, present and past (Vedran, Silja, Søren and

Stani, we have missed you!), because they all contributed to make my experience at CMoL unique, and among all the things I am going to miss, surely the table soccer matches and late-afternoon procrastination-sessions with Pia, Karis and Cecilia, have a special place.

This PhD scholarship is funded by the Danish National Research Foundation, CMoL and the Niels Bohr Institute, University of Copenhagen.

Abstract

This PhD thesis consists of three research projects revolving around the common thread of investigation of the properties and biological functions of Toxin-Antitoxin loci. Toxin-Antitoxin (TA) loci are transcriptionally regulated via an auto-inhibition mechanism called conditional cooperativity, based on cooperative binding of toxin-antitoxin complexes to operator DNA that depends on the stoichiometric ratio between the toxin and the antitoxin. More specifically, toxin and antitoxin can form heteromers with different stoichiometric ratios, and the complex with the intermediate ratio works best as a transcription repressor. This allows transcription at low toxin level, strong repression at intermediate toxin level, and then again transcription at high toxin level

In the first project, we reveal the biological function of conditional cooperativity by constructing a mathematical model of one particular *E.coli* TA system, the *relBE* locus. We show that the model reproduces the experimentally observed response to nutritional stress. We further demonstrate that conditional cooperativity stabilizes the level of antitoxin in rapidly growing cells such that random induction of *relBE* is minimized. At the same time it enables quick removal of free toxin when the starvation is terminated.

In the second project, we explore the features and the potential biological role of conditional cooperativity, in a more general perspective, that can be applied to the regulation of chromosome encoded TA loci in *E.coli* in general. In this context, we will neglect the cooperativity in the binding, and focus on the fact that the regulation depends on the ratio between the toxin and the antitoxin. For this reason, we talk about *conditional regulation* instead of *conditional cooperativity*. Such regulation has two interesting features: first, it provides a non-monotonous response to the concentration of one of the proteins, and second, it allows ultrasensitive response mediated by the sequestration of the active heteromers. We study conditional regulation in simple feedback motifs, and show that it can provide bistability for a wide range of parameters. We then demonstrate that the conditional cooperativity in toxin-antitoxin systems combined with the growth-inhibition activity of free toxin can mediate bistability between a growing state and a dormant state.

The final project aims at unraveling the connection between stochasticity in the expression of TA loci in *E.coli* and the phenomenon of bacterial persistence. Persistence is a form of antimicrobial tolerance that is not associated with DNA

mutation that confers resistance, but rather with a spontaneous switch of a cell to a physiological state characterized by slow or non-growth that impairs the effectiveness of antibiotics. The action of TA loci has often been invoked in the attempt of explaining the mechanism of persisters formation. We suggest a stochastic description of the activity of chromosome-encoded TA loci, aiming at providing insights about the mechanisms that support the stochasticity in persister formation.

Dansk Resume

Denne PhD afhandling består tre forskningsprojekter der handler om den røde tråd af efterforskning af biologiske funktioner af Toxin-antitoxin loci. Toxin-antitoxin (TA) loci er transkriptionelt reguleret via en auto-hæmning mekanisme kaldet *conditional cooperativity*, baseret på kooperativ binding af toxin-antitoxin komplekser til operatør DNA. Reguleringen afhænger af det støkiometriske forhold mellem toksinet og antitoxin. Mere specifikt, kan toksin og antitoxin danne heteromere med forskellige støkiometriske forhold, og komplekset med den mellemliggende forhold fungerer bedst som en *transcription repressor*. Dette tillader transskription ved lav toksin niveau, stærk undertrykkelse på mellemniveau toksin niveau og derefter igen transskription ved høj toksin niveau.

I det første projekt, afslører vi den biologiske funktion af betingede kooperativitet, ved at konstruere en matematisk model af den særlige *E.coli* TA system, *relBE* locus. Vi viser, at modellen reproducerer eksperimentelt observerede reaktion ernæringsmæssig stress. Vi viser endvidere betinget kooperativitet stabiliserer niveauet af antitoxin i hurtigt voksende celler, således at tilfældig induktion af *relBE* minimeres. Samtidig er det muligt hurtig fjernelse af frit toksin når sult afsluttes.

I det andet projekt, udforske vi de funktioner og den potentielle biologiske rolle betinget kooperativitet i et mere generelt perspektiv, der kan anvendes til reguleringen af kromosom-kodede TA loci i *E.coli* i almindelighed. I denne sammenhæng vil vi forsømme den kooperativitet i bindingen, og fokusere på det faktum, at forordningen, afhænger af den forholdet mellem toksinet og antitoxin. Derfor taler vi om *conditional regulation* i stedet for *conditional cooperativity*. En sådan regulering har to interessante træk det første giver det en ikke-monoton respons på koncentrationen af et af proteinerne, og dels gør det muligt ultrafølsomt reaktion medieret ved beslaglæggelse af de fungerende heteromere. Vi studerer betinget regulering i simple feedback-motiver, og vise, at det kan give bistabilitet for en bred vifte af parametre. Vi derefter vise, at den betingede kooperativitet i toxin-antitoxin systemer kombineret med væksthæmning aktivitet fri toksin kan mægle bistabilitet mellem en voksende stat og en sovende tilstand. Det endelige projekt sigter mod optrevling forbindelsen mellem stokastik i ekspressionen af TA loci i *E.coli* og fænomenet af bakteriel *persistence*. Persistence er en form for antimikrobiel tolerance, som ikke er forbundet med DNA-mutation, der bibringer resistens, men snarere med en spontan omstilling af en celle til en fysiologisk til-

stand karakteriseret af en langsom eller ikke-vækst, som forringer effektiviteten af antibiotika. Virkningen af TA loci er ofte blevet påberåbt i forsøget på at forklare den mekanisme af persisters formation. Vi foreslår stokastisk beskrivelse af aktiviteten af kromosom-kodede TA loci, med det formål give indsigt i de mekanismer, der understøtter den stokastik i persisters formation.

Publication List

- Cataudella, I., Trusina, A., Sneppen, K., Gerdes, K., and Mitarai, N. (2012). Conditional cooperativity in toxin-antitoxin regulation prevents random toxin activation and promotes fast translational recovery. *Nucleic acids research*, 40(14), 6424-6434.
- Cataudella, I., Sneppen, K., Gerdes, K., and Mitarai, N. (2013). Conditional Cooperativity of Toxin-Antitoxin Regulation Can Mediate Bistability between Growth and Dormancy. *PLoS computational biology*, 9(8), e1003174.

Contents

1	Introductory Concepts	3
1.1	Gene Expression Regulation	3
1.2	Modeling Chemical Reactions	5
1.2.1	Law of Mass Action	5
1.2.2	Statistical Mechanics Approach	7
1.3	Modeling Gene Expression	10
1.3.1	Transcription Regulation : the ODE approach	10
1.3.2	The Gillespie Algorithm	12
1.4	Prokariotic Toxin-Antitoxin Loci	14
1.4.1	Toxin-Antitoxin Loci	14
1.4.2	Biological Role of TA loci	16
2	The <i>relBE</i> system and its role in the nutritional stress response	19
2.1	The <i>relBE</i> locus	20
2.1.1	Conditional Cooperativity	20
2.2	The Model	22
2.2.1	The <i>relBE</i> regulatory network	22
2.2.2	The Stochastic Model	25
2.2.3	The reactions scheme	25
2.2.4	Modeling the transition to amino-acid starvation	28
2.3	Results	29
2.3.1	Aminoacid starvation drives the switch to toxin activation	29
2.3.2	Single Cell activation of RelE is binary	31
2.3.3	Conditional Cooperativity primes fast exit from RelE dominated state and prevents random toxin activation	33
2.3.4	Robustness against parameter change	34
2.4	Conclusion	36

3	Conditional Regulation and Bistability	39
3.1	Conditional Regulation	41
3.1.1	The Promoter Activity	42
3.1.2	Bistability in a simple feedback motif	43
3.2	A Simple Peristers Model	47
3.2.1	Conditional Regulation and Peristers	47
3.2.2	Toxin Accumulation feedbacks on growth rate	49
3.2.3	Robustness to parameter change	50
3.3	Conclusion	54
4	Stochasticity in the activity of TA systems and Persisters	59
4.1	The switching rate	61
4.1.1	Master Equation	61
4.1.2	Potential Landscape	63
4.1.3	Kramer's escape rate	66
4.1.4	The switching rate strongly depends on the parameters choice	68
4.2	Stochastic Model of TA activity	73
4.3	Considering the effect of multiple TA systems	75
4.3.1	Stability consideration	75
4.3.2	Stochastic model of interaction of 10 TA systems	77
4.4	Conclusion and future work	80
5	Conclusive Remarks	83
	Bibliography	85
	Appendices	93
A	Extimation of Maximal Promoter Activity α_0	95
B	Reference parameters in calculation of rates of persistence	97
C	Reference parameters in the stochastic model of TA activity	99
D	Reference parameters in stability analysis for the multiple TA systems	101

E	Reference parameters in the stochastic model for the multiple TA systems	103
F	Derivation of Kramers escape rate	105
G	Attached article: Conditional cooperativity in toxin-antitoxin regulation prevents random toxin activation and promotes fast translational recovery	111
H	Attached article: Conditional Cooperativity of Toxin-Antitoxin Regulation Can Mediate Bistability between Growth and Dormancy	133

Introduction

Biological systems are characterized by a high level of complexity. Thanks to the great technological advancement in the field of biology in the *post genomic era*, the extent of this complexity has been exposed even further: Enormous amount of new data are available, and several new molecular process taking place inside cells have been elucidated. Even if we restrict our attention to prokaryotic cells, the simplest phenotypical features will be the result of a complex network of several molecular components interacting on different levels. Mathematical and computational modeling has thus become an essential tool to approach this complexity.

In this thesis, I am mainly concerned with the process of regulation of gene expression, which relies on complex networks of interacting genes and proteins, that up- and down-regulate each other. The approach used throughout this thesis is to focus on one specific *pathway*, that constitutes a small subcomponent of such a network. Through mathematical modeling, one can address its functional properties and at the same time gain insights on the basic design principles of the pathway.

More specifically, the work presented here, although divided in three separate projects, develops around one common thread: the attempt to unravel the biological function of toxin-antitoxin (TA) loci. Those are DNA regions, found in *E.coli* as well as in other bacteria and archae, that encodes for both a cytotoxic protein and a cognate antidote.

In Chapter 1 I summarize the basic concepts from mathematical modeling and molecular biology, employed throughout all the thesis.

In Chapter 2, I discuss a project that focuses on the investigating the role played by one specific TA locus in *E.coli*, the *relBE* locus, in *stress response*, and in particular, in the response to *amino-acid starvation*. The *relBE* system is one of the most thoroughly investigated prokaryotic TA loci, and measurements of several fundamental biochemical quantities are available in literature. For this reason, the

relBE system will serve as a reference point throughout the all thesis.

The investigation is carried beyond the specificity of one single system: in Chapter 3, the focus is shifted to exploring the potential of TA loci in *E.coli* as genetic modules capable of mediating *bistability* in the state of the bacterium, which might support the occurrence of heterogeneous behavior within a population of genetically identical cells.

The interest for molecular mechanisms that can support such an occurrence, lies in the connection with a phenomenon known as *bacterial persistence*. This is a form of anti-microbial tolerance, that has its basis in the arising of heterogeneous phenotypes in a clonal cell population, not mirrored by genotypic mutations, as in the case of antibiotic resistance, and is considered to be intrinsically *stochastic* in nature.

In Chapter 4 I tackle the problem of addressing the stochasticity in the expression of TA loci in *E.coli*, in the attempt to connect it to bacterial persistence. The latter project, although it provides a valid descriptive framework for the interconnection between toxin-antitoxin loci and persistence, is still a *work in progress*, and the future perspective are discussed in the conclusion of the chapter.

Chapter 1

Introductory Concepts

The aim of this chapter is to summarize the basic concepts that have been employed to perform the work presented in this thesis. In order to do so, I first describe the mathematical and computational techniques used and discuss them in relation to their application to models of gene regulatory network. Furthermore, since this thesis focuses specifically on the regulatory network of genetic elements known as *prokariotic toxin-antitoxin loci*, in the end of the chapter I will provide a short summary of the main biological features of those.

1.1 Gene Expression Regulation

Gene expression is the process by mean of which the information contained in a gene is converted into a functional gene product, that can be a protein, tRNA, sRNA or ribosomal rRNA. The process of gene expression in prokariotic cells can be schematically described by the following basic steps:

- Transcription: where a specific DNA segment is copied, by RNA-polymerase, into messenger RNA (mRNA).
- Translation: where a ribosome binds to the mRNA and recruits amino-acids according to the sequence specified by the mRNA, decoding this way messenger RNA into an amino-acids chain (polypeptide).
- Protein Folding: where the synthesised polypeptide folds into a functional three-dimensional structure.

Regulation of gene expression encompasses a wide range of mechanisms that result in an increase or decrease in the level of gene product for a given gene. It covers the fundamental role of allowing cells to adapt to a changing environment and respond to external signals. Gene Regulatory Networks (GRN) describe the interaction between the several molecular players that characterized the state of a cell. More specifically, GRNs include the indirect interaction between different genes, mediated by their gene products, and the direct interaction between each gene and the several chemical species, (RNA, proteins and other kinds of signaling molecules) that affect the expression of that gene. Each node on the network represents a certain molecular component like a DNA segment, RNA, or a protein and the links between nodes describe the type of interaction (binding, conformational change, degradation, phosphorylation, etc.). Mathematical modeling of GRN provides a powerful tool to capture the essential features connected to the expression of a certain gene, or a set of genes. Furthermore, it allows to obtain predictive results on the behavior of the system that can be tested against experimental observations.

In this thesis I mainly focus on investigating the behavior of *small* gene regulatory network, where the regulation occurs mainly at the transcriptional level, and is mediated by simple chemical reactions, like *binding* of proteins to DNA, and among each other. For this reason this is the type of GRN I will refer to in the rest of this chapter.

1.2 Modeling Chemical Reactions

1.2.1 Law of Mass Action

Let us consider a simple chemical reaction, for example a titration experiment where we consider the binding of a transcription factor TF to an operator site O on a piece of DNA.



The law of mass action states that *in equilibrium* the concentration of the reaction product [OTF] is directly proportional to the product of the concentrations of the reactants [1]:

$$[\text{OTF}] \propto [\text{O}][\text{TF}]. \quad (1.2)$$

The constant of proportionality can be derived considering the condition of *equilibrium*. A reversible reaction is in equilibrium when the ratio reactant/product is constant over time. This condition is satisfied when the flux of the *forward* reaction $\text{O} + \text{TF} \xrightarrow{k_{on}} \text{OTF}$ is equal to the flux of the *backward* reaction $\text{OTF} \xrightarrow{k_{off}} \text{O} + \text{TF}$. This translates into:

$$k_{on}[\text{O}][\text{TF}] = k_{off}[\text{OTF}], \quad (1.3)$$

hence one can define the constant of proportionality in equation 1.2 as $\frac{1}{K}$, with K defined as:

$$K = \frac{k_{on}}{k_{off}} = \frac{[\text{O}][\text{TF}]}{[\text{OTF}]} \quad (1.4)$$

K is called the dissociation constant for the binding reaction 1.1. An intuitive interpretation of the identity of K can be given if we consider that all the concentrations considered so far, refer to *free* concentrations in solution. The total concentrations are defined as:

$$[\text{TF}_{\text{tot}}] = [\text{TF}] + [\text{OTF}] \quad (1.5)$$

$$[\text{O}_{\text{tot}}] = [\text{O}] + [\text{OTF}]. \quad (1.6)$$

It follows that the *occupied* fraction of the operator is

$$\frac{[\text{OTF}]}{O_{\text{tot}}} = \frac{[\text{OTF}]}{[\text{OTF}] + [\text{O}]} = \frac{\frac{[\text{O}][\text{TF}]}{K}}{[\text{O}]\left(\frac{[\text{TF}]}{K} + 1\right)} = \frac{[\text{TF}]}{1 + \frac{[\text{TF}]}{K}}. \quad (1.7)$$

Analogously the fraction of the operator that is free is

$$\frac{[\text{O}]}{O_{\text{tot}}} = \frac{[\text{O}]}{[\text{OTF}] + [\text{O}]} = \frac{[\text{O}]}{[\text{O}]\left(\frac{[\text{OTF}]}{[\text{O}]} + 1\right)} = \frac{1}{1 + \frac{[\text{TF}]}{K}}. \quad (1.8)$$

Normally the number of operator sites is much smaller than the number of TF molecules, hence $[TF_{\text{tot}}] \approx [TF]$. It follows that the K can be interpreted as the concentration of $[TF]$ required for the fraction of the occupied operator to be $\frac{1}{2}$ [2].

Cooperativity

Let us generalize what discussed so far to the case where *cooperative* binding of n transcription factors TF is required for formation of a stable complex with the operator O.



with K , effective dissociation constant, defined as

$$K = \frac{[\text{O}][\text{TF}]^n}{[\text{OTF}_n]}. \quad (1.10)$$

In this situation it can be shown that the fraction of occupied promoter can be calculated as

$$\frac{\frac{[\text{TF}]^n}{K}}{1 + \frac{[\text{TF}]^n}{K}} = \frac{\left(\frac{[\text{TF}]}{K_m}\right)^n}{1 + \left(\frac{[\text{TF}]}{K_m}\right)^n} \quad (1.11)$$

where is the constant K_m that can be interpreted as the concentration of the transcription factor TF at which the fraction of occupied promoter is $\frac{1}{2}$ and not the effective dissociation constant K derived from the law of mass action 1.10. Only in the case $n = 1$ the two coincide. Equation 1.11 is referred to as the Hill's equation [3] and n is the Hill's coefficient. The Hill's coefficient quantifies the *cooperativity* of the described binding reaction. More specifically, $n > 1$ implies that the binding is *enhanced* by the presence of others TFs bound to the operator. The higher the hill coefficient, the sharper is the dependence of the fraction of the occupied

promoter on the variation of the concentration of the transcription factor around K_m , as it is shown in Fig 1.1, where the dependence of Hill's function 1.11 on the concentration of the transcription factor [TF], for $n = 2$ and $n = 4$ are illustrated.

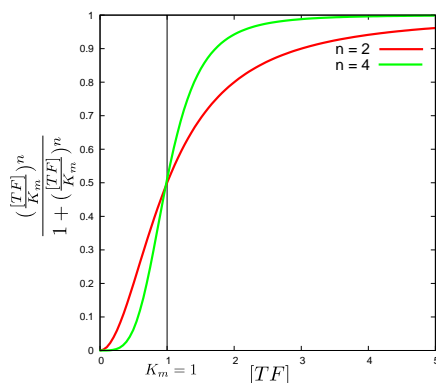


Figure 1.1: Schematic representation of the dependence of the occupancy fraction of the operator $\frac{(\frac{[TF]}{K_m})^n}{1 + (\frac{[TF]}{K_m})^n}$ on [TF] for Hill's coefficient 2 (red line) and 4 (green line). $K_m = 1$

1.2.2 Statistical Mechanics Approach

In the previous section we derived the formula for the fraction of occupied operator O, given the dissociation constant K for the simple binding reaction 1.1, using the law of mass action. In this section, we show how the same result can be obtained using a *statistical mechanics* approach.

Let us consider N identical transcription factor molecules TF (non interacting among each other) in a volume V , and one single operator site O. The probability for one TF to be bound to O, is related to the difference in Gibbs Free Energy between the bound and unbound state: $\Delta G' = G'(bound) - G'(unbound)$. Here when $\Delta G' < 0$ the 'bound' state has a lower free energy, and it is hence more favorable. The system, constituted by the N TF molecules, can be found in two possible state: the "ON" state, where one TF is bound to the operator while $N - 1$ TF are free, and the "OFF" state, where all the N molecules are free. The statistical weight of each state can be calculated as the product between the number of ways the state can be realized and the Boltzmann factor $e^{-\frac{E}{k_B T}}$ of the

state. The statistical weight for the ON state is [2]

$$Z(ON) = \frac{1}{(N-1)!} \left(\int_V dr^3 \int \frac{dp^3}{h^3} e^{-\frac{p^2}{2mK_B T}} \right)^{N-1} \cdot e^{-\frac{\Delta G'}{k_B T}} \quad (1.12)$$

where the integrals count over all the possible positions in the volume V and values of the momentum in the momentum space, for each free molecule. The factor $\frac{1}{(N-1)!}$ avoids multiple counting of realizations that differ by a permutation of molecules, given the fact they are indistinguishable. The division by h^3 accounts for the discreteness of the phase-space required by quantum mechanics. The term $e^{-\frac{\Delta G'}{k_B T}}$ is the Boltzmann factor for the binding of one TF to O. Analogously we can define the statistical weight of the OFF state as:

$$Z(OFF) = \frac{1}{N!} \left(\int_V dr^3 \int \frac{dp^3}{h^3} e^{-\frac{p^2}{2mK_B T}} \right)^N \quad (1.13)$$

Integration of 1.12 yields:

$$Z(ON) = \frac{V^{N-1} \left[\left(\frac{2\pi m k_B T}{h^2} \right)^{\frac{3}{2}} \right]^{N-1}}{(N-1)!} e^{-\frac{\Delta G'}{k_B T}} \quad (1.14)$$

using Stirling's formula ($N! \approx \left(\frac{N}{e}\right)^N$) and within the approximation $\frac{N-1}{N} \approx 1$, we obtain

$$Z(ON) \propto \left(\frac{c}{\rho} \right)^{N-1} e^{-\frac{\Delta G'}{k_B T}} \quad (1.15)$$

where $\rho = \frac{N}{V}$ and $c = \left(\frac{2\pi m k_B T}{h^2} \right)^{\frac{3}{2}}$. For the OFF state we can write

$$Z(OFF) \propto \left(\frac{c}{\rho} \right)^N. \quad (1.16)$$

The partition function for the system constituted by the N identical TF molecules in the volume V is $Z = Z(ON) + Z(OFF)$. Hence, the probability P_{ON} to find the system in the ON state is

$$P_{ON} = \frac{Z(ON)}{Z} \quad (1.17)$$

and the probability P_{OFF} for the system to be in the OFF state

$$P_{OFF} = \frac{Z(OFF)}{Z}. \quad (1.18)$$

The ratio between the probability of the ON state and the OFF state is

$$\frac{P_{ON}}{P_{OFF}} = \frac{\rho}{c} e^{-\frac{\Delta G'}{k_B T}}. \quad (1.19)$$

The latter is equivalent to the ratio between the bound and free fraction of the operator calculated in the previous section using the laws of mass action

$$\frac{P_{ON}}{P_{OFF}} = \frac{[OTF]}{[O]} = \frac{[TF]}{K} \quad (1.20)$$

with K dissociation constant for the binding reaction 1.1. If we identify ρ with $[TF]$ we can *unify* the statistical mechanics description and the one based on the law of mass action by identifying

$$K = c \cdot e^{\frac{\Delta G'}{k_B T}}. \quad (1.21)$$

Both the dissociation constant and the factor c have the dimension of amount of substance per unit volume, i.e. of a *concentration*. If we define ΔG as binding energy *per mole* and we measure the volumes in liters, we obtain the final equality

$$K = [1M] \cdot e^{\frac{\Delta G}{RT}}. \quad (1.22)$$

The statistical weights obtained can be normalized with respect to $Z(OFF)$, we then write

$$Z(ON) = [TF] e^{-\frac{\Delta G}{RT}} \text{ and } Z(OFF) = 1. \quad (1.23)$$

By substituting the statistical weights in the form just presented into the probability of the ON state we obtain

$$P_{ON} = \frac{Z(ON)}{Z(ON) + Z(OFF)} = \frac{[TF] e^{-\frac{\Delta G}{RT}}}{1 + [TF] e^{-\frac{\Delta G}{RT}}} \quad (1.24)$$

which is completely equivalent to the result obtained by applying the law of mass action, provided that one identifies $e^{-\frac{\Delta G}{RT}}$ with $\frac{1}{K}$ as in equation 1.22.

1.3 Modeling Gene Expression

1.3.1 Transcription Regulation : the ODE approach

In this section I address the problem of quantitatively describing gene expression as a dynamical process.

Let us consider the expression of gene g encoding for a protein, G , in the simple case where the regulation occurs at the *transcriptional* level. In the simplest level of description, this is a process consisting of two-steps, mRNA synthesis (transcription) and protein synthesis (translation). The dynamics of the process can be described by a set of Ordinary Differential Equations (ODE). The behavior over time of the concentration of the mRNA (m) and of the protein G is governed by the balance between synthesis of new molecules and degradation as follows:

$$\frac{dm}{dt} = P - \gamma_m m \quad (1.25)$$

$$\frac{dG}{dt} = \beta m - \gamma_G G, \quad (1.26)$$

where P represents the rate (concentration per unit time) of production, β is the translation rate per mRNA molecule, while γ_m and γ_G are the degradation rates¹. The production term P will be described according to the exact mechanism of regulation of transcription. In particular, we need to distinguish between two cases:

- A) transcription of g is initiated by the transcription factor TF binding to the operator site of the promoter - TF is an activator.
- B) transcription of g is inhibited by the transcription factor TF binding to the operator site of the promoter - TF is a repressor.

In case A) the production rate will be proportional to the probability of the operator site to be occupied by the transcription factor TF. Conversely, in case B), P will be proportional to the probability of the operator site to be free. Taking into account the formulas for the probability of occupation obtained in the previous section 1.7,1.8 we can write

$$\text{A) } P \propto \frac{\frac{[TF]}{K}}{1 + \frac{[TF]}{K}}$$

¹for the sake of simplicity i only illustrate the simple case where degradation is linear

$$\text{B) } P \propto \frac{1}{1 + \frac{[TF]}{K}}$$

where, again, K is the dissociation constant for the binding reaction of TF to the operator. Equations 1.25, for case A) can be then written as

$$\frac{dm}{dt} = \frac{\alpha[TF]}{K + [TF]} - \gamma_m m \quad (1.27)$$

$$\frac{dG}{dt} = \beta m - \gamma_G G. \quad (1.28)$$

Instead for case B) the ODE system 1.25 becomes

$$\frac{dm}{dt} = \frac{\alpha K}{K + [TF]} - \gamma_m m \quad (1.29)$$

$$\frac{dG}{dt} = \beta m - \gamma_G G. \quad (1.30)$$

where in both cases α represents the maximal level of mRNA synthesis.

The production rate in both equations 1.27 and 1.29 has the form of the famous Michaelis-Menten equation relating the reaction rate to the substrate concentration for an enzymatic reaction [4, 5], provided that TF has the role of the substrate and mRNA synthesis rate is interpreted as the reaction rate.

In the case illustrated, we have assumed that the binding of the transcription factor to the operator is not cooperative. Extension to the case where the binding involves cooperativity is straightforward, provided that we express the occupancy probability of the operator (or the probability to be free) as in 1.11. In the case where cooperative-binding of 2 TF is needed to activate transcription, for example, transcription of g mRNA be described by the following equation:

$$\frac{dm}{dt} = \frac{\alpha[TF]^2}{K + [TF]^2} - \gamma_m m. \quad (1.31)$$

1.3.2 The Gillespie Algorithm

The ODE approach suggested in the previous section, although appropriate in several circumstances, does not allow to take into account explicitly the *discrete* and *stochastic* nature of a process involving several interacting chemical species. In these cases it becomes relevant to include the *fluctuation* in the level of the molecular species involved, in the description of the process.

The standard approach for a stochastic description of such system is to write down the Master Equation. This governs the time evolution of the probability distribution of the system to be found in a state characterized by a given molecular level for each of the N molecular species.

It is also possible to simulate numerically the time evolution of the system, through the implementation of an algorithm for stochastic simulations proposed by Gillespie in 1977 [6], commonly referred to as the *Gillespie algorithm*. I will now describe the basic structure of the algorithm, after having introduced some basic concepts regarding the probabilistic description of the system and the notation used.

Let us assume, in a fixed volume V , we have a spatially uniform mixture of X_i molecules of chemical species S_i with $i = 1, \dots, N$, interacting through M specified reaction channels, each labelled as R_μ , with $\mu = 1, \dots, M$.

The basic assumption is that for each reaction channel R_μ the reaction rate a_μ at a given time t , is fully determined by the number of molecules per chemical species $\vec{X} = (X_1, \dots, X_N)$.

The time evolution of the system depends on the probability $P(\tau, \mu)d\tau$ that given the state of the system \vec{X} at time t , the next chemical reaction will occur between $t + \tau$ and $t + \tau + d\tau$ AND it will be of the kind μ .

$P(\tau, \mu)$ can be expressed as the product between the probability that given the state \vec{X} no reaction will occur between t and $t + \tau$, and the probability of a reaction of the type R_μ occurring within the time interval $t + \tau$ and $t + \tau + d\tau$. It can be shown that one then obtains [6]

$$P(\tau, \mu) = \begin{cases} a_\mu e^{-a_0 \tau} & \text{if } 0 \leq \tau \leq \inf \\ 0 & \text{otherwise} \end{cases}$$

where $a_0 = \sum_{\nu=1}^M a_\nu$ is the probability per unit time that *any* reaction would occur, given the system is in the state \vec{X} . It is possible to generate a pair of random

variables (τ, μ) distributed according to $P(\tau, \mu)$ as follows:

$$\tau = \frac{1}{a_0} \ln\left(\frac{1}{r_1}\right) \quad (1.32)$$

$$\mu : \text{ so that } \frac{\sum_{\nu=1}^{\mu-1} a_\nu}{a_0} < r_2 \leq \frac{\sum_{\nu=1}^{\mu} a_\nu}{a_0} \quad (1.33)$$

where r_1 and r_2 are random numbers uniformly distributed within the interval $[0, 1]$. A stochastic simulation of the system described above can be implemented as follows:

Initialization

Set initial values for X_i ; $i = 1, \dots, N$

Set $t = 0$

Step 1

Calculate a_μ according to X_i ; $i = 1, \dots, N$

Calculate $a_0 = \sum_{\nu=1}^M a_\nu$

Step 2

Generate r_1 and r_2 from a uniform random number distribution in $[0, 1]$

Calculate $\tau = \frac{1}{a_0} \ln\left(\frac{1}{r_1}\right)$

Take μ so that $\frac{\sum_{\nu=1}^{\mu-1} a_\nu}{a_0} < r_2 \leq \frac{\sum_{\nu=1}^{\mu} a_\nu}{a_0}$

Step 3

Update time $t = t + \tau$

Update X_i ; $i = 1, \dots, N$ according to R_μ

Go to Step 1.

A stochastic simulation method of the kind described above can be called *exact* [6], in the sense that each Gillespie realization represents a random trajectory in phase space, that reflects the probability distribution that one would obtain by solving analytically the Master Equation governing the time evolution of the system.

1.4 Prokariotic Toxin-Antitoxin Loci

1.4.1 Toxin-Antitoxin Loci

In this work, the dynamics of expression of the TA loci is investigated in connection to their involvement in the response to amino-acid starvation, and in the phenomenon of bacterial persistence. These concepts are going to be clarified in the following sections.

Prokaryotic toxin-antitoxin loci (TA loci) are frequently found both in bacteria and archae [7,8]. A TA locus encodes for two components: a *toxin* that inhibits cell growth, and an *antitoxin* that counteracts this toxic activity. So far, three types of Toxin-Antitoxin loci have been identified. In Type I and Type III TA loci, the role of the antitoxin is played by small RNAs [9, 10], while in the case of type II TA systems, the antitoxin is a protein that inhibits the toxin by forming tight complexes with it [11]. The study presented in this thesis is only concerned with type II TA loci. Type II Toxin-Antitoxin loci have been divided into gene families according to toxin sequence similarities, some are plasmid-encoded (e.g. *ccd* locus on the plasmid F, *parDE* on the RK2 plasmid, *highBA* locus on the Rts1 plasmid and *phd/doc* on the P1 plasmid), while the remaining are chromosome-encoded (e.g. *relBE* and *mazEF* of *E.coli* and *vapBC* of *Salmonella Enterica*) [11]. In this thesis, we focus on the activity of TA loci in *E.coli*. This contains 11 TA loci: 10 of those, encodes for a toxin that is an mRNA endonuclease (mRNase), namely an enzyme that mediates cleavage of the mRNA. More specifically, six of them cleave mRNA positioned at the ribosomal A-site (RelE, YoeB, HigB, YahV, YafO and YafQ) [12–16], while the remaining 4 (MazF, ChpB, MqsR and HicA) cleave mRNA in a site-specific but ribosome-independent fashion [7, 17, 18]. The 11th TA locus is *hipAB*, that does not belong to any of the previously mentioned families. The toxin HipA, inhibits translation by phosphorylation of the Elongation Factor TU [19]. TA loci in *E.coli* have the following common features [20]:

- The toxin inhibits translation.
- The antitoxin auto-regulates transcription of the TA locus [11].
- The toxin and the antitoxin form complexes that bind stronger than the sole antitoxin, and cooperatively, to the operator region, hence the toxin work as a co-repressor of transcription [21].

- Transcription of all investigated TA loci is regulated through a complex mechanism named *conditional cooperativity*, basically consisting in the toxin working both as a co-repressor and a de-repressor of transcription according to the ratio between the concentration of the toxin and the antitoxin. This will be discussed in further detail in the next section [21–24].
- The antitoxin is translated at a higher rate than the toxin [20].
- The antitoxin is degraded by the cellular protease Lon [7, 25–27].

1.4.2 Biological Role of TA loci

Nutritional Stress Response

Bacteria have evolved strategies to cope with the stress induced by shortage or lack of nutrients, such as amino-acids, glucose or carbon sources. The response to nutritional stress consists in a down-regulation of protein and nucleic acids production, and a concomitant up-regulation of amino-acid synthesis and proteins degradation. In other words, the cell goes into its metabolic base level in order to optimize resource utilization and maximize its chances of survival during the period of crisis. These adjustments are known as *stringent response* [28]. The well known trigger to activation of stringent response is the accumulation of the alarmone guanosin-tetra-phosphate (ppGpp) and guanosine-penta-phosphate (pppGpp) [29].

A TA locus can work as a module that has the capability of inducing rapid adjustments of protein synthesis, through modulation of the toxin activity. Such a tool, would provide a strong benefit to a bacterium that is facing amino-acid starvation. This argument is topped with accumulating experimental evidences suggesting that TA loci might be involved in the cellular response to amino-acid starvation. As it will be discussed in further detail in the next chapter, in fact, Christensen *et al* in 2001 [25] discovered that amino-acid starvation stimulates transcription of one of the TA loci in *E.coli* K-12, the *relBE* locus, and that the presence of the *relBE* locus facilitates growth slow-down in starved cells. Furthermore, the protease that is responsible for degradation of all the anti-toxins in *E.coli* TA loci, Lon, is known to be activated during amino-acid starvation [30].

Bacterial Persistence

In 1994 Joseph Bigger discovered that that if a culture of *Staphylococcus* that had been treated with penicillin, was re-plated and incubated for 24 hours, surviving colonies would be recorded. These colonies could re-grow into a population that was again susceptible to penicillin. Bigger named these cells *persisters* to distinguish them from cells that had evolved a genetic mutation that conferred them resistance [31].

Persister cells correspond to a sub-population of multi-drug tolerant bacteria, that are genetically indistinguishable from the rest of bacterial population. The phenomenon of persistence can be then described as the emergence of *phenotypical heterogeneity* within a *genetically homogenous* population.

Persisters are currently understood as cells that enter a dormant state via a mechanism that is drug-independent and stochastic [32, 33]. A common interpretation [20, 34] is that being in a slow- or non-growing state, protects them from the antibiotics, since most antibiotics efficiently kill only growing bacteria [35]. In particular, experiments performed by Balaban *et al.* on *E. coli* in micro-fluidic chambers, in fact, confirmed that persister cells belong to a pre-existing (with respect to addition of antibiotic) sub-population of non- or slow-growing cells. If this subpopulation is generated during *stationary phase*, when the bacterial population is characterized by an over-all slow growth because of external factors such as nutritional stress, they are referred to as Type I persisters. When instead persisters are formed because of *spontaneous* switching from exponential growth to a dormant state, they are referred to as Type II persisters [32]. Although bacterial persistence constitutes obviously a problem of medical relevance, as it compromises the effectiveness of anti-microbials, the exact molecular mechanism behind it is not understood yet.

The first evidence for a genetic basis of persistence was the discovery of the *hip* (High Persistence) phenotype of *E. coli*-K12. It has been shown that mutations in the *hipA* gene resulted in a strongly increased persistence frequency [36–39].

Interestingly, it was discovered that the *hipA* gene actually belongs to a Toxin-Antitoxin module, the *hipAB* locus [40, 41]. The intriguing connection between bacterial persistence and the activity of TA loci in *E. coli* spans far beyond the discovery of the *hip* phenotype. For example, a correlation between high TA-mRNA level and persisters fraction, has been demonstrated. [33, 42]. Furthermore Maisonneuve *et al.* in 2011. [43] showed that progressive deletion of the 10 chromosome-encoded TA loci in *E. coli*-K12 resulted in a significant reduction in the persisters fraction, confirming the involvement of the TA modules activity in the persistent phenotype.

Chapter 2

The *relBE* system and its role in the nutritional stress response

In 2001, Christensen *et al.* [25] discovered the first (p)ppGpp-independent nutritional stress response module in *E. coli*: The *relBE* locus. The *relBE* locus is a Toxin-Antitoxin module that encodes for the cytotoxin RelE and the antitoxin RelB. Christensen *et Al.* showed that over-expression of RelE severely inhibits translation and that the presence of the *relBE* toxin-antitoxin locus causes a significant reduction in the translation level during amino acid starvation. They compared the rate of translation in *wild type* (*relBE*⁺) *E.coli* K-12 and the Δ *relBE* strain with deletion of the *relBE* locus, before and after induction of starvation for serine. As expected the rate dropped quite significantly in both cases, but for the strain where the *relBE* locus was present, the post-starvation level was almost 2-fold lower than the value for the Δ *relBE* strain. These results suggest that amino acid starvation is responsible for activation of the toxin RelE.

In order to investigate the role played by the *relBE* locus in the response to starvation, and comprehend the mechanism characterizing its transcriptional regulation, I propose a model of the dynamics of the *relBE* operon activity. The results of this study, carried through via mathematical modeling and numerical simulations, are presented in this chapter.

The work discussed in this chapter resulted in a publication, that is attached in appendix G.

2.1 The *relBE* locus

The *relBE* locus is a chromosome-encoded Toxin-Antitoxin locus in *E.coli* K-12. It is constituted by two genes *relB* and *relE*. *relE* encodes for the cytotoxin RelE and *relB* for the antitoxin RelB, that inhibits RelE toxicity by forming tight complexes with it. The two genes belong to the same operon and are transcribed by the same promoter situated upstream of *relB* [44]. The antitoxin RelB is degraded by the protease Lon [25], at a high rate, with its half-life been measured to be $\sim 3 \text{ min}$ [21]. The toxin RelE, on the other hand, is metabolically stable and its concentration decays solely because of dilution due to cell division. Its turnover time, in fast growth conditions, is thus $\sim 30 \text{ min}$, the estimated average doubling time for exponentially growing *E.coli* cells.

The steady state concentrations of the toxin and the antitoxin have been measured [45] to be around $500 - 1000 \text{ nM}$ for RelB and $50 - 100 \text{ nM}$ for RelE. RelB level is thus ~ 10 times higher than RelE during the exponential growth phase. Given the 10 fold difference in the half-lives, is then safe to assume that RelB is translated 100 times more often than RelE.

The toxin RelE is an RNA-interferase that cleaves mRNA positioned at the ribosomal A-site in a codon-dependent fashion, impairing translation. Consequently RelE expression inhibit cell growth and colonies formation [12].

When RelE is sequestered in complexes with the antitoxin RelB, the cleavage of mRNA is inhibited, and cell growth is not affected. RelB is mostly found in the form of dimers RelB_2 and the toxin and the antitoxin can form complexes in the two stoichiometric ratios RelB_2RelE and $\text{RelB}_2\text{RelE}_2$ [45].

RelB and RelE contribute to auto-regulate the *relB* locus expression: RelB dimers repress the promoter while RelE acts as a co-repressor, namely when it binds RelB dimers, it enhances their affinity for the operator region [21, 45]. The details of this interaction will be discussed in the next subsection.

2.1.1 Conditional Cooperativity

The *relBE* operon *relO* consists of two binding sites.

Overgaard *et al.* in 2008, showed that toxin-antitoxin complexes, in the stoichiometric ratio of RelB_2RelE , can bind *cooperatively* to the two binding sites, with a much higher affinity than the RelB dimers alone, conferring strong repression of the promoter. The same study also showed that over-expression of RelE

in living cells causes an increase in the synthesis of *relBE* mRNA, suggesting that the over-expression induces de-repression of the *relBE* promoter.

It was shown in conclusion, that the ON/OFF state of the promoter depends on the RelB:RelE *ratio*, rather than on the absolute concentration of the two proteins. RelE acts as a co-repressor at low concentration and as a de-repressor at higher concentrations. In particular, for RelB:RelE ratios above 2:1 RelE strongly enhances RelB binding to the operator *relO*, thus inducing repression of the promoter. For ratios below 2:1 further addition of RelE doesn't affect the promoter state, until RelB:RelE ≈ 1 , when over-expression of the toxin results in disruption of previously formed repressor complexes [21].

This peculiar behavior can be understood by realizing the fact that toxin-antitoxin complexes can be formed in two different stoichiometric ratios : RelB₂RelE and RelB₂RelE₂ and the latter has no affinity to the operator region of the *relBE* promoter. [46]. For RelB:RelE ratios 2:1 and above, the most abundant stoichiometric form of the toxin-antitoxin complex is RelB₂RelE, resulting in strong repression of the promoter. But when RelE level exceeds RelB and the ratio is close 1:1 and below, the equilibrium is pushed towards the alternative stoichiometric ratio, RelB₂RelE₂, titrating away RelB₂RelE and inducing de-repression of the promoter.

The *relBE* locus complex auto-regulation mechanism, with the state of the promoter determined by the relative concentration of the proteins encoded by the locus, is called *Conditional Cooperativity* [21]. The term *conditional* in conditional cooperativity, refers to the promoter state depending on the ratio, rather than absolute concentration of the regulator proteins, while the term *cooperativity* is used because regulation of the promoter is achieved through cooperative binding of complexes of the regulators to the operator sites.

A schematic visualization of the discussed effect of conditional cooperativity on the promoter activity in two different RelB:RelE ratios range is given in Fig2.1.

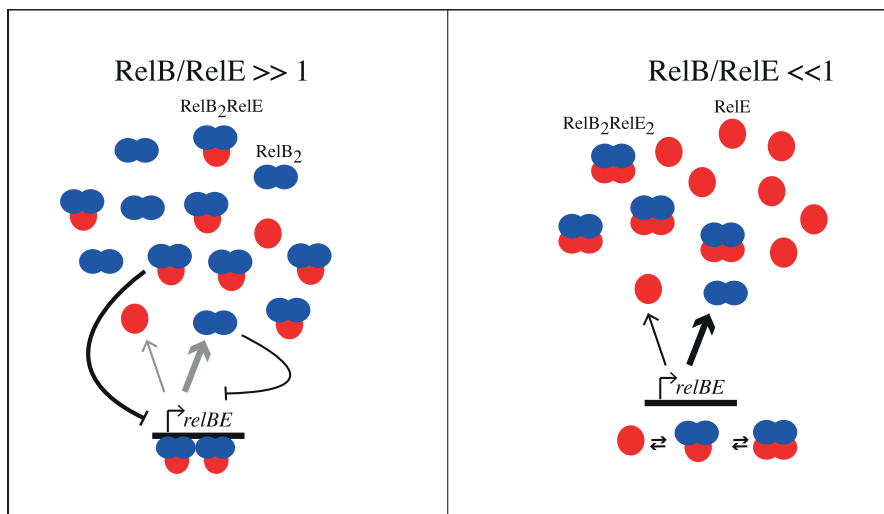


Figure 2.1: Visualization of conditional cooperativity due to the formation of $\text{RelB}_2\text{RelE}_2$, that does not repress the promoter

2.2 The Model

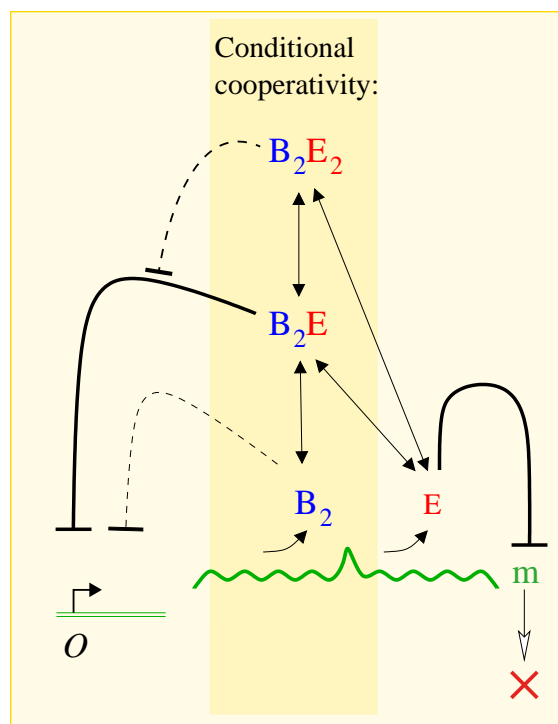
2.2.1 The *relBE* regulatory network

In this section I will clarify what are the essential features that define the *relBE* regulatory network and how they have been included in the model. A graphical depiction of the *relBE* network is given in Fig.2.2.

When the two binding sites of the operator site *relO* (indicated as *O* in figure) of the *relBE* promoter are empty, the promoter is de-repressed and *relBE* mRNA (*m*) is synthesized. The *relBE* mRNA is then translated to produce both RelB and RelE molecules.

In the model, transcription of the *relBE* locus and translation of the *relBE* mRNA are considered separately.

RelB forms tight dimers, so from now on we assume that RelB is always in the form of dimers RelB_2 . In Figure 2.2 RelB dimers are indicated as B_2 and RelE monomers are referred to as E . Free RelE monomers (E_f) cleave intra-cellular mRNA, including *relBE* mRNA, resulting in a negative feedback on their own production. Apart from the RelE-mediated cleavage, the mRNA is also subject to active degradation. The *relBE* mRNA half-life has not been measured, but in the model I used $\sim 5 \text{ min}$, corresponding to the high-end of a typical half-life of mRNA in *E.coli*, so that it is possible to keep the maximal promoter activity and the translation rate within biologically plausible range, given the constraint of the



B = *RelB* - antitoxin, E = *RelE* - toxin.

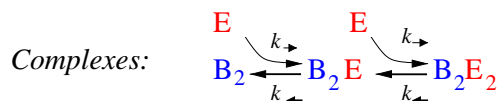


Figure 2.2: *relBE* locus regulatory network as considered in the model. O represents the operator site *relO*, m is the *relBE* mRNA while B and E are *RelB* and *RelE*, respectively. The toxin-antitoxin complexes in the two stoichiometric form *RelB*₂*RelE* and *RelB*₂*RelE*₂ are indicated by B_2E and B_2E_2 . The arrows with a flat ending represent negative interaction, as in repression or degradation. Positive interactions, the ones that result in an increase in the concentration of one molecule type or in a higher reaction rate, are indicated by arrows with a pointy ending. Finally, the dashed-lined arrows indicate weak or indirect interactions.

measured steady-state value for the concentration of *RelE* and *RelB*.

It is worth mentioning at this point, that on average there are 4 chromosomes in an exponentially-growing *E. coli* cell. The maximal promoter activity is calculated from the overall steady state mRNA level (as shown in detail in appendix A), so it refers to the total transcription product of the 4 loci belonging to the 4 chromosomes.

As mentioned in section 2.1 free *RelB* has a fast turnover, while *RelE* is metabolically stable and it is only diluted because of cell division. Degradation of *RelB* depends on whether it is in its free *RelB*₂ form or in complex with *RelE*.

The latter have been observed to be more stable [45], thus the half-life of RelB₂ in complexes, τ_c , is taken to be 4 times longer than for free dimers. Cell division has not been taken into account in the model explicitly, but it affects RelE half-life.

RelB₂ and RelE bind to each other to form RelB₂RelE. Two RelB₂RelE complexes can form a strong cooperative binding to the operator site and repress the promoter. RelB₂ dimers alone also bind to the operator and repress the promoter, but this repression is much weaker than the one conferred by cooperative binding of RelB₂RelEs.

Repression by a single RelB₂RelE has not been considered in the model, since the Hill coefficient for the binding to *relO* has been measured to be close to 2 [21]. But binding of the two RelB₂RelEs to the operator is assumed to be happening in two steps, one molecule at the time, with binding of the second molecule showing a much lower value of the dissociation constant ($K_{D3} > K_{D2}$). Binding constants are estimated to reproduce the experimentally observed repression fold of the promoter, that is ~ 800 in fast growth conditions [44].

RelB₂RelE complexes also bind free RelE monomers to form RelB₂RelE₂ complexes, which have no affinity to the operator region. Formation of these RelB₂RelE₂ complexes depletes the repressor complex pool, counteracting repression of the promoter. This is the main feature of *conditional cooperativity*.

We further consider that RelB₂RelE complex formation can occur *on* the operator, resulting in de-repression of the promoter. We call this mechanism *stripping*, as it consists in a free RelE molecule binding a B₂E complex already bound to the operator and cause its release from the binding site, with consequent de-repression of the promoter. This mechanism has been shown to happen in vitro [21].

2.2.2 The Stochastic Model

The *relBE* regulatory network described in the previous section, consists of a set of chemical reactions involving a certain number of molecular species. We perform stochastic simulations of this chemical process, where the amount of each molecular species is considered as a discrete variable, i.e. as the number of molecules of that kind. Concentrations are converted to number of molecules considering that one molecule in an average *E.coli* cell, corresponds to 1 nM ¹.

2.2.3 The reactions scheme

The state of the system at a given time is defined by the amount of the following molecular species

- m - *relBE* mRNA
- B_f - Free RelB dimers
- E_f - Free RelE monomers.
- B_2E - RelB₂RelE complex
- B_2E_2 - RelB₂RelE₂ complex

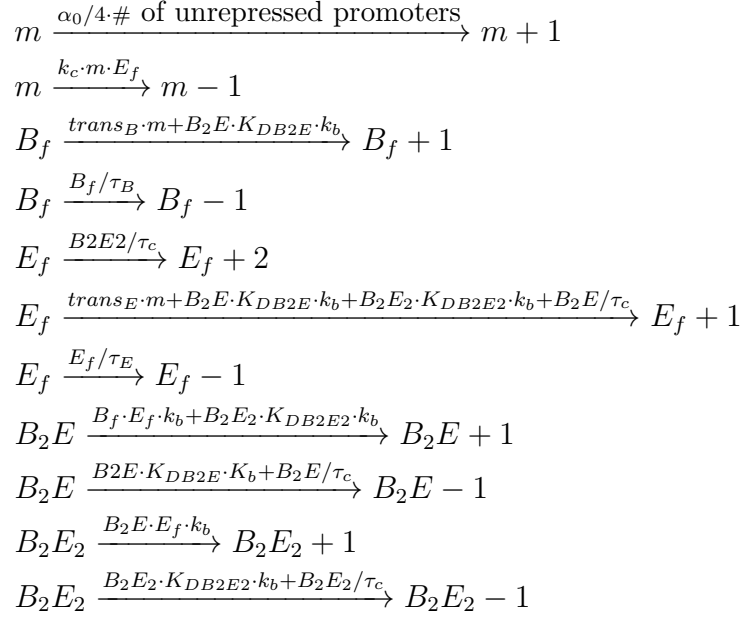
The total copy number of RelB₂ and RelE are given by

$$\begin{aligned} B_T &= B_f + B_2E + B_2E_2 \\ E_T &= E_f + B_2E + 2B_2E_2 \end{aligned}$$

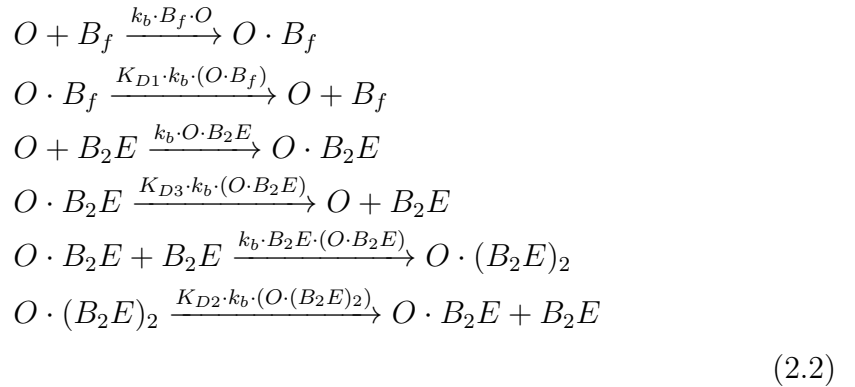
¹ *E.coli* cells have a volume $\approx 1\mu\text{m}^3$ and

$$1\text{nM} = \frac{10^{-9}\text{mol}}{\text{dm}^3} = \frac{10^{-24}\text{mol}}{\mu\text{m}^3} = \frac{10^{-24} \cdot N_A}{\mu\text{m}^3} \text{molecules} \approx \frac{1}{\mu\text{m}^3} \text{molecule} \quad (2.1)$$

We simulate the behavior of the system over time by means of Gillespie Algorithm. Each chemical reaction is then treated as a discrete stochastic event, happening at a given rate. The reactions that involve synthesis, degradation, complex formation and dissociation are the following:

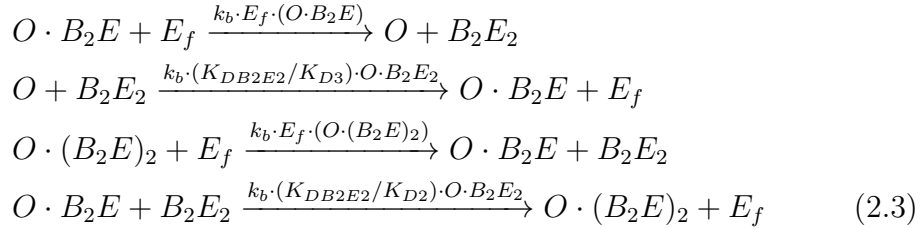


The following reactions refer to the operator (*O*) dynamics.



The last set of reaction describes this peculiar mechanism that we refer to as *stripping*, that was mentioned in the previous section. It consists in free RelE molecules binding a RelB₂RelE complex that is already bound to the operator, causing the release of the latter from the operator, and the reverse reaction of

those.



Symbol and Meaning	Description	Value	Units	Reference
α_0 total promoter activity		154.665	$nM \min^{-1}$	see tex
$[B2]_{ss}$ steady state total concentration of <i>RelB</i> dimers		200	nM	see text cf [45]
$[E]_{ss}$ steady state total concentration of <i>RelE</i>		44	nM	see text cf [45]
τ_m <i>mRNA</i> halflife		7.2	min	see text cf [47]
τ_B <i>RelB</i> halflife		4.3	min	see text cf [45]
τ_E <i>RelE</i> halflife		43	min	see text
τ_c <i>RelB</i> ₂ halflife in complexes		17	min	see text cf [45]
n_H Hill's coefficient		2.3		[45]
$trans_B$ <i>RelB</i> translation rate		15	min^{-1}	see text
$trans_E$ <i>RelE</i> translation rate $trans_B/50$		0.3	min^{-1}	see text
k_{bind} binding on-rate $4\pi Da/V_{cell}$		3.8	min^{-1}	[2]
$\frac{K_d B_2E}{[B_2][E]} = K_d B_2E$ dissociation constant for B2E complexes formation		0.3	nM	[21]
$\frac{K_d B_2E_2}{[B_2E][E]} = K_d B_2E_2$ dissociation constant for B2E2 complexes formation		0.3	nM	
$k_u B_2E$ dissociation rate for B2E		1.14	nM	
$k_u B_2E = k_{bind} \times K_d B_2E$				
$k_u B_2E_2$ dissociation rate for B2E2		1.14	nM	
$k_u B_2E_2 = k_{bind} \times K_d B_2E_2$				
K_{D1} dissociation constant for B binding to DNA		10	nM	see text cf [44]
K_{D2} dissociation constant for second B2E bound to DNA		0.04	nM	see text cf [44]
K_{D3} dissociation constant for first B2E binding to DNA		30	nM	see text cf [44]
k_c cleavage rate		2.0	$nM^{-1} min^{-1}$	see text cf [12]

Table 2.1: Set of parameters used in the stochastic simulation, in exponential growth condition. The value of the maximal promoter activity α_0 (cfr Table 2.1) calculation is shown in appendix A.

In each run the behavior of the system is simulated over a total time range of 600 minutes, through three different phases. From $t = 0$ to $t = 200$ the set of parameters used in the simulation is the one given in Table 2.1 and it is relative to a cell in fast growth conditions. At time $t = 200$, as it will be described in

more detail in section 2.3 the value of some of the parameters is modified to mimic amino acid starvation conditions. The system is let evolve in such conditions for 300 minutes. At time $t = 500$ all the parameters are moved back to their original values, describing fast growth (see Table 2.1). This is done to investigate the system *recovery* once the nutritional stress is over.

2.2.4 Modeling the transition to amino-acid starvation

There are three main processes taking place during amino-acid starvation

- The overall translation rate in the cell is reduced to $\frac{1}{10}$ of the pre-starvation level, independently of the *relBE*, as measured by Christensen *et al.* in the *relBE*⁻ strain [25].
- Cell division slows down dramatically or stop completely, affecting dilution of RelE.
- The activity of the protease Lon, responsible for degradation of RelB increases [30].

According to these observations, the value of some key parameters were changed to mimic amino-acid starvation (AS) conditions. Table 2.2 summarizes the parameters defining the transition and their values pre- and post- starvation.

Parameter	Pre-Starvation	Post-Starvation
$trans_B$	15 min^{-1}	1.5 min^{-1}
$trans_E$	0.3 min^{-1}	0.03 min^{-1}
τ_E	43 min	24 h
τ_B	4.3 min	0.5375 min
τ_c	17.2 min	2.15 min

Table 2.2: $trans_B$ and $trans_E$ are the translation rates of, respectively, *RelB* and *RelE*. Their values change to $\frac{1}{10}$ of pre-starvation, in accord with the drop in overall translation detected in the experiments. [25]. The half-life of RelE, τ_E , becomes $24h$, since it reflects cell division, that stops during amino-acid starvation. The value of $24h$ is somewhat arbitrary, it was chosen to be much longer than the total simulated time (5 hours). This way within the investigated time-range the toxin can virtually accumulate indefinitely. At last, the Increased activity of Lon protease upon starvation, is reflected in a shorter half-life for *RelB*₂ dimers, both in their free form (τ_B) and in complexes with the toxin (τ_c)

2.3 Results

2.3.1 Aminoacid starvation drives the switch to toxin activation

Figure 2.3 illustrates the population averaged response of the *relBE* locus expression to amino-acid starvation. As it can be seen in the upper panel of fig. 2.3, the transition to AS condition happening at 200 min , induces a dramatic increase in the level of free toxin. Concomitantly with the accumulation of free toxin, a drop in the concentration of the free antitoxin *RelB*₂ is detected, as it is shown in the middle panel of 2.3. This is expected, given the lower translation rate, together with the enhanced degradation of the antitoxin. Finally in agreement with the experimental results by Christensen *et al* [25], the onset of amino-acid starvation coincides with a spike in the *relBE* mRNA level. This spike is explained as follows: as accumulation of free *RelE* starts, the promoter gets de-repressed resulting in a rapid increase in the *relBE* mRNA level. As *RelE* keeps accumulating, though, it cleaves *relBE* mRNA, with a consequent drop in the concentration of the mRNA.

Comparison between Fig. 2.3 and 2.4 shows that toxin activation depends on degradation of *RelB*₂ in complexes. If this feature is removed, in fact, one is faced

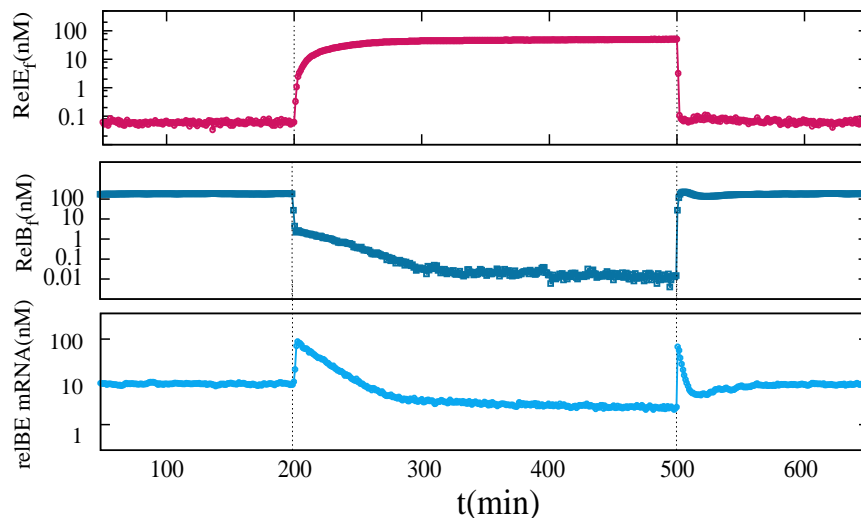


Figure 2.3: Time courses averaged over 1000 cells, for free RelE (upper panel), RelB (middle panel) and *relBE* mRNA (bottom panel), illustrating how the system switches between a state of high antitoxin to a state of high free toxin.

with only a modest increment in RelE concentration, that remains on average below $1nM$ - which translates into less than one molecule per cell.

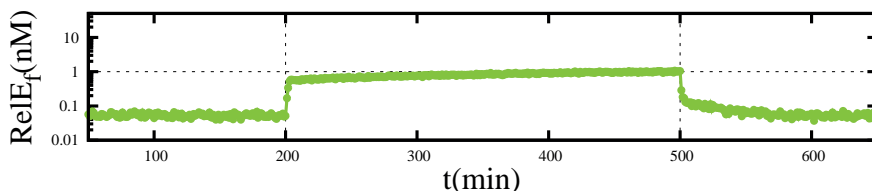


Figure 2.4: Development of free RelE in case that there is no active degradation of RelB in complexes, thus RelB in complex the same half-life as τ_E . Free RelE is seen to remain low, in contrast to behavior of standard model (Fig 2.3 middle panel) where RelB in complex is degraded a factor 4 times slower than in complex but still degraded much faster than RelE.

Once starvation is over at 500 *min*, translation, alongside with cell division, is restored. At this point in time the promoter is de-repressed because of *conditional cooperativity*. Therefore RelB production is heavily boosted. On top of that, RelB turnover slows down because Lon activity is not enhanced in rich medium conditions. The resulting increase in the concentration of RelB₂ allows the free RelE level to return to non-starved levels quite fast, as it can be noticed by observing the behavior of RelB_f, RelE_f and *relBE* mRNA in Fig 2.3.

Stripping

In Section 2.2 I briefly mentioned a mechanism that I referred to as *stripping*. It consist in free *RelE* molecules *invading* the $relO \cdot RelB_2RelE$ complex inducing the release of $RelB_2RelE$ from the operator.

Stripping contributes to the excess-RelE mediated de-repression of the promoter. Conditional cooperativity consists in the formation of $RelB_2RelE_2$ complex *in the bulk* that depletes the repression factors ($RelB_2RelE$) pool resulting, effectively, in de-repression of the promoter. With stripping in addition, RelE actively *pulls away* the transcription factor from the operator binding site. It is possible to have conditional cooperativity without stripping, but not vice-versa.

If the on-off dynamics was fast, the presence of stripping would not affect the time-scale of the accumulation of *RelE* upon starvation. In this case, though, the average residence time of $(RelB_2RelE)_2$ on the operator is long, estimated to be roughly 6 *min*². In this case stripping facilitates de-repression of the promoter at lower concentrations of free *RelE*. This, in turn, means that *relBE* mRNA synthesis is boosted before *RelE* has accumulated enough to make mRNA cleavage significant, resulting in the peak in *relBE* mRNA. Increased *relBE* mRNA level means, of course, increased synthesis of RelB, that can "fight back", despite the enhanced degradation rate, delaying further accumulation of free RelE. Figure 2.5 shows the behavior of the system without stripping. As it can easily be seen, no peak in the level of *relBE* mRNA is detected upon starvation, and the rise in the concentration of free RelE is much faster than in the standard case.

2.3.2 Single Cell activation of RelE is binary

In this section I describe the dynamics of protein concentration at single cell level.

In Fig 2.3 one observes a steady accumulation of free toxin over time, over the starvation period.

When looking at single trajectories, as in Figure 2.6 it becomes immediately clear that increase in the concentration of *RelE* upon starvation, doesn't happen in a graded fashion. It is a sudden switch that typically does not occur immediately after the onset of starvation but rather with a certain time delay.

Figure 2.7 shows the probability distribution $P([E_f, t])$ of a cell having a certain

²Calculated considering a repression fold due to two $RelB_2RelE$ binding to the operator ~ 800 and a diffusion limited on-rate estimated to be $0.06 \text{ min}^{-1} \text{ molecule}^{-1}$ [2]

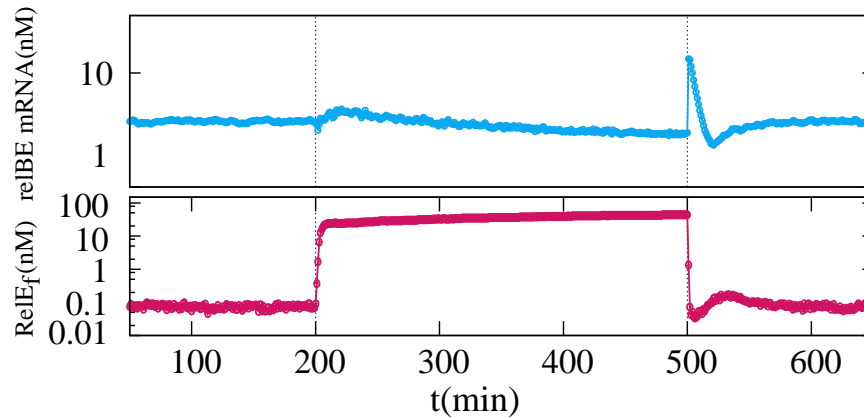


Figure 2.5: Average trajectory of *relBE* mRNA and free RelE without stripping. Compared to in Fig. 2.3, entry into the toxin dominated state is faster.

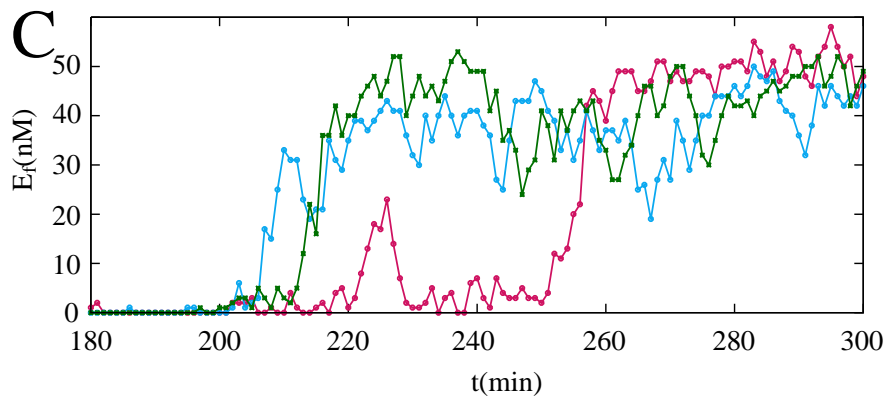


Figure 2.6: The dynamics at entrance to the starvation at the single cell level. Three examples are shown, and the total amount of free RelE is plotted as function of time, from time 180 to time 300.

concentration E_f of free RelE at time t . There is a high peak at low RelE free concentration at the very onset of starvation. But a second peak, corresponding to high ($\sim 45nM$) free RelE concentration, appears already after 10 minutes from the transition to starvation conditions. The low probability for an intermediate $[E_f]$ value suggests that each cell switches from a state with low concentration of free toxin to a toxin-dominated state quickly.

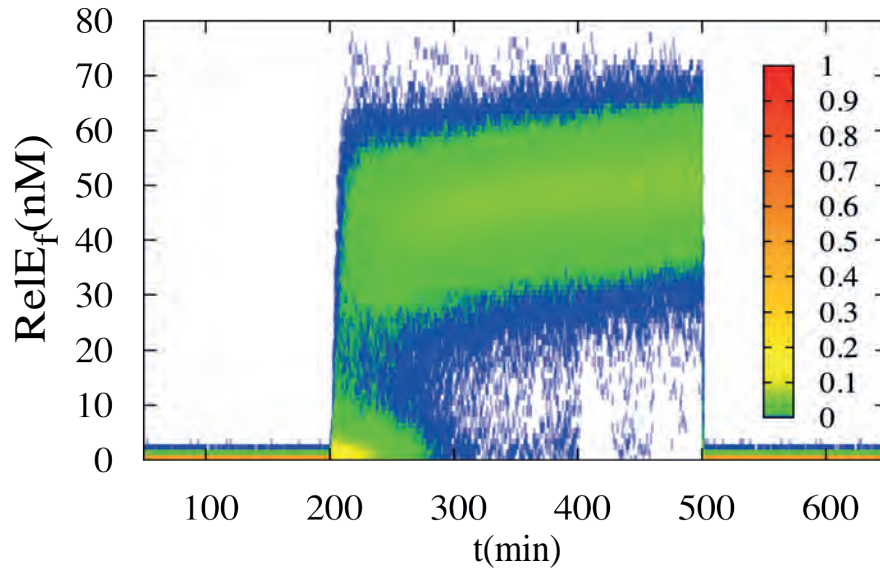


Figure 2.7: Probability distribution $P([E_f], t)$ of a cell having a certain concentration $[E_f]$ nM of free RelE at a given moment t .

2.3.3 Conditional Cooperativity primes fast exit from RelE dominated state and prevents random toxin activation

In order to unravel the role of conditional cooperativity, we compared the behavior of the system with and without conditional cooperativity. For the latter case, we prevent $\text{RelB}_2\text{RelE}_2$ formation completely. This way accumulation of free RelE, even above $2[\text{RelB}_2]$, will not result in a decrease in the abundance of the repression factor RelB_2RelE .

Figure 2.8 A. shows that the presence of conditional cooperativity guarantees fast recovery from the toxin-dominated state, once starvation is over. During the starvation period, $[\text{RelE}] \gg [\text{RelB}_2]$, in this circumstance conditional cooperativity guarantees that the promoter is de-repressed already during starvation, accelerating the exit from the toxin-dominated state as soon as the stress is terminated. The lack of conditional cooperativity also allows the system to reach higher level of free RelE during the starvation phase, making, of course recovery harder.

Our model also shows conditional cooperativity to have an effect on keeping homeostasis. In fact, it reduces the probability of having a high level of RelE in the non-starved phase, as it is shown in Figure 2.8 B. In fast growth conditions the total concentration of RelB is ~ 10 times higher than total RelE, implying

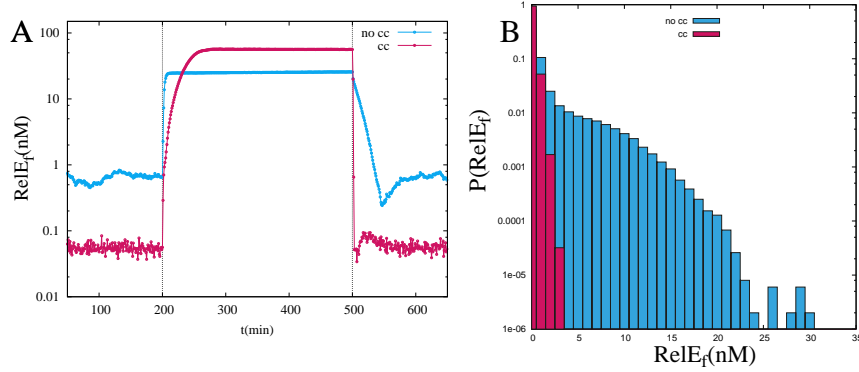


Figure 2.8: Role of conditional cooperativity. A: The time evolution of free RelE level for the system with (red) and without (blue) conditional cooperativity. The system is starved for amino acid from 200 to 500 min. B: Probability distribution of free RelE in the non-starved state without conditional cooperativity (blue) and with conditional cooperativity (red). Free RelE takes higher value without conditional cooperativity.

that all the toxin is sequestered in complex with the antitoxin and there is no free RelE available. If the level of RelB drops, allowing the presence of free RelE, conditional cooperativity ensures additional RelB.

2.3.4 Robustness against parameter change

The model of the *relBE* system presented involves several parameters. To make sure that the main results are not dependent on fine-tuning of the parameters I tested the robustness of the model against parameter change. The parameters used in table 2.1 have been changed one by one, by 2^n -fold with $n \in [-3, 3]$ and I tested that the model still work within the new parameter set. The model is defined as *working* if the following conditions are satisfied:

i) $[RelE_f] < 1nM$ in fast growth state; ii) $[RelE_f] \geq 10nM$ within 20 minutes from the switch to starvation; iii) $[RelE_f] < 1nM$ within 5 minutes after starvation is terminated.

The results of the test are summarized in Fig.2.9. Condition i) - that states that the level of free RelE has to be below $1nM$ in non-starved state, is very easily satisfied. Only if the dissociation constant K_{DB_2E} for $RelB_2RelE$ complex formation becomes very weak, preventing RelB from efficiently keeping RelE sequestered in complexes, i) is compromised.

Condition ii) - fast accumulation of free RelE upon starvation - is the most

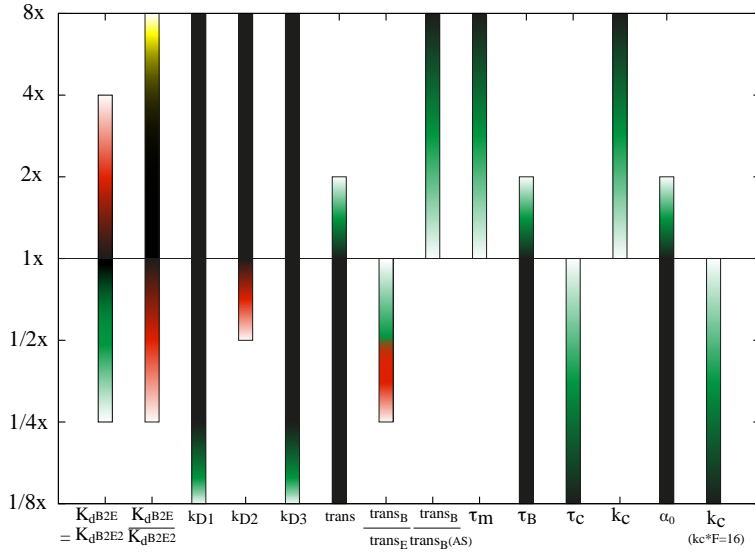


Figure 2.9: Summary of the model behavior against parameter changes. For each parameters (horizontal axis), fold change of the values from our reference values are tried one by one. The color gradients indicate how the model deviates from the reference behavior: yellow indicates too many free toxins in the healthy states, green indicates too slow rise of free RelE at aa starvation, and red indicates too slow drop of toxins after the removal of aa starvation. In the first entry, $K_dB_2E = K_dB_2E_2$, the ratio of the dissociation constants K_dB_2E and $K_dB_2E_2$ are kept to be one, but the value itself is changed. In the second entry, the ratio $K_dB_2E/K_dB_2E_2$ is changed, while keeping smaller dissociation constant to be the reference value 0.3 nM. For the entry *trans*, the translation rates for RelB and RelE are changed by the given folds, while $trans_B/trans_E$ and $trans_B/trans_B(AS)$ ($trans_B(AS)$ is the translation rate of RelB during the aa starvation) are kept to the reference values. For the entry $trans_B/trans_E$ and $trans_B/trans_B(AS)$ the given ratio is changed with keeping the value of the translation for RelB $trans_B$ to be 15 /min. For the entry τ_B (τ_C), the lifetime of the RelB₂ (RelB's in the complexes) are changed with keeping the 1/8 fold reduction of the lifetime during the aa starvation. For the entry k_c (the 12th entry), the value of the cleavage rate is changed, while for the entry $k_c(k_c \times F = 16)$ (the last entry), the value of k_c and the fold-change of the RelB degradation rate F are changed, so that $k_c \times F$ is kept to the reference value 16.

delicate criterion. In the *relBE* system, in normal growth condition, it is *vital* that the level of free toxin is kept as low as possible, even fluctuations in RelE concentration have to be kept under control. For this reason it is not surprising that most of the reference parameters cited in Table 2.1 lie in a region of the parameter space where inhibition of raise is the free toxin is a priority, and they are just borderline sufficient to satisfy condition ii).

The third criterion iii) -namely fast exit from the toxin-dominated state - is

violated when production of RelB becomes impaired. This circumstance can occur because the ratio $\frac{trans_B}{trans_E}$ between the translation rate of RelB and RelE is too low, or if the repression of the promoter provided by *RelB₂RelE* is too intense.

Finally, the robustness of the model against change in the maximal transcription rate α_0 it's biologically important. Even though this effect was not taken into account explicitly in the model, it is very natural to assume that accumulation of free RelE would provide a negative feedback on the cell growth rate, that, in turn, would negatively affect the transcription rate [48]. We find that our model is robust against a $\frac{1}{8}$ - to 2-fold change in α_0 , which suggest that including the negative feedback on growth rate in the model would not invalidate the conclusions.

2.4 Conclusion

I built a model of the *relBE* locus transcription regulation that takes into account explicitly the intrinsically stochastic nature of the chemical reactions that compose the regulatory network. The latter was then used to investigate the dynamical behavior of the system through the transition from rich-medium culture conditions to amino-acid starvation, and to monitor how a cell would recover once starvation is over.

The model allowed to unravel several interesting features concerning the *relBE* locus activity.

- a fast entry into a toxin-dominated state *requires* RelB dimers to be degraded by Lon not only in their free form, but also when in complex with RelE.
- The activation of the toxin, RelE, in response to amino-acid starvation is not graded, but switch-like.
- Conditional cooperativity mediates fast recovery from the toxin-dominated state and prevents random activation of the toxin in non-starved state.

Switching behavior is known to be related to a positive feedback loop in many biological systems [49, 50]. In the present case the positive feedback loop facilitating the switch is given by accumulation of toxin that leads to inhibition of

antitoxin synthesis through *relBE* mRNA cleavage, which, in turn, allows RelE to accumulate further.

Conditional cooperativity, preventing unwanted activation of the toxin in the exponential growth phase, plays a role in ensuring survival itself, to a cell that is provided with a toxin-antitoxin module. This conclusion is intriguing, especially when one considers that all the bacterial toxin-antitoxin modules studied so far present a similar mechanism [20].

Chapter 3

Conditional Regulation and Bistability

In the previous chapter we demonstrated that *conditional cooperativity* in the regulation of the *relBE* locus is involved in the cell's ability to recover effectively and efficiently after having been exposed to amino-acid starvation, and prevents random toxin activation in non-starved state.

As briefly mentioned in Chapter 1 section 1.4, all chromosome and plasmid-encoded Toxin-Antitoxin loci that have been investigated so far have been shown to be regulated through *conditional cooperativity*. The *relBE* locus of *E. coli* [21,45], *vapBC* of *Salmonella enterica*, *phd/doc* of plasmid P1 [23,51,52] and *ccdA/ccdB* of plasmid F are included among those. This circumstance suggests a biological relevance for conditional cooperativity, beyond the response to amino-acid starvation observed in the case of the *relBE* locus.

In the previous chapter the function of conditional cooperativity has been investigated in a set-up that takes into account details that are rather specific to the *relBE* system. The aim of the study presented in this chapter is to explore the features and the potential biological role of conditional cooperativity, in a more general perspective, that can be applied to the regulation of type II TA loci in general.

As mentioned in Chapter 1 Toxin-Antitoxin loci have been suggested to be involved in the phenomenon of bacterial *persistence* [20,32,38,39,43], whereas the exact underlying molecular mechanism is not understood yet and it is currently a hot research topic [53].

Nevertheless, if we keep in mind that persisters are currently understood as

cells in a slow- or non-growing state, a possible interpretation of the phenomenon is then that this dormant (persister) state might be a consequence of stochastic activation of the toxin. This would be supported by the TA locus regulatory network exhibiting bi-stability between a fast-growing antitoxin-dominated state and a dormant toxin-dominated one. This hypothesis has been investigated, with focus on the *hipAB* locus in particular, by Lou et al. in 2008. [54]. They concluded that the above mentioned bistability is possible, as long as a high (≥ 4) Hill coefficients are assumed in the binding of the Toxin-Antitoxin complex to the operator, along with growth-inhibition mediated by free toxin. In their study conditional cooperativity was not taken into account.

In the current chapter we investigate conditional cooperativity as a mechanism that can mediate bistability between growth and dormancy, via heteromer-formation, without the need of a high hill coefficient.

The work presented in this chapter resulted in the publication attached in Appendix H.

3.1 Conditional Regulation

To analyze the function of conditional cooperativity as a regulatory mechanism *mediated by heteromer formation*, and to explore the potential of such mechanism, I built a simplified model of a generic type II Toxin-Antitoxin locus, inspired on the *relBE* system, where the antitoxin A and the toxin T can form complexes in two stoichiometric forms



where AT is the only active complex, that confers repression to the promoter, while free A, T and ATT do not exert direct transcriptional regulation. For simplicity, weak repression of the promoter due to binding of the antitoxin A alone is not considered, and the binding of AT to the operator is not assumed to be cooperative.

Since we are not considering cooperativity in the binding of AT to the operator anymore, from now on I will refer to the regulatory mechanism examined simply as *conditional regulation*, instead of *conditional cooperativity*.

The concentration of AT and ATT are calculated according to the laws of mass action as follows :

$$[AT] = \frac{[A_f][T_f]}{K_T} \quad (3.3)$$

$$[ATT] = \frac{[AT][T_f]}{K_{TT}} \quad (3.4)$$

where K_T and K_{TT} are the dissociation constants for, respectively AT and ATT complex formation, and $[A_f]$ and $[T_f]$ are the concentration of free A and T calculated considering conservation of mass :

$$[A] = [A_f] + [AT] + [ATT] \quad (3.5)$$

$$[T] = [T_f] + [AT] + 2[ATT] \quad (3.6)$$

Figure 3.1 shows the behavior of the concentration of [AT] as a function of [T]

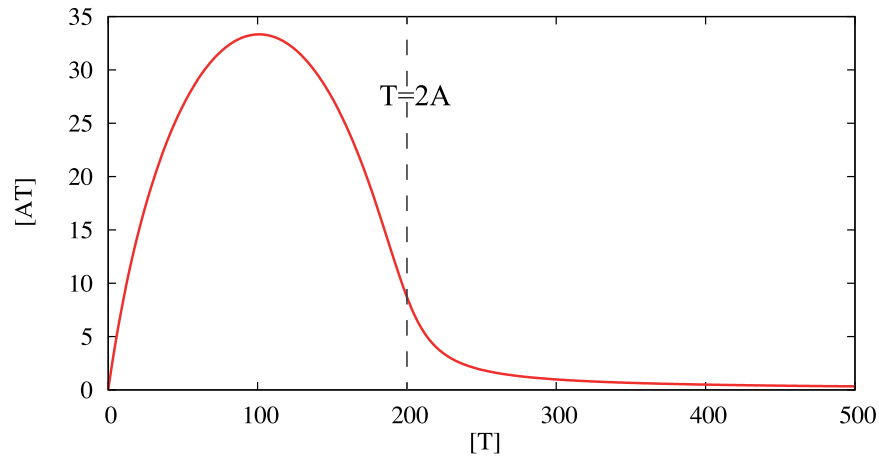


Figure 3.1: Concentration of the heteromer AT as function of the toxin concentration $[T]$, for a fixed value of the antitoxin concentration $[A] = 100$ and $K_T = K_{TT} = 1$. Notice that the concentrations are given as a-dimensional quantities.

for a fixed value of $[A]$. As expected $[AT]$ concentration starts accumulating from 0 as $[T]$ increases, and it peaks at $[T] = [A]$. For $[T] \geq [A]$, $[AT]$ starts decreasing, as a consequence of formation of $[ATT]$ complexes that sequester away ATs. For $[T] \geq 2[A]$ virtually all ATs have been sequestered by free T into ATT complexes and $[AT]$ drops to 0.

3.1.1 The Promoter Activity

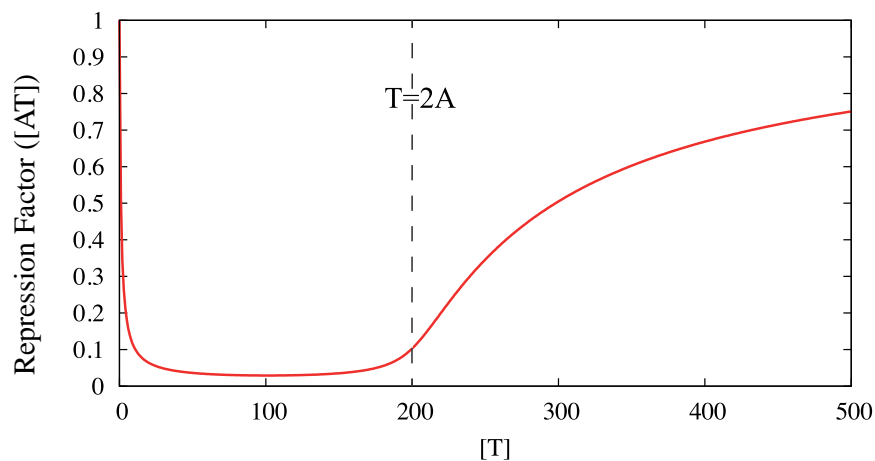


Figure 3.2: Promoter activity $\propto \frac{1}{1+[AT]}$ as function of the toxin concentration $[T]$, for a fixed value of the antitoxin concentration $[A] = 100$ and $K_T = K_{TT} = 1$. Notice that the concentrations are given as a-dimensional quantities

Figure 3.2 shows the promoter activity as a function of $[A]$, for fixed $[A] = 100$. The behavior of the promoter activity $\propto \frac{1}{1+[AT]}$ mirrors the behavior of $[AT]$ as a function of $[A]$ and $[T]$ shown in 3.1.

The promoter is de-repressed for $[T] \simeq 0$, when $[AT]$ is also ~ 0 , it undergoes maximal repression for $[T] = [A]$, where $[AT]$ peaks, and transcription is finally resumed for $[T] \geq 2[A]$, thanks to the sequestration of the repression units AT into ATT heterocomplex, mediated by accumulation of free T. The derepression around $[T] = 2[A]$ shows *ultra-sensitive* behavior, if the dissociation constants K_T and K_{TT} are small enough¹. This behavior is a straightforward consequence of the ultra-sensitive behavior of $[AT]$ around $[T] = 2[A]$, where just a factor two change in $[T]$ results in dramatic sequestration of AT, as it can be seen in Fig. 3.1.

Another peculiar feature of the present system, whose consequences will be discussed later, is that the promoter activity is a non-monotonic function of $[T]$. At low absolute concentration, an increase in $[T]$ induces repression, while in the T-dominated regime ($[T] > [A]$) further accumulation of the toxin results in de-repression.

3.1.2 Bistability in a simple feedback motif

I investigate the dynamical behavior of the concentration of the toxin T in the case where its production is negatively regulated by the AT complex, as described in the previous section, and the value of A is kept fixed. The simple regulatory network is described by the equation:

$$\frac{d[T]}{dt} = \frac{\sigma}{1 + \frac{[AT]}{K_O}} - [T], \quad (3.7)$$

where σ is the maximal production rate for T and K_O is the dissociation constant for AT binding to the promoter. $[AT]$ is calculated, for a given $[A]$ and $[T]$, as in Eq. 4.32. The concentration of $[A]$ is kept fixed, which is equivalent to make the assumption that production of A is controlled by a constitutive promoter, and $[A]$ level is in steady-state. So $[A]$ plays the role of an external parameter.

Transcription of T-encoding mRNA and translation of T proteins are not taken into account as separate processes in this model. The maximal production rate σ incorporates the mRNA steady state level and the translation rate per mRNA

¹in the case of the In *relBE* system the dissociation constants are indeed very strong, in the nanomolar regime, cfr Table 2.1 in Chapter 2

molecule. In this section we set $K_T = K_{TT} = 1$ and express all the concentrations in units of toxin-antitoxin binding strength. The time unit is chosen to be the life-time of the toxin T.

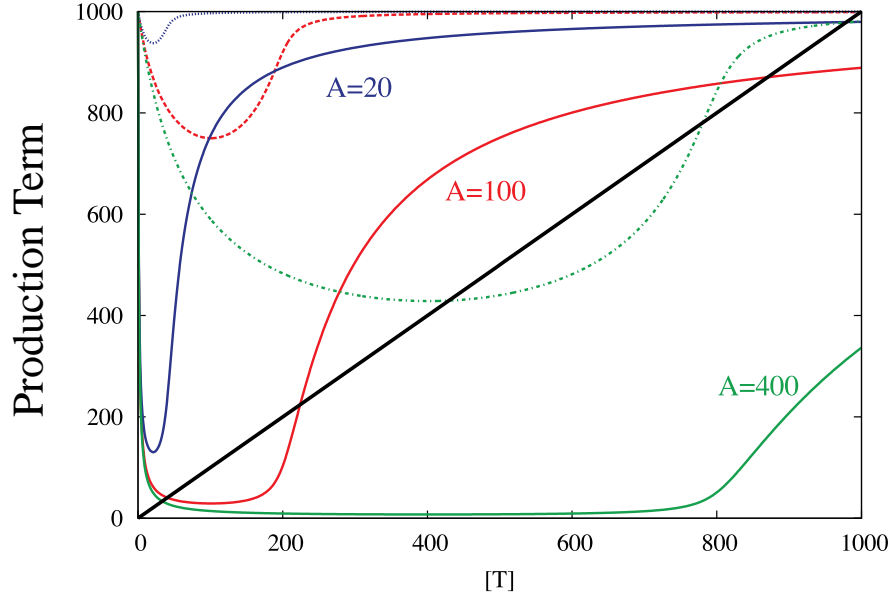


Figure 3.3: Production term of Eq.3.7 as a function of T, for $K_0 = 1$ (solid lines), $K_0 = 10$ (dashed lines) and for three different values of [A]. [A] = 20 = blue line, [A] = 100 = red line, [A] = 400 = green line. The solid black line represents the degradation term.

In figure 3.3 the production term of Eq 3.7 as function of [T], for three different values of [A], is plotted in color lines. Solid and dashed lines refer, respectively, to stronger and weaker AT binding to the promoter. The solid black line represent the linear degradation term in Eq 3.7. The repression is strongest at $[T] = [A]$ in all cases, as that depends on the stoichiometric ratio of the toxin-antitoxin complexes only, and analogously sharp de-repression always happens at $[T] = 2[A]$. The higher the value of [A], though, the higher the repression factor at $[T] = [A]$. For a given value of [A], a tighter binding of AT to the promoter also confers stronger repression. Each crossing of the production and degradation terms in the plot represents a steady state for equation 3.7. For $K_0 = 1$ and low value of the antitoxin concentration, $[A] = 20$, equation 3.7 admits only one solution, for high values of T, $[T] \simeq 1000$. As the values A is shifted to a higher level ($[A] = 100$), the production and degradation term cross three times, namely the system exhibits bistability. The two stable solutions correspond to a low T (uninduced) state and a high T (induced) state respectively, while the unstable solution occurs at an intermediate value. If the value of A is pushed even further ($[A] = 400$), the

stable state corresponding to high T concentration is lost, and the system becomes mono-stable, with solution at low T concentration.

The dashed lines show that, for weaker binding of AT to the promoter $K_O = 100$, bi-stability is still supported, as long as the value of A is increased accordingly (cf. Fig.3.3, green-dashed line).

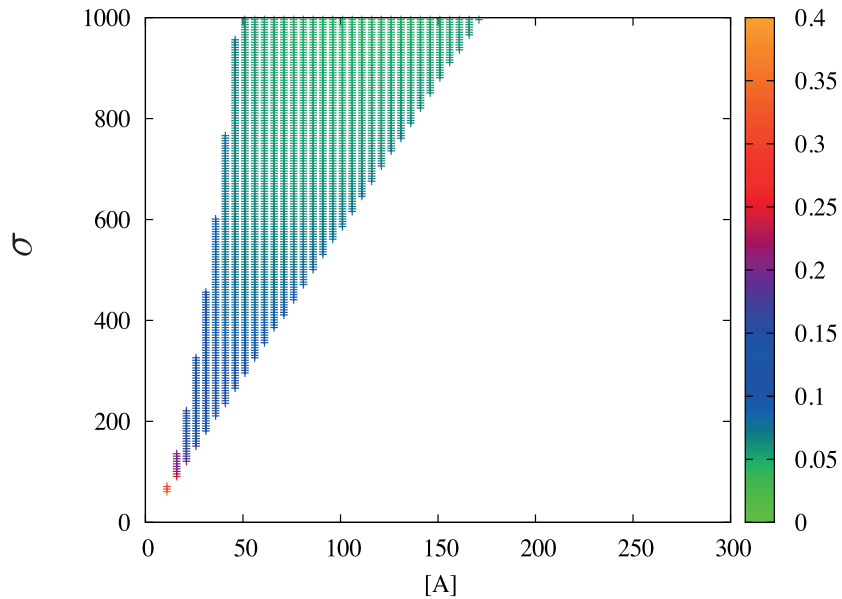


Figure 3.4: Region in the parameter space that shows bistability for $K_O = 1$. Each point on the plot represent a combination of σ and $[A]$ that allows the equation to have two stable solutions. The color of the point reflect the $T(\text{low})/T(\text{high})$ ratio.

Figure 3.4 shows the robustness of bistability with respect to change in relevant parameters, i.e. the maximal production rate for T, σ , and the total concentration of the antitoxin $[A]$.

For each value of σ , if the concentration of A is too low, the system is monostable and induced, while if $[A]$ exceeds a certain threshold, the high T fixed point is lost, and the system is monostable, with a fixed point corresponding to low T concentration. Analogously, for a given value of $[A]$, for too high values of σ the antitoxin-dominated fixed point vanishes, while on the contrary, if production of T is insufficient, achieving a high T state becomes impossible.

The color of each bistable point in the phase diagram represent the ratio between the low-T and the high-T fixed point. Higher values of σ result in higher $[T]$ in the T-dominated solution, and thus in a lower ratio. The effect of the value of $[A]$ on the ratio, instead, appears to be less pronounced. Remarkably, conditional

regulation in the simple regulatory network provides bi-stability in a wide range of parameters, in absence of cooperativity in the binding of AT to the operator. The reason behind this is that in Eq 3.7 the non-linearity in the denominator, necessary to achieve bi-stability, is obtained through the ultra-sensitive decrease in AT concentration around $[T] = 2[A]$ mediated by protein-protein sequestration. The minimal requirements to obtain bi-stability in the level of a protein in a genetic regulatory network are a *positive feedback* and a source of *ultra-sensitivity* resulting in a sigmoidal response function to the input signal [55–57]. In the present case, conditional regulation provides a positive feedback to accumulation of toxin, T, and sequestration mediated by formation of heteromers provides ultrasensitivity. Bistability in a genetic network, mediated by sequestration due to protein-protein interaction *alone* has also been demonstrated in literature before [58].

The other peculiar feature of the promoter activity with conditional regulation, the non-monotonic behavior, guarantees the un-induced steady state to occur always for a finite amount of [T]. The biological relevance of this circumstance will be discussed later.

3.2 A Simple Peristers Model

3.2.1 Conditional Regulation and Peristers

In the previous section it has been shown that *conditional regulation* supports bi-stability in a wide range of parameters in a simple feedback loop motif. In order to explore the essential features of the mechanism of persister formation, in this section we build a model of the activity of a TA module, regulated via conditional regulation.

The reference to the *relBE* system is maintained in the choice of parameters, because details of molecular mechanisms and parameters (cf. Table 2.1) are well known for this system.

The model consists in the following equations :

$$\frac{d[A]}{dt} = \frac{\sigma_A}{1 + \frac{[AT]}{K_O}} - \Gamma_A[A], \quad (3.8)$$

$$\frac{d[T]}{dt} = \frac{\sigma_T}{1 + \frac{[AT]}{K_O}} - [T] \quad (3.9)$$

where the concentration of [AT] is calculated as in eq. 4.32. A graphic representation of the model in eq. 3.8 and 3.9 is given in fig. 3.5 A1. In equations 3.8 and 3.9 A and T production is considered coupled, in the sense that they are assumed to be encoded from the same promoter. Their translation rates, though, are different, as it is reflected by the different values of σ_A and σ_T . In particular, σ_A is assumed to be ~ 100 times higher, in analogy with the case of the *relBE* locus. This does not result in a loss of generality in the model, since in all the Type II TA loci investigated so far, the translation rate of the antitoxin has been measured to be higher than the one of the toxin [11].

The other common features of all known type II TA loci are the fact that the toxin is metabolically stable, while the antitoxin has a fast turnover and conditional cooperativity mediated autoregulation. The half-life of the toxin is then set by the *E.coli* doubling time in log-phase growth in rich medium to be ~ 30 min, while for the antitoxin is set to be ~ 3 min.

The feedback loop described by equations 3.8 and 3.9, however, cannot exhibit bi-stability. The reason lies in the fact that in this simple motif, the toxin and the antitoxin production are regulated identically. When the promoter undergoes sharp de-repression around $[T] = 2[A]$ the production of the antitoxin is also

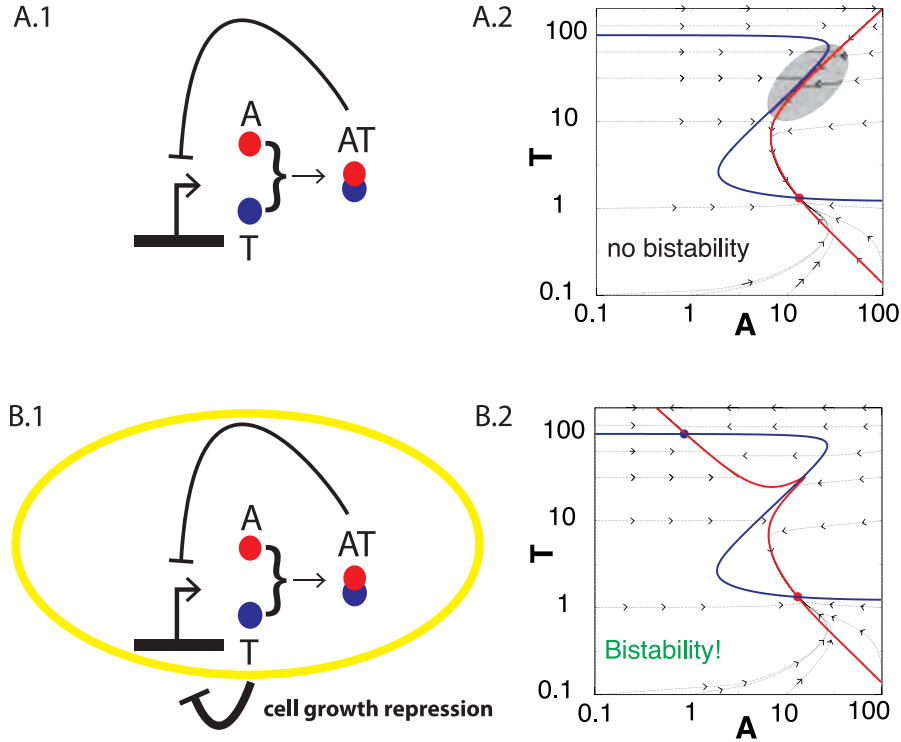


Figure 3.5: (A1) Schematic representation of the genetic circuit described by our model eqs. (3.8 and 3.9) for TA system with CR. (A2) Null-clines for the system of eqs. (3.8 and 3.9). Blue line $\frac{dT}{dt} = 0$, Red line $\frac{dA}{dt} = 0$. No combination of parameters gives bistable steady states. Infact, for comparable values of A and T the two null clines become parallel, as shown in the area highlighted in grey. Dashed lines with arrows show the flow to the fixed point. (B1) Schematic representation of the genetic circuit described by the model (3.11). (B2) Null-Clines for the system of eqs. (3.11). with $\beta_M = \beta_C \approx 10$. Blue line $\frac{dT}{dt} = 0$, Red line $\frac{dA}{dt} = 0$. Dashed lines with arrows show the flow to the stable fixed points.

enhanced, and the latter is large enough that it is impossible to achieve a stable steady state in the toxin-dominated regime. Figure 3.5 A2, shows an example of null clines for the system given by eq 3.8 and 3.9. It can be clearly seen that only one fixed point is found, occurring for high A and low T. For comparable values of T and A the null clines become almost parallel, as shown in the grey area, as a consequence of the identical regulation of production of T and A. Parameter scanning spanning from $\frac{1}{8}$ to 8 fold of the reference parameters (listed in Table 3.1) were performed, and no combination of them showed bi-stability.

σ_A	10000
σ_T	100
Γ_A	10
$K_T = K_{TT}$	0.004
K_O	0.15

Table 3.1: Reference Parameters. The values of the parameter are unitless. The cell generation constitutes the unit time $\tau_u = 43 \text{ min}$, while the concentration unit is 1/10000 of the maximal production of antitoxin per cell generation. $C_u \simeq 70$ to keep the reference to the *relBE* system.

3.2.2 Toxin Accumulation feedbacks on growth rate

Toxins encoded by Type II TA loci, by mean of inhibition of translation [20], slow down or completely halt cell growth. Variations in the growth rate are known to affect transcription, translation and cell division rate [48, 59]. For these reasons, the toxin-induced growth-arrest needs to be taken into account explicitly in a meaningful description of the activity of a TA locus. Within the framework of the present model this consists in including two effects :

- Free toxin accumulation inhibits protein synthesis: by free toxin activity. This inhibition can also happen indirectly, via growth-rate dependent inhibition of global transcription [48].
- The toxin turnover depends on dilution due to cell division. If cell division is inhibited by the free toxin activity, the half-life of the toxin is prolonged accordingly.

A graphics representation of the extended regulatory network is given in fig. 3.5 B1. The extension of the model in 3.8 and 3.9 is expressed by the following set of equations :

$$\begin{aligned} \frac{dT}{dt} &= \frac{\sigma_T}{\left(1 + \frac{[AT]}{K_O}\right) (1 + \beta_M [T_f])} - \frac{1}{1 + \beta_C [T_f]} \cdot [T] \\ \frac{dA}{dt} &= \frac{\sigma_A}{\left(1 + \frac{[AT]}{K_O}\right) (1 + \beta_M [T_f])} - \Gamma_A \cdot [A] \end{aligned} \quad (3.10)$$

$[T_f]$ reduces protein production, and the parameter β_M quantifies this effect, per $[T_f]$ molecule. The choice to use the same parameter, β_M , for the inhibition of translation of both T and A is justified by the assumption that accumulation of free toxin acts on the mRNA level, where toxin and antitoxin are coupled.

Analogously, β_C represents the cell growth-inhibition per free toxin molecule. The degradation rate of A is not affected by changes in the growth rate, since it is very fast. We are introducing in the model a positive feedback on accumulation of free toxin: inhibition of translation impairs the antitoxin capability of counteracting the toxin and the toxin half-life is prolonged. In principle, the term dependent on β_M reduces production of both T and A to the same extent, but the antitoxin, with its short lifetime is effectively more affected.

As it can be seen in Fig. 3.5 B2, including the effect of the growth-rate mediated positive feedback on toxin accumulation, allows the system to show bi-stability. In Fig 3.5 B we use $\beta_M = \beta_C \approx 11$ so that the effect on [T] of the newly introduced term, is balanced off and the shape of the T-null cline is conserved in fig 3.5 A and B. On the contrary, the A-null cline is affected, as for high values of [T], solutions of $\frac{dA}{dt} = 0$ tend to occur for lower values of [A].

As it was mentioned before, the toxin-mediated inhibition of protein production and cell division is caused by the combination of several effects. Thus the numerical values of β_M and β_C are not easy to infer. It was thus necessary to evaluate the robustness of the bistable behavior, with respect to significant change in the value of β_M and β_C .

Figure 3.6 shows the results of parameter scanning over several order of magnitude in the value of β_M and β_C . Each point on the plot is a combination of β_M and β_C that gives bi-stability. The color coding represents the ratio between the dilution rate at low and high T steady state $[1 + \beta_c T_f(\text{high})]/[1 + \beta_c T_f(\text{low})]$. The system exhibits bi-stability for a wide range of β_M and β_C values, but the increase in the generation time, parametrized by β_C , plays a more fundamental role in bi-stability. For too large values of β_M the positive effect of the β_C term on accumulation of T is counteracted by the strong inhibition of T production. For similar values of β_M and β_C the system is always bi-stable, provided that $\beta_M = \beta_C > 1$

3.2.3 Robustness to parameter change

The dependence of the system behavior on β_M and β_C has been discussed in the previous section. We also study the effect of the ratio between the translation rate of the antitoxin and the toxin $\frac{\sigma_A}{\sigma_T}$ on bistability, as it determines the relative steady state concentration of the two proteins, and expect a pretty significant effect. Figure 3.7 shows the area, in the $\beta_M - \beta_C$ plane where the system exhibits

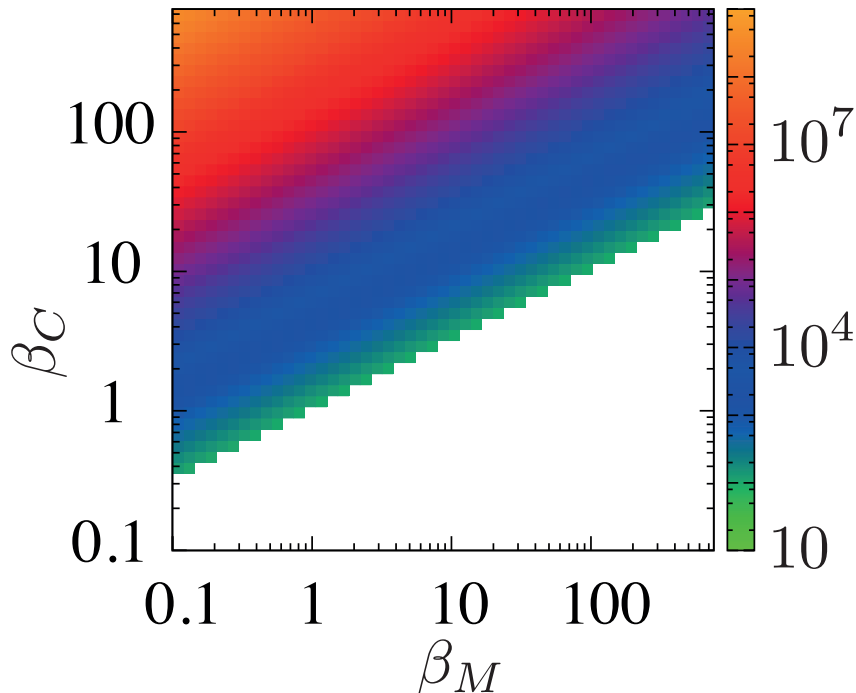


Figure 3.6: The state diagram of the bistability. Every point in the plot represents a combination of (β_M, β_C) that makes the system bistable. The color code represents ratio between T dilution rate calculated upon the low- T steady state and the high- T steady state, $[1 + \beta_C T_f(\text{high})]/[1 + \beta_C T_f(\text{low})]$.

bi-stability for four different values of the $\frac{\sigma_A}{\sigma_T}$ ratio. The ratio is varied by keeping σ_T fixed to 100 and changing σ_A . Only ratios $\frac{\sigma_A}{\sigma_T} > 10$ are considered, since lower ratios would represent non-biological circumstances, as an antitoxin-dominated state would not be possible because of the fast antitoxin degradation. As expected, when the value of the ratio is large, a stronger growth-rate mediated feedback is needed to stabilize the toxin-dominated steady state, and this is reflected by the *shift* of the bistable region towards higher values of β_M and β_C . On the contrary, for relatively small value of the ratio, $\frac{\sigma_A}{\sigma_T} = 20$, for high values of β_C , the stability of the antitoxin-dominated steady state is lost, as a very small amount of free toxin is enough to activate the positive feedback via growth rate.

To underline the generality of the presented results we performed scanning of the rest of the parameters. We fixed one parameter at the time, while the remaining were scanned randomly, over a sample of 1000 parameters sets, with the change in each parameter spanning between $\frac{1}{8}$ and 8 fold from the reference value in Table 3.2, on a logarithmic scale. The results of the scanning are summarized in figures 3.8. Bistability is a robust feature of the discussed feedback loop motif.

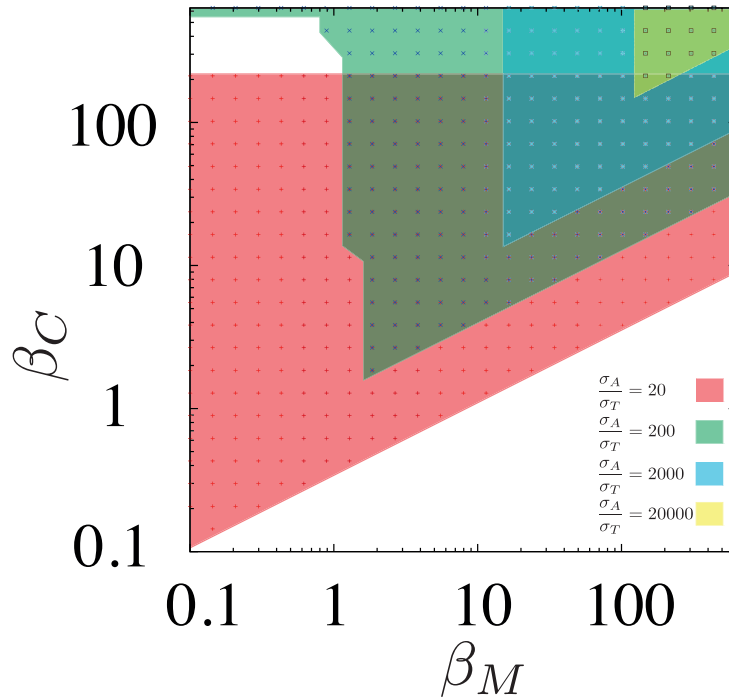


Figure 3.7: Bistable region for various values of $\frac{\sigma_A}{\sigma_T}$, with $\sigma_T = 100$. The remaining 6 parameters are fixed to the reference values. The shaded regions represents the area in the 2D parameters space β_M, β_C that shows bistable behavior.

The fraction of the samples that show bistability spans from a minimum of 20% to a maximum of 80%.

Finally, we investigated the effect of the change in the values of the dissociation constant for the AT and ATT toxin-antitoxin complex formation more extensively. The value of $K_T = K_{TT}$ was changed up to 64-fold higher than the reference value. The role of these parameters is particularly relevant, as the value of K_T and K_{TT} quantifies the sharpness of the transition to de-repressed promoter occurring at $[T]=2[A]$, or in other words, they determine the ultra-sensitivity of the conditional regulation. As it can be seen in Fig 3.9, the fraction of parameter sets that allow bi-stability decrease gradually with increasing value of K_T and K_{TT} . But even with a rather extreme 64-fold increase up to 20% of the sample shows bistability.

	X [60]	\rightarrow	\rightarrow	\tilde{X}
σ_A	$16628nMmin^{-1}$	$\frac{\sigma_A \cdot \tau_u}{C_u}$	$\frac{16628nMmin^{-1} \cdot 43min}{71.5nM}$	10000
σ_T	$166.28nMmin^{-1}$	$\frac{\sigma_T \cdot \tau_u}{C_u}$	$\frac{166.28nMmin^{-1} \cdot 43min}{71.5nM}$	100
K_O	1 nM	$\frac{K_O}{C_u}$	$\frac{1nM}{71.5nM}$	0.015
K_T	0.3 nM	$\frac{K_T}{C_u}$	$\frac{0.3nM}{71.5nM}$	0.004
K_{TT}	0.3 nM	$\frac{K_{TT}}{C_u}$	$\frac{0.3nM}{71.5nM}$	0.004
Γ_A	$0.2min^{-1}$	$\Gamma_A \cdot \tau_u$	$0.2min^{-1} \cdot 43min$	10
Γ_T	$0.02min^{-1}$	$\Gamma_T \cdot \tau_u$	$0.02min^{-1} \cdot 43min$	1
β_C	$0.16nM^{-1}$	$\beta_C \cdot C_u$	$0.16nM^{-1} \cdot 71.5nM$	11
β_M	$0.16nM^{-1}$	$\beta_C \cdot C_u$	$0.16nM^{-1} \cdot 71.5nM$	11

Table 3.2: Reference parameter values used in used in Fig 3.5. The cell generation constitutes the unit time $\tau_u = 43 min$, while the concentration unit is 1/10000 of the maximal production of antitoxin per cell generation. $C_u \simeq 70$ to keep the reference to the *relBE* system.

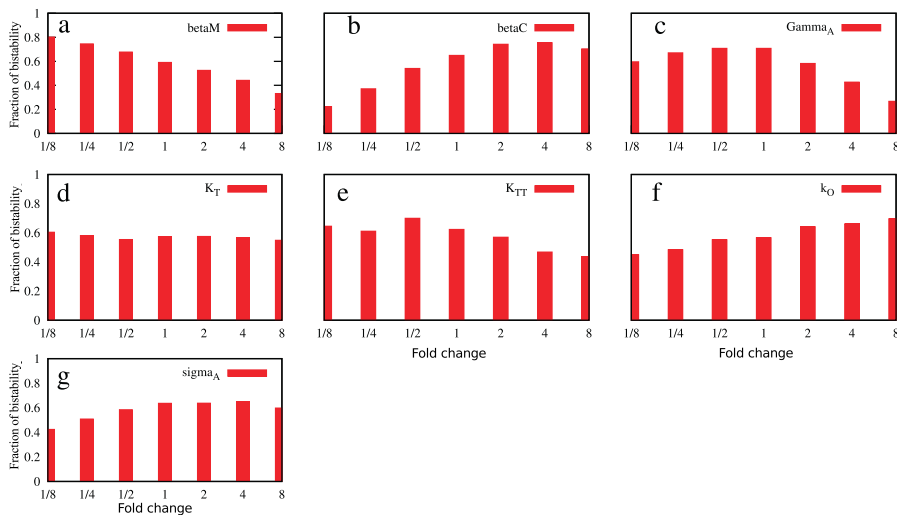


Figure 3.8: Robustness of bistability against parameters change. We fix $\sigma_T = 100$ and $\Gamma_0 = 1$, and vary rest of the parameters. In (a) β_M is changed systematically between $\frac{1}{8}$ and 8 fold of the value used in the main text $\beta_M^0 = 11.4475$; we change it between $\frac{1}{8} \cdot \beta_M^0 = 1.4309$ and $8 \cdot \beta_M^0 = 91.58$ with a pace given by $2^n \cdot \beta_M^0$ with an integer $n \in [-3, 3]$. For each value of β_M , we sample the rest of the parameters randomly and independently of each other, and they can take any values from the set $2^n \cdot (\text{the reference value})$ with $n \in [-3, 3]$. The reference values are given in Table 3.2. We collect a sample of 1000 points in the parameter space. The bars in the histogram represent the fraction of this sample of points in the parameter space that still shows bistable behavior. The same procedure is then carried out for β_C (b), Γ_B (c), K_T (d), K_{TT} (e), K_O (f) and σ_A (g)

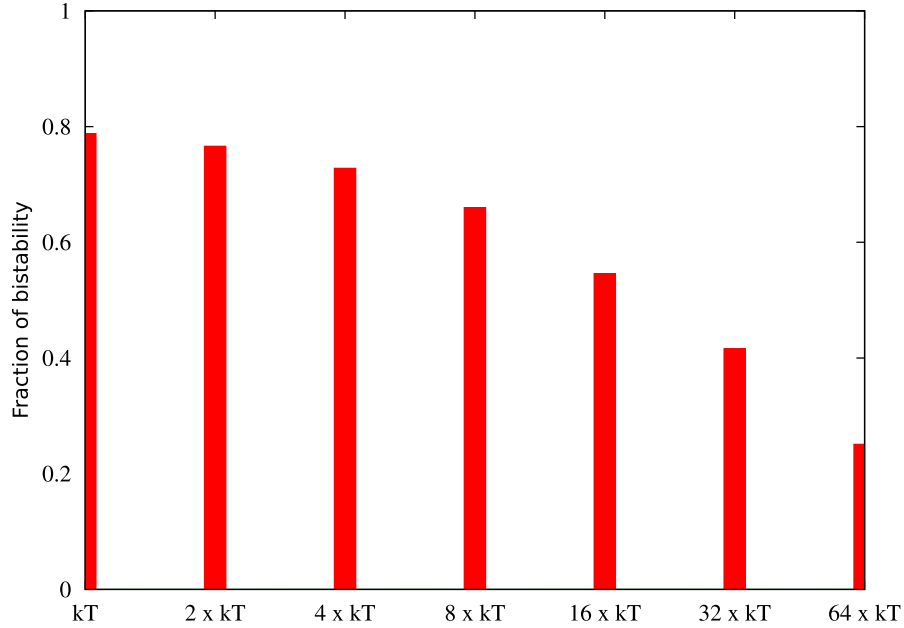


Figure 3.9: Robustness of bistability against the change of the dissociation constants K_T and K_{TT} . We set $K_T = K_{TT}$, and increase them systematically from the reference value (0.004) to 64 fold of the reference value. Since the dissociation constants set the concentration of A and T at which AT and ATT formation is significant, we fix $\sigma_A = 10000$ and $\Gamma_A = 10$ in addition to fixing $\sigma_T = 100$ and $\Gamma_0 = 1$. We then sample the rest of the parameters randomly in the base 2 logarithmic scale, within 1/8 to 8 fold of the reference value. We tried 1000 parameter sets for each values of $K_T = K_{TT}$. The plot shows the fraction of the parameter set that shows the bistability. We see that the number of bistability parameter sets decrease gradually with fold increase of the dissociation constants.

3.3 Conclusion

Equations 3.11 constitute a minimal model of the activity of a Toxin-Antitoxin module, that includes the two key ingredient of *conditional regulation* and growth-rate mediated positive feedback on toxin accumulation. It was shown that the described system exhibits robust bi-stability in a wide range of parameters, between a growing, antitoxin-dominated state, and a toxin-dominated state, characterized by a significant slow down in growth-rate.

The robustness against parameter change, combined with the fact that the model does not include details of the molecular mechanism on how the toxin functions, ensures that the results presented do not refer uniquely to the *relBE* system. The validity of the presented results can be extended to describe the behavior of all the type II TA loci in *E.coli* that are confirmed to be regulated via conditional cooperativity, provided that the following common characteristics are

included [20, 21, 24, 45, 51]

- conditional-cooperativity mediated auto-regulation
- stable toxin mainly diluted because of cell division and unstable antitoxin
- toxin-mediated inhibition of protein synthesis and thus cell growth

. The simple model presented only provides the minimal ingredients to obtain a persister state, namely bistability between a toxin-dominated and an anti-toxin dominated steady state. However, to capture the stochastic nature of the phenomenon of bacterial persistence, it is necessary to include in the model the intrinsic stochasticity of the dynamics, as it will be discussed in further detail in the next chapter.

Nevertheless, the results obtained with the present model, contain interesting insights on the connection between conditional regulation and persisters formation.

Persister cells can be classified in two fundamental categories, known as Type I and Type II persisters. [32, 38]. Switch to persisters state caused by external stress generates Type I persisters, while formation of Type II persisters relies on a spontaneous occurrence.

Conditional regulation mediated bi-stability offers the basis for the existence of a persister state for the TA system described by equations 3.11, thus can be related to type II persisters formation. On the other hand, as briefly mentioned before, the non-monotonic behavior of the promoter activity in a TA system with conditional regulation ensures that the low-toxin steady state occurs at finite [T]. The latter circumstance means, that there is always a finite amount of toxin stored in the cell in the form of AT complex. When the concentration of the anti-toxin is sufficiently high, the toxin is sequestered in complexes and no toxic activity detected. However, when the overall protein production is impaired by external factors, like nutritional stress, the stored toxin can be used for fast switching to a dormant state. Therefore, the non-monotonicity can be responsible for facilitating the switch to type I persister state.

The role of conditional regulation with respect to type I and II persisters formation is schematically summarized in Figure 3.10. The plot in the upper panel shows conditional-regulation mediated bi-stability, suggesting that a spontaneous switching between the two stable fixed point might be the key mechanism of type II persisters formation. The plot in the grey area in the lower panel shows, how

a drop in the overall translation rate can *push* the system towards a stable state, characterized by a higher toxin concentration, potentially a type I persister state.

Conditional regulation is a mixed feedback motif, where protein-protein interaction is combined with transcriptional regulation. In literature there exist several examples of system showing bistable behavior thanks to ultra-sensitivity mediated by protein-protein interaction [58,61,62]. Furthermore, the effect of growth rate-mediated feedbacks on bistable systems has been discussed in recent literature [48,59]. The uniqueness of the regulatory feedback investigated in this study is that it includes combination of both effects. The need for taking into account both these mechanisms stems from the fact that T and A are produced from the same operon, and hence identically regulated at the transcriptional level. When only one of the mechanisms mentioned is present it is then difficult to obtain bistability [54], which is instead achieved by regulating the level of products of the operon through a combination of growth modulation and hetero-complex formation.

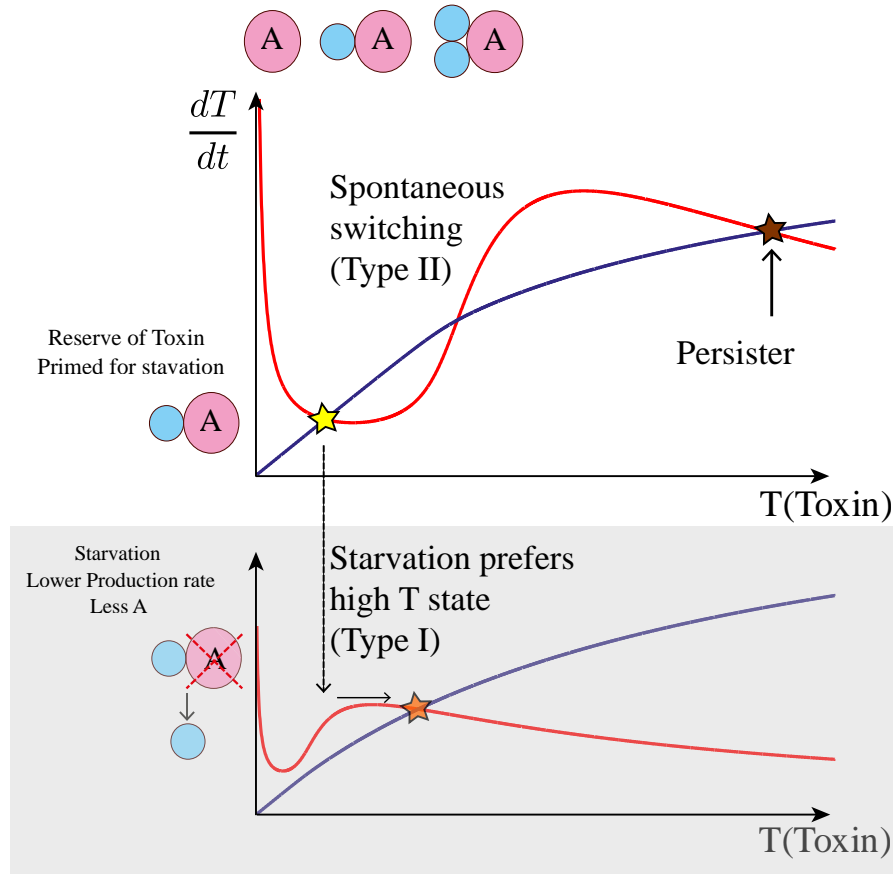


Figure 3.10: Schematic role of conditional regulation in persisters formation: The red curves show the toxin production rate and the blue lines give the degradation rate, both from eq. (3.11). Both terms depend on A , and here we make approximation that A is always in steady state (eq.3.11 with $dA/dt = 0$) for given T , because dynamics of A is much faster than T due to high production and degradation rate. Since production term of A and T are proportional to each other and A is degraded at a constant rate, resulting A concentration is proportional to the production term of T (red curves). The scales of curves are modified from actual functional forms so that the characteristic behaviours can be grasped easily. The ultra-sensitivity mediated by protein-protein binding combined with feedback from free toxin activity is reflected in the peak of the production rate and drop of the degradation rate, resulting in bistability of the system. This accounts for the type II persister where a cell can spontaneously switch to and out of the persister state. The non-monotonicity of the conditional regulation secures that some toxins are stored in antitoxin dominated state, helping the transition to the stress-induced activation of toxin [60], which becomes the base for type I persister formation.

Chapter 4

Stochasticity in the activity of TA systems and Persisters

So far we have shown that the presence of TA a locus regulated by conditional cooperativity provides the basis for robust bi-stability between a fast growing A-dominated state and a T-dominated, perister state [63]. Identifying the key ingredients for the bi-stable behavior is, though, not enough for capturing the essence of bacterial persistence, that is an intrinsically *stochastic* phenomenon. It is necessary to address the problem of cells *switching* between the two steady states.

In this chapter I provide a *stochastic description* of the TA module activity. In order to do so, the chemical reactions that constitute the regulatory network of the TA system, must be described through a master equation [64, 65]. The latter follows the evolution of the probability of the system to be in a state characterized by certain concentrations values, rather than the time evolution of *average* concentrations. We then derive the potential landscape function for the network [66] and through an implementation of the Kramers escape rate calculation [67] we address the problem of the switch between the two steady states. Furthermore, to address the details of the dynamics of the stochastic process I perform simulations of a stochastic version of model of the TA activity proposed in the previous chapter, and extend it to be able to simulate the behavior of a system constituted by multiple cross-interacting TA systems.

The results shown in this chapter are not yet conclusive. Further investigation has to be carried on to fully understand the connection between the stochasticity in the dynamics of the TA activity and persisters formation, as it will de discussed

in detail in the conclusion.

4.1 The switching rate

4.1.1 Master Equation

In the ODE model defined in eq. 3.11, the state of the TA activity at time t , is fully characterized by the concentration the toxin T and the antitoxin A . The level of the two stoichiometric forms of the toxin-antitoxin complexes AT and ATT was calculated, for a given A and T , through the laws of mass action, considering the conservation of mass (see equations 3.3 and 3.5 in chapter 3).

This model can be formulated in terms of master equations. However, in the attempt to attain the simplest level of description possible, we assume A to be always in the steady state for a given level of toxin, because of its fast turnover dynamics. This approximation results in no loss of generality, as all Type II TA loci are characterized by a stable toxin, while the antitoxin is degraded by cellular protease [20]. The steady state value of A , for a given value of T , is obtained, from equations 3.11, with $\frac{dA}{dt} = 0$, as follows:

$$A(T, t) = \frac{\frac{\sigma_A}{\Gamma_A}}{(1 + \beta_M T_f(A, T))(1 + \frac{AT(A, T)}{K_O})}. \quad (4.1)$$

Equation 4.1, solved taking into account the conservation law and law of mass action 3.3 and 3.5, yields the A level for a given T , which in turn allows to determine $AT(T)$ and $ATT(T)$ as functions of the sole T . The state of the system can then be described by the discrete stochastic variable T , total number of toxin molecules, and the activity of the TA system is modeled through the following Master Equation:

$$\begin{aligned} \frac{\partial P(T, t)}{\partial t} = & \frac{\sigma_T}{(1 + \frac{AT(T-1)}{K_O})(1 + \beta_M T_f(T-1))} \cdot P(T-1, t) \\ & - \frac{\sigma_T}{(1 + \frac{AT(T)}{K_O})(1 + \beta_M T_f(T))} \cdot P(T, t) \\ & + \frac{\Gamma_0 \cdot (T+1)}{(1 + \beta_C T_f(T+1))} \cdot P(T+1, t) \\ & - \frac{\Gamma_0 \cdot T}{(1 + \beta_C T_f(T))} \cdot P(T, t). \end{aligned} \quad (4.2)$$

Equation 4.2 describes the time evolution of the probability $P(T, t)$ of the system

to be in a state characterized by a given value of T at time t . As in the deterministic model 3.11, σ_T is the maximal production rate for the toxin, K_O is the dissociation constants for the binding of the AT complex to the operator, β_M and β_C quantify the negative feedback on the growth rate due to accumulation of toxin and Γ_0 is the rate of toxin dilution due to cell division.

The notation in equation 4.2 can be simplified by defining :

$$r(T, t) = \frac{\sigma_T}{\left(1 + \frac{AT(T, t)}{K_O}\right)(1 + \beta_M T_f(T, t))} \quad (4.3)$$

$$s(T, t) = \frac{\Gamma_0 \cdot T}{(1 + \beta_C T_f(T, t))} \quad (4.4)$$

where $r(T, t)$ expresses the rate of production of one molecule of toxin, while $s(T, t)$ is the rate of degradation of one molecule of toxin. With this simplification Eq. 4.2 becomes

$$\begin{aligned} \frac{\partial P(T, t)}{\partial t} = & r(T - 1) \cdot P(T - 1, t) \\ & - r(T) \cdot P(T, t) \\ & + s(T + 1)P(T + 1, t) \\ & - s(T) \cdot P(T, t). \end{aligned} \quad (4.5)$$

4.1.2 Potential Landscape

For a one-dimensional master equation as in eq. 4.2, one can define the potential landscape that characterize the steady state distribution, which in turn can be used to evaluate the switching rate as a Kramers escape problem.

In order to derive it, I perform the Kramer-Moyal expansion of the master equation 4.5, truncate it at the second order and obtain a second-order Fokker-Planck equation. By comparison with the standard form of the Fokker-Planck equation for a particle in a potential, I obtain the desired potential landscape for the bi-stable dynamics of the TA system.

From Master Equation to Fokker-Planck Equation

In the formalism of the step operators E^S defined as $E^S f(x) = f(x + S)$ Equation 4.5 can be re-written as:

$$\frac{\partial P(T, t)}{\partial t} = (E^{-1} - 1)r(T)P(T, t) + (E^1 - 1)s(T)P(T, t). \quad (4.6)$$

By treating T as a continuous variable, x , and assuming $P(x, t)$ is a smooth function of x , the step operator can be expanded as $E^S = 1 + \sum_{k=1}^{\infty} \frac{(S\Delta x)^k}{k!} \frac{\partial^k}{\partial x^k}$. If the expansion is truncated at the second order one obtains

$$\begin{aligned} \frac{\partial P(x, t)}{\partial t} &= -\frac{\partial}{\partial x} \left\{ \left[\left(r(x) - s(x) \right) \cdot P(x, t) \right] - \frac{\partial}{\partial x} \left[\frac{1}{2} \left(s(x) + r(x) \right) \cdot P(x, t) \right] \right\} \\ &= -\frac{\partial}{\partial x} \left\{ \left[\left(\frac{\sigma_T}{\left(1 + \frac{AT(x)}{K_O}\right)(1 + \beta_M T_f(x))} - \left(\frac{\Gamma_0 \cdot x}{(1 + \beta_C T_f(x))} \right) \right) P(x, t) \right] \right. \\ &\quad \left. - \frac{\partial}{\partial x} \left[\frac{1}{2} \left(\left(\frac{\Gamma_0 \cdot x}{(1 + \beta_C T_f(x))} \right) + \frac{\sigma_T}{\left(1 + \frac{AT(x)}{K_O}\right)(1 + \beta_M T_f(x))} \right) P(x, t) \right] \right\} \end{aligned} \quad (4.7)$$

where obviously,

$$r(x) = \frac{\sigma_T}{\left(1 + \frac{AT(x)}{K_O}\right)(1 + \beta_M T_f(x))} \quad (4.8)$$

$$s(x) = \frac{\Gamma_0 \cdot x}{(1 + \beta_C T_f(x))}. \quad (4.9)$$

Derivation of the potential energy landscape

Now we consider the standard form of the Fokker-Plank Equation in a potential $U(x)$:

$$\frac{\partial P}{\partial t} = -\frac{\partial}{\partial x} \left[-\mu(x) \frac{dU}{dx} \cdot P(x, t) - \frac{\partial}{\partial x} \left(D(x) P(x, t) \right) \right] \quad (4.10)$$

This can be re-written in term of the effective potential defined by $\frac{dV(x,t)}{dx} = \left(\frac{dU}{dx} + \frac{1}{\mu(x)} \frac{dD}{dx} \right)$ as

$$\frac{\partial P}{\partial t} = -\frac{\partial}{\partial x} \left\{ - \left(\mu(x) \frac{dV}{dx} \right) \cdot P(x, t) - D(x) \cdot \frac{\partial P(x, t)}{\partial x} \right\} \quad (4.11)$$

$V(x, t)$ is the effective potential that includes both the 'drift' term and the contribution given by noise. We are interested in finding its functional form. It is worth noticing that, by comparison of Equation 4.11 with the *continuity equation* 4.12 we obtain the flux $J(x, t)$ as

$$\frac{\partial P}{\partial t} = -\frac{\partial J}{\partial x}, \quad (4.12)$$

$$J = - \left[\left(\mu(x) \frac{dV}{dx} \right) \cdot P(x, t) + D(x) \cdot \frac{\partial P(x, t)}{\partial x} \right] \quad (4.13)$$

If we now compare equations 4.7 and 4.10 we can identify

$$D(x) = \frac{1}{2} \left(s(x) + r(x) \right) \quad (4.14)$$

$$\frac{dU}{dx} = \frac{s(x) - r(x)}{\mu(x)}. \quad (4.15)$$

If we further identify $D(x) = \mu(x)$, $P_0(x) \sim e^{-V(x)}$ is the steady-state distribution satisfying $J(x, t) = 0$ and

$$\frac{dU}{dx} = \frac{s(x) - r(x)}{\frac{1}{2} \left(s(x) + r(x) \right)},$$

that implies

$$\begin{aligned} \frac{dV(x)}{dx} &= \frac{dU}{dx} + \frac{1}{\mu(x)} \frac{dD}{dx} \\ &= \frac{2\left(s(x) - r(x)\right) + \frac{ds}{dx} + \frac{dr}{dx}}{s(x) + r(x)} \end{aligned} \quad (4.16)$$

Integration of 4.16 yields the functional form of the effective potential landscape for the system described by Equation 4.2.

An example of the potential $V(x)$, obtained through numerical integration, is given in Fig 4.1. The parameters used to numerically evaluate $V(x)$ are indicated in Table B.1 $V(x)$ has the form of a bistable potential, with two well-separated minima. One occurs at low values of x , and the other at high values of x .

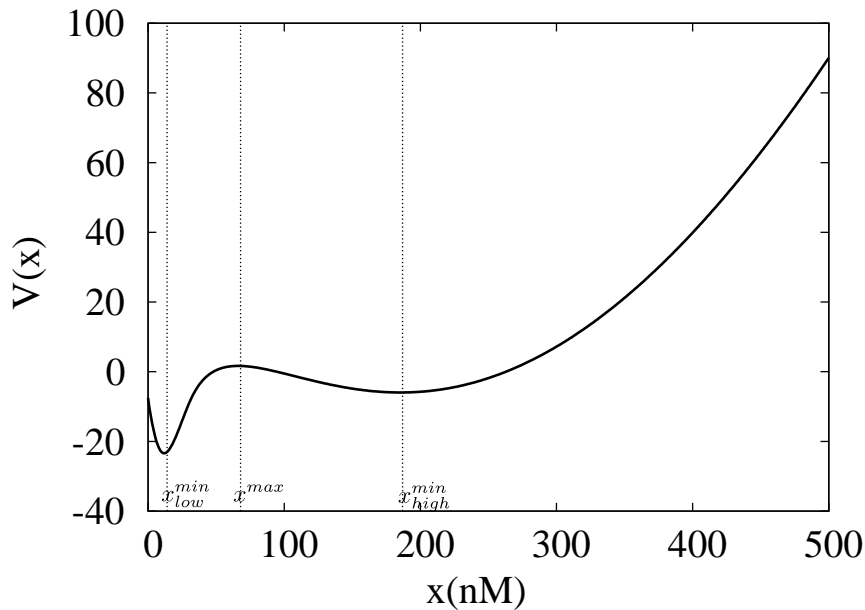


Figure 4.1: Result of the numerical integration of equation 4.16. The potential $V(x, t)$ exhibits two well-separated minima, x_{low}^{min} and x_{high}^{min} and a maximum x^{max} . The minima are labelled *low* and *high* since they correspond to states of the system described in 4.7 characterized by, respectively, low and high amount of toxin. The parameter set used is listed in appendix

4.1.3 Kramer's escape rate

The Kramers escape technique [67] allows to calculate the rate at which a Brownian particle trapped in a potential well escapes over a potential barrier.

In the previous section it has been shown how the present problem of the dynamics of the activity of a TA system can be mapped onto the description, through Fokker-Plank equation, of the motion of a Brownian particle subject to a bi-stable potential. The analogy holds as long as we consider that in the case of the TA system, the stochastic variable $X(t)$ represents, instead of the position of the particle, a given concentration of the toxin. Furthermore, the source of noise in the case of Brownian motion is thermal fluctuation, while in the present case is the fluctuation in the number of particles given by intrinsic noise [68].

In figure 4.1 we have shown a typical potential landscape $V(x)$. The two minima are labelled as x_{low}^{min} and x_{low}^{max} . In the present section we calculate the escape rate from x_{low}^{min} to x_{low}^{max} (and vice-versa), describing the A-dominated and T-dominated states respectively. One necessary assumption for the Kramers escape calculation to be used, is the quasi-stationary assumption, namely $\frac{\partial P(x,t)}{\partial t} \approx 0$. The latter assumption holds, if the flux from x_{low}^{min} to x_{low}^{max} and vice-versa is low¹.

Taking into account $\mu(x) = D(x)$ equation 4.13 for the flux J becomes:

$$J = -D(x) \left[\frac{dV}{dx} P(x,t) + \frac{\partial P(x,t)}{\partial t} \right] \quad (4.17)$$

Because of the quasi-stationary approximation, the flux J , from x_{low}^{min} to x_{low}^{max} (and vice-versa), has to be independent of both x and t . In particular, for each direction we assume

$$J = p \cdot r, \quad (4.18)$$

where p is the probability to initially be in the potential well, and r is the rate of escape from the well.

Using the quasi-stationary approximation and assuming that the probability distribution around each minima can be approximated with the *equilibrium* probability distribution that would be obtained if the potential barrier located at x^{max} were infinite, it is possible to calculate p . Once p is known, the rate r can be cal-

¹Within the current framework, the quasi-stationary approximation should be a safe assumption for biologically relevant cases

culated from eq. 4.17. Following the derivation shown in appendix F, one obtains:

$$r_{A \rightarrow T} = \frac{D(x^{max})}{2\pi} e^{-(V(x^{max}) - V(x_{low}^{min}))} \sqrt{|V''(x^{max})|} \sqrt{V''(x_{low}^{min})}, \quad (4.19)$$

$$r_{T \rightarrow A} = \frac{D(x^{max})}{2\pi} e^{-(V(x^{max}) - V(x_{high}^{min}))} \sqrt{|V''(x^{max})|} \sqrt{V''(x_{high}^{min})}, \quad (4.20)$$

where $D(x)$ is given in eq. 4.14 and x^{max} , x_{low}^{min} , x_{high}^{min} are the stationary points of the bi-stable potential, as noted in Fig. 4.1. $r_{A \rightarrow T}$ is the escape rate from the minimum of $V(x, t)$ located at x_{low}^{min} and can be identified with the rate of persisters formation. $r_{T \rightarrow A}$ is the rate at which a persisters cell switches back to fast growth rate, or the escape rate from x_{high}^{min} .

4.1.4 The switching rate strongly depends on the parameters choice

The reference parameters used to evaluate the potential $V(x, t)$ in Fig. 4.1 are listed in Table B.1 in Appendix B. The reason behind the choice of parameters was to keep within the same order of magnitude of the measures relative to the *relBE* system, to avoid parameter range that are not biologically plausible. In the described parameters set, calculation of the escape rates yields the following results:

$$r_{A \rightarrow T} \simeq 10^{-13} (\text{generation time})^{-1} \quad (4.21)$$

$$r_{T \rightarrow A} \simeq 3 \times 10^{-07} (\text{generation time})^{-1} \quad (4.22)$$

Notice that these rates describe the probability of a cell to switch to persistence *per* cell generation, in the growing state. The rates can be then mapped onto the probability of one switch to happen within a cell population that is constituted by r^{-1} cells, and this way one can relate the rate $r_{A \rightarrow T}$ to persistence frequency, provided that one assumes that the growth rate in the T-dominated state is negligible and both the switching rates are *low*. Measured values for the frequency of persisters are $\sim 10^{-4}$, for type II persisters [43]. Direct measures of the resuscitation rate $r_{T \rightarrow A}$ are hard to perform, given the low frequency of persisters cell, so the only reference point is the value estimated in the model of persistence as a switch in a two-state model by Balaban *et. al.*, where the presented value is $\sim 0.07 (\text{generation time})^{-1}$ [32].

Obviously the results obtained using the reference parameters set are not suited to reproduce the observed rates. We performed parameters scanning, in order to search for calculated rates closer to the experimental observation, and investigate the sensibility of the model with respect to the key-parameters in the model.

Dependence on $\frac{\sigma_T}{\sigma_A}$

The ratio in the translation rate of the toxin and the antitoxin $\frac{\sigma_T}{\sigma_A}$, is obviously a critical parameter in determining the value of the switching rate. Figure 4.2 illustrates how a higher $\frac{\sigma_T}{\sigma_A}$ ratio results in a lower potential barrier to overcome to switch from the low toxin to the high toxin steady state, facilitating the switch

to persister state. On the other hand, though, higher $\frac{\sigma_T}{\sigma_A}$ stabilizes the high toxin steady state, inhibiting resuscitation.

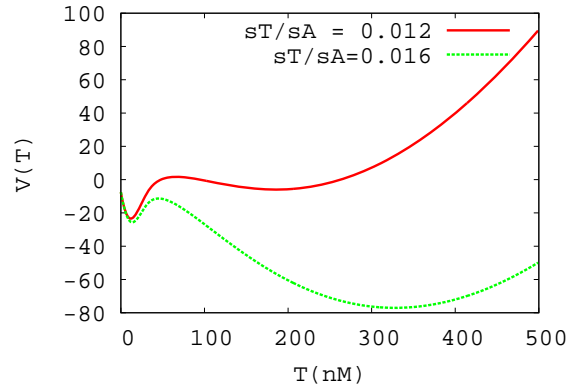


Figure 4.2: Potential landscape $V(x, t)$ as a result of the numerical integration of equation 4.16. Green line $\frac{\sigma_T}{\sigma_A} = 0.016$, Red line $\frac{\sigma_T}{\sigma_A} = 0.012$. The remaining parameters are fixed to the values indicated in Table B.1

In figure 4.3 and figure 4.4 the dependence of the switching to persister and resuscitation rates on the $\frac{\sigma_T}{\sigma_A}$ is explored in a more systematic way. From the above consideration follows that the rate of persisters formation increases with increasing $\frac{\sigma_T}{\sigma_A}$, while on the contrary the resuscitation rate decreases. In both cases the dependence of the rate on the ratio is quite dramatic, a change in the ratio around 20% can result, for example, in 4 order of magnitude difference in the rate of switch to persistence (cf. $\frac{\sigma_T}{\sigma_A} = 0.016$ and $\frac{\sigma_T}{\sigma_A} = 0.02$).

Dependence on β_M and β_C

As explained in detail in Section 3.2.2, the presence of a positive feedback on toxin accumulation, mediated by growth inhibition, is a necessary ingredient in obtaining bi-stability. For this reason we investigate how the form of the potential landscape and consequently the rate to and from the persister state depends on the strength of the feedback. For simplicity we assume $\beta_M = \beta_C = \beta$. As Figure 4.5 shows, increasing the strength of the positive feedback on the toxin, lowers the height of the potential barrier to overcome to switch to persistence but it stabilizes the high toxin steady state, inhibiting this way, resuscitation. As a consequence, as it can be inferred from Figures 4.6 and 4.7 $r_{A \rightarrow T}$ increases with increasing β , while $r_{T \rightarrow A}$ decreases. It is worth noticing, though, that within the constraint of $\beta_M = \beta_C = \beta$ the absolute value of the resuscitation rate is so low that the dependence on the

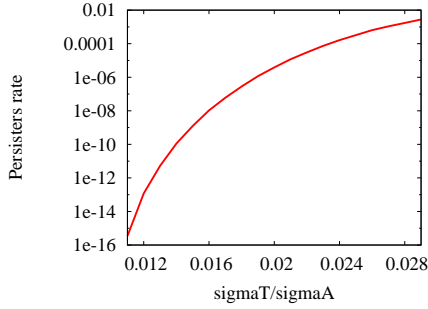


Figure 4.3: Dependence of the rate of switching to persistence $r_{A \rightarrow T}$ on the ratio $\frac{\sigma_T}{\sigma_A}$ between translation rate of the antitoxin and the toxin. $\frac{\sigma_T}{\sigma_A}$ is varied between 0.011 (compatible with the observation of the steady state values of the toxin-antitoxin pair RelE-RelB) to 0.029

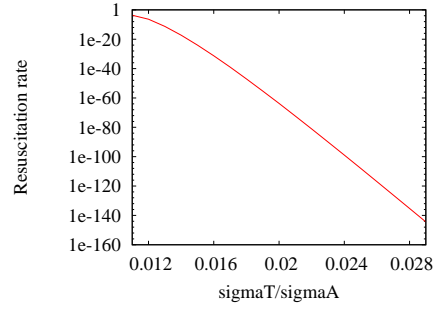


Figure 4.4: Dependence of the resuscitation rate $r_{T \rightarrow A}$ on the ratio $\frac{\sigma_T}{\sigma_A}$ between translation rate of the antitoxin and the toxin. $\frac{\sigma_T}{\sigma_A}$ is varied over the same range mentioned in the caption of Fig 4.3

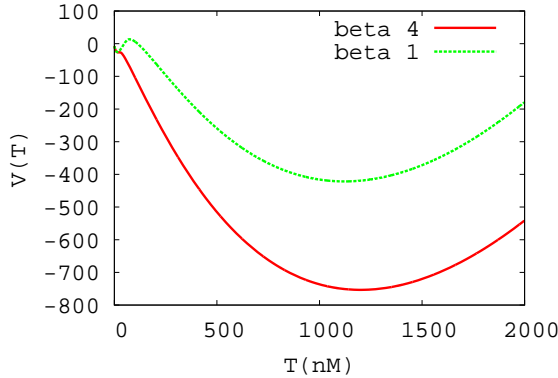


Figure 4.5: Potential landscape $V(x, t)$ as a result of the numerical integration of equation 4.16. Green line $\beta_M = \beta_C = 1 \text{ nM}^{-1}$, Red line $\beta_M = \beta_C = 4 \text{ nM}^{-1}$ The remaining parameters are fixed to the values indicated in Table B.1

exact value of β within the investigated range is practically irrelevant. As in previous case, both rates are very sensitive to change in β .

Dependence on Γ_A

The importance of exploring the dependence on the degradation rate of the antitoxin Γ_A lies in the fact that all investigated antitoxin belonging to *E. coli* K-12 TA loci are substrate of the protease Lon [14, 25, 27], that is known to be activated during nutritional stress [30]. A connection between persistence and growth-arrest

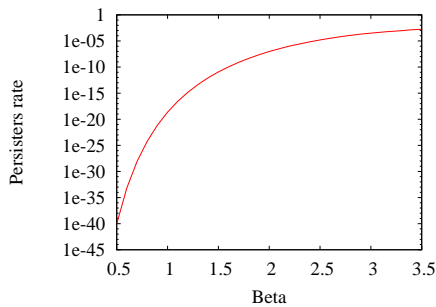


Figure 4.6: Dependence of the rate of switching to persister rate $r_{A \rightarrow T}$ on β . β is varied between 0.5 nM^{-1} and 3.5 nM^{-1}

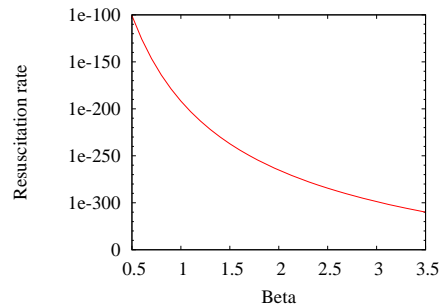


Figure 4.7: Dependence of the resuscitation rate $r_{T \rightarrow A}$ on β . β is varied over the same range mentioned in the caption of Fig 4.3

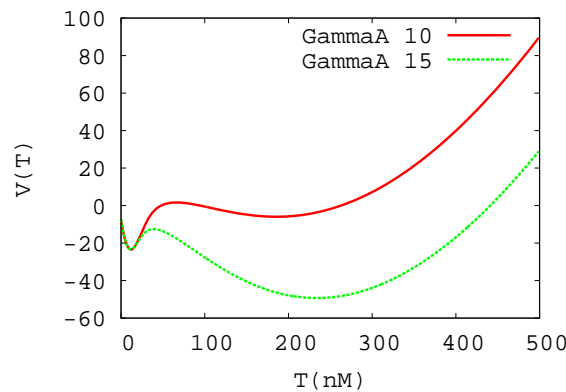


Figure 4.8: Potential landscape $V(x, t)$ as a result of the numerical integration of equation 4.16. Green line $\Gamma_A = 10$ (generation time) $^{-1}$, Red line $\Gamma_A = 15$ (generation time) $^{-1}$. The remaining parameters are fixed to the values indicated in Table B.1

induced by nutritional stress [32], as well as a correlation between persisters formation and fluctuation in the level of (p)ppGpp, the alarmone that triggers stringent response, has been shown in literature [69], as it will be discussed in the end of this chapter.

The reference value of Γ_A is ~ 10 (generation time) $^{-1}$. A higher degradation rate for the anti-toxin results in a more stable high toxin state and in a lower potential barrier for the transition to persistence, as it can be seen in Fig 4.8. Thus, as expected, it favors the persister state.

This results in $r_{A \rightarrow T}$ increasing as Γ_A is increased, while the resuscitation rate $r_{T \rightarrow A}$ decreases. Both rates are extremely sensitive to the degradation of the antitoxin. Increasing Γ_A of about 50% (cfr $\Gamma_A = 10$ (generation time) $^{-1}$ and

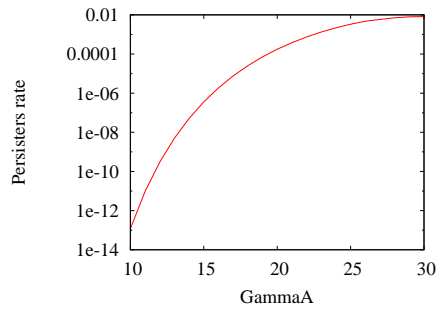


Figure 4.9: Dependence of the rate of switching to persister rate $r_{A \rightarrow T}$ on the degradation rate for A Γ_A . Γ_A is varied between 10 (generation time)⁻¹ and 30 (generation time)⁻¹

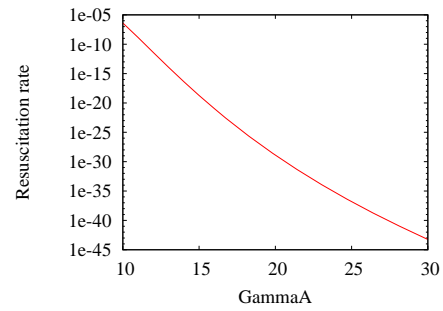


Figure 4.10: Dependence of the resuscitation rate $r_{T \rightarrow A}$ on the life-time of A Γ_A . Γ_A is varied over the same range mentioned in the caption of Fig 4.3

$\Gamma_A = 15$ (generation time)⁻¹) can determine a change in the value of $r_{A \rightarrow T}$ up to 6 orders of magnitude (cf. $\Gamma_A = 10$ and $\Gamma_A = 15$).

4.2 Stochastic Model of TA activity

So far we have been concerned with addressing the rate of switching between the steady states of the TA module regulatory network by Kramers escape approach. In order to capture the full dynamics of the system and test the prediction obtained through the Kramers escape calculations, we simulate a stochastic model of the TA activity using the Gillespie algorithm.

The state of the system at each time t is completely defined by the total amount of the antitoxin A and toxin T. The formation of toxin-antitoxin complex is not modeled explicitly. At each time-step, for a given value of A and T, the amount of AT and ATT complex is computed numerically, solving equations:

$$[AT] = \frac{[A_f] \cdot [T_f]}{K_T} \quad (4.23)$$

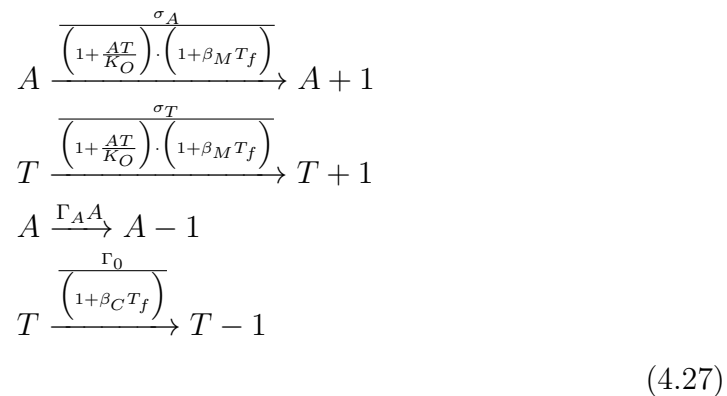
$$[ATT] = \frac{[AT] \cdot [T_f]}{K_{TT}} \quad (4.24)$$

with the constraint:

$$A = [A_f] + [AT] + [ATT] \quad (4.25)$$

$$T = [T_f] + [AT] + 2[ATT] \quad (4.26)$$

The list of reaction included in the model is:



As in the deterministic model presented in 3.11, the rate of production, of both T

and A is limited by the amount of free toxin T_f . Analogously, the rate of dilution of T through cell division, is affected by the amount of free toxin.

Figure 4.11 shows the typical outcome of a simulation. The parameters used are relatively far from the reference parameters shown in Table B and were chosen to be able to observe both the switches on a time-scale that is possible to simulate numerically. The Kramers escape rate predictions for the current set of parameters are indicated in 4.28 and show a reasonable agreement in the switching time scale.

$$r_{A \rightarrow T} \simeq 10^{-4} (\text{generation time})^{-1} \quad (4.28)$$

$$r_{T \rightarrow A} \simeq 2 \times 10^{-4} (\text{generation time})^{-1} \quad (4.29)$$

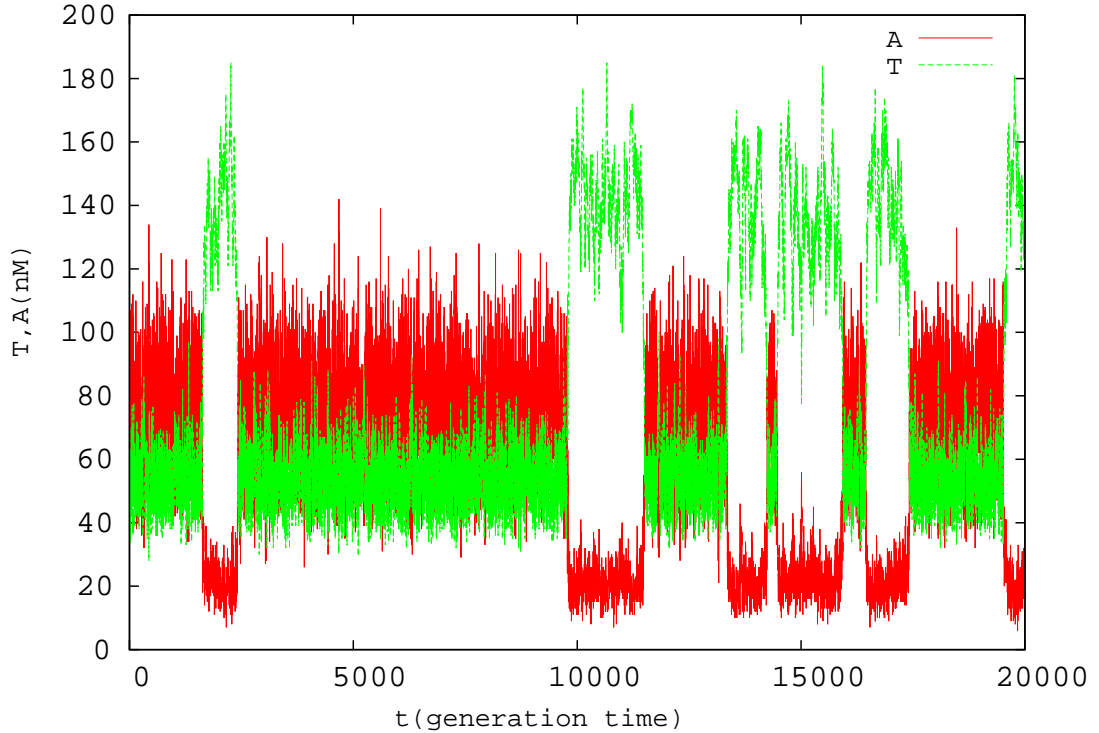


Figure 4.11: Time course of a Gillespie simulation as described in 4.31. The time evolution of the amount of Toxin (T) is indicated in green, while the red line refers to the amount of antitoxin (A). Within the chosen set of parameters, listed in C, it is possible to detect both the switch from fast growth to persist state and the resuscitation from persistence to growth.

4.3 Considering the effect of multiple TA systems

In 2011 Maissonneuve *et al.* investigated the effect on the persister frequency, of progressive deletion of the 10 TA loci of *E.coli* K-12. They demonstrated that the deletion of 10 TA loci results in a dramatic $\sim 10^2$ -fold decrease in the frequency of persister cell formation. Nevertheless, the reduction due to progressive deletion of TA loci is *gradual*, as the effect of multiple TA loci is *cumulative* and deletion of a single TA locus, independently of its identity, has a small effect on persister rate [43].

In this section I propose an extension of the model of TA activity aimed at addressing the combined effect on bi-stability and persister formation of multiple TA loci.

4.3.1 Stability consideration

The equivalent formulation of 3.11, for the i -th TA system, in the case of combined effect of n TA systems is

$$\begin{aligned} \frac{dA_i}{dt} &= \frac{\sigma_A}{\left(1 + \frac{AT_i}{K_O}\right) \cdot \left(1 + \beta_M \sum_{i=1}^n T_{fi}\right)} - \Gamma_A A_i \\ \frac{dT_i}{dt} &= \frac{\sigma_T}{\left(1 + \frac{AT_i}{K_O}\right) \cdot \left(1 + \beta_M \sum_{i=1}^n T_{fi}\right)} - \frac{\Gamma_0}{\left(1 + \beta_C \sum_{i=1}^n T_{fi}\right)}, \quad i = 1, 2, \dots, n \end{aligned} \quad (4.30)$$

where, for the sake of simplicity, the value of the parameters is assumed to be the same for each TA system. The *cross-interaction* between different TA system is mediated by T_f , and is fully contained in the terms $1 + \beta_M \sum_{i=1}^n T_{fi}$ and $1 + \beta_C \sum_{i=1}^n T_{fi}$. The underlying assumption is that the n TA modules only "feel" each other through the slow-down in protein production and growth due to the additive contribution of the n free toxins. In the present study $n = 10$ unless otherwise noted.

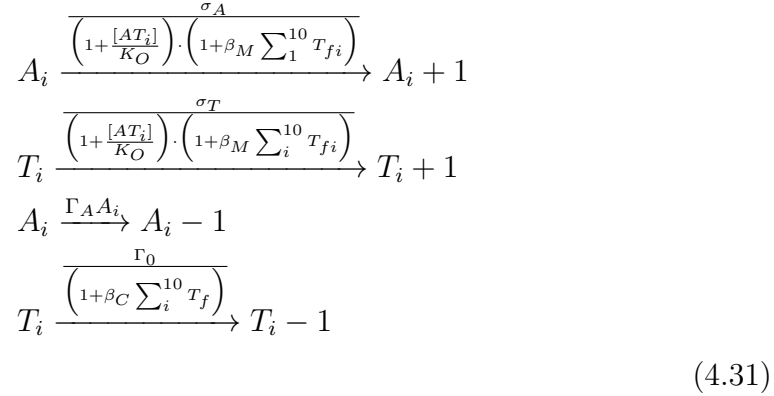
Within the strong assumption of all TA systems being identical, the steady-state with $T_1 = T_2 = \dots T_n = \tilde{T}$ and $A_1 = A_2 = \dots A_n = \tilde{A}$ should exist, which implies that, at least around this steady-state, the coupling of n TA systems *corresponds* to changing β_M and β_C simultaneously by n fold in one TA system. Hence, the strong dependence of the switching rate on $\beta_M = \beta_C = \beta$ seen in figures 4.6

and 4.7 translates into a strong dependence on the number of TA systems.

4.3.2 Stochastic model of interaction of 10 TA systems

In order to investigate the dependence of the rate of switching to persisters on the numbers of interacting TA systems, and discuss it in the light of the experiments from Maisonneuve et al. [43], I built a stochastic version of the model specified in Equations 4.30 for the dynamics of multiple interacting TA system. Stochastic simulation were performed via a Gillespie algorithm implemented as follow :

The state of each TA system (labelled by i) is specified by the discrete variables corresponding to the amount of toxin T_i and antitoxin A_i relative to that system. At each time step one of the 10 TA system is chosen randomly, and its state updated according to:



where for each system i , AT_i and T_{fi} are computed numerically according to:

$$[AT_i] = \frac{[A_{fi}] \cdot [T_{fi}]}{K_T} \tag{4.32}$$

$$[ATT_i] = \frac{[AT_i] \cdot [T_{fi}]}{K_{TT}} \tag{4.33}$$

with the constraint:

$$[A_i] = [A_{fi}] + [AT_i] + [ATT_i] \tag{4.34}$$

$$[T_i] = [T_{fi}] + [AT_i] + 2[ATT_i] \tag{4.35}$$

The interaction between the different systems is considered to be additive, as described in detail in the previous section 4.3.1.

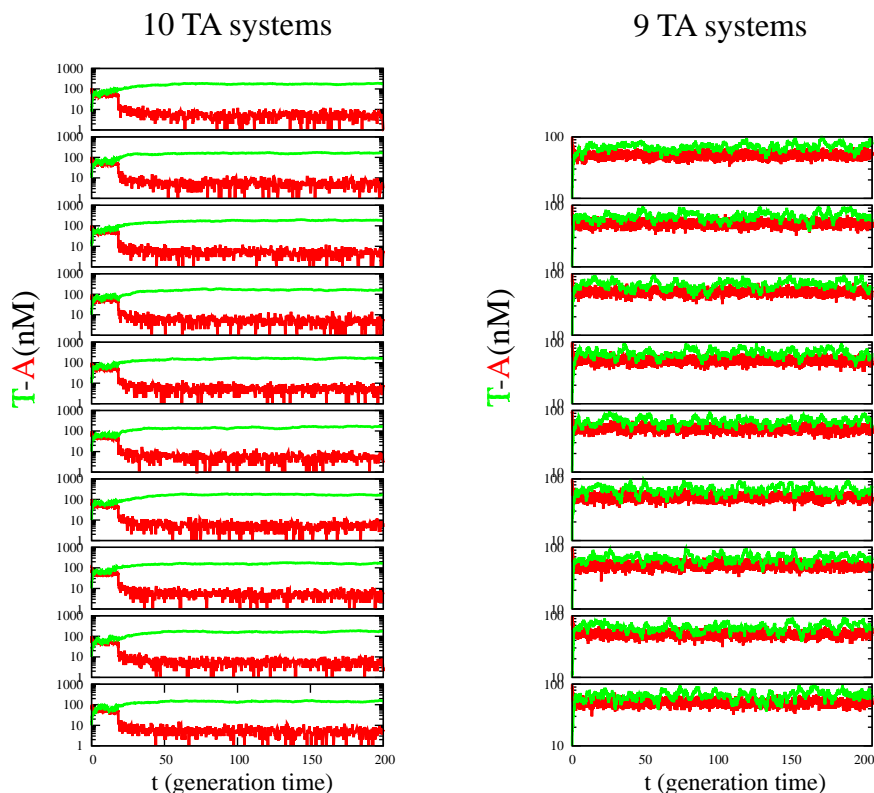


Figure 4.12: Left Panel: Stochastic time course of the activity of 10 cross-interacting TA systems. Each plot represent the time course of a single TA. The green line : Toxin (T) level, red line Antitoxin A. The switch to persisters state is detected within ~ 20 generation time. Right Panel: Stochastic time course of the activity of 9 cross-interacting TA systems. Each plot represent the time course of a single TA. The green line : Toxin (T) level, red line Antitoxin A. Within 200 generation time no switch to persister state is detected.

Figure 4.12 shows the time evolution of 10 (left panels) and 9 (right panel) interacting TA system. Each system is started from initial conditions that mimic the low-T state, and the the switch to a persister state, characterized by $T \gg A$ is monitored. In the case of 10 TA systems, the switch is detected within a very short time (~ 20 generation time). Removing only one TA system, already results in a dramatic change in the dynamics, as no switching is detected within 200 generations time.

To give any precise quantitative conclusion on the dependence of life-time of the A-dominated state on the number of TA systems, one should compare, of course, quantities averaged over a statistically significant sample of Gillespie simulations,

rather than a single trajectory. Nevertheless the observed dynamics *suggests* that the persists level is extremely sensitive to the number of interacting TA systems present. This circumstance is not in agreement with the weak dependence of the persists level on *one* further TA module deletion observed by Maisonneuve *et al* [43].

4.4 Conclusion and future work

We built a model in the attempt to explain bacterial persistence in terms of stochastic activation of the toxin in TA systems. We calculated the rate of persister formation and the resuscitation rate, using an implementation of the Kramers escape rate calculation. Furthermore, to capture the full dynamics of the TA activity and observe the switch, we performed stochastic simulation, using the Gillespie algorithm. The results of the Gillespie simulations show reasonable agreement with the calculated rates, therefore ensuring that the approximation used for the calculation of the switching rates, consisting in A being kept constantly in steady state, is not too strong.

Unfortunately it was not possible to find a combination of parameters that gives a value for the rate of persister formation and a value of the resuscitation rate compatible with the measured values [32, 43]. At the same time, the model lacks robustness to parameter change, as the computed value of both the persister and resuscitation rate are extremely susceptible to change in the parameters value, as shown in section 4.2.

When analyzing the behavior of the system against parameter change, we observed that the level of persister increases with increased degradation rate for the antitoxin. This finding is compatible with the emerging idea, supported by recent literature, of a connection between fluctuations in the level of cellular (p)ppGpp and higher levels of persistence [69]. The alarmone (p)ppGpp is the triggering signal for stringent response, and is known to up-regulate the activity of the Lon protease, that degrades the anti-toxins [30]. Within the scenario of (p)ppGpp mediated persistence, the persister formation rate would be dominated by (p)ppGpp fluctuations, and the resuscitation could be interpreted as being due to the existence of a slow-growth mediated negative feedback on (p)ppGpp. This would explain why in the present model, we cannot reproduce plausible rates.

Furthermore the effect of taking into account the activity of 10 cross-interacting TA systems has been investigated through stochastic simulations. We observed that the presence of multiple 10 systems stabilizes the high T state, facilitating the switch from fast-growth to persistence. This is in qualitative agreement with what has been observed by Maisonneuve *et al.* in 2001 [43]. However, in the stochastic simulation, the dependence of the rate of persisters formation on the number of TA system, was unfortunately found to be very sharp, which is in contrast with the gradual dependence found in [43].

On the other hand, when considering persisters formation as triggered by fluctuations in (p)ppGpp, one can imagine a relation between the fraction of a population showing (p)ppGpp level above a certain threshold and the fraction of the population that undergoes the transition to persistence. In the framework of our model, variation in the degradation rate of the anti-toxin Γ_A is a proxy for a variation in the (p)ppGpp level, because stringent response is known to activate Lon [30]. Furthermore, as discussed in section 4.3.1 increasing the value of $\beta_M = \beta_C = \beta$ in the system described by eq. 3.11 in chapter 3, can be used as a proxy for increasing the number of cross-interacting TA modules in the system described by eq. 4.30, within the strong approximation of all TA loci to be identical and in the same steady-state. Figure 4.13 is shown to discuss the interplay between (p)ppGpp-mediated higher degradation of the antitoxin and multiple TA system. It summarizes the stability of the steady states of system 3.11 for increasing Γ_A and β . The fact that the dependence of the threshold value for Γ_A above which the fast-growth state loses stability on the number of TA systems is graded, roughly linear, may be compatible with the observations by Maisonneuve *et al.* of a graded dependence of the persisters fraction on the number of interacting TA systems.

In conclusion, within the framework of our model, the sole stochasticity in the activation of the Toxin in the TA systems, is not a satisfactory explanation for the formation of persister cells. Although the presented model allows to reproduce some qualitative features of the process of persisters formation, additional mechanism need to be taken into account in order to be able to capture fully the quantitative aspects of the phenomenon.

As it will be discussed in further detail in the next chapter, future development of this work could consist in coupling the activity of the TA systems to the (p)ppGpp regulatory network.

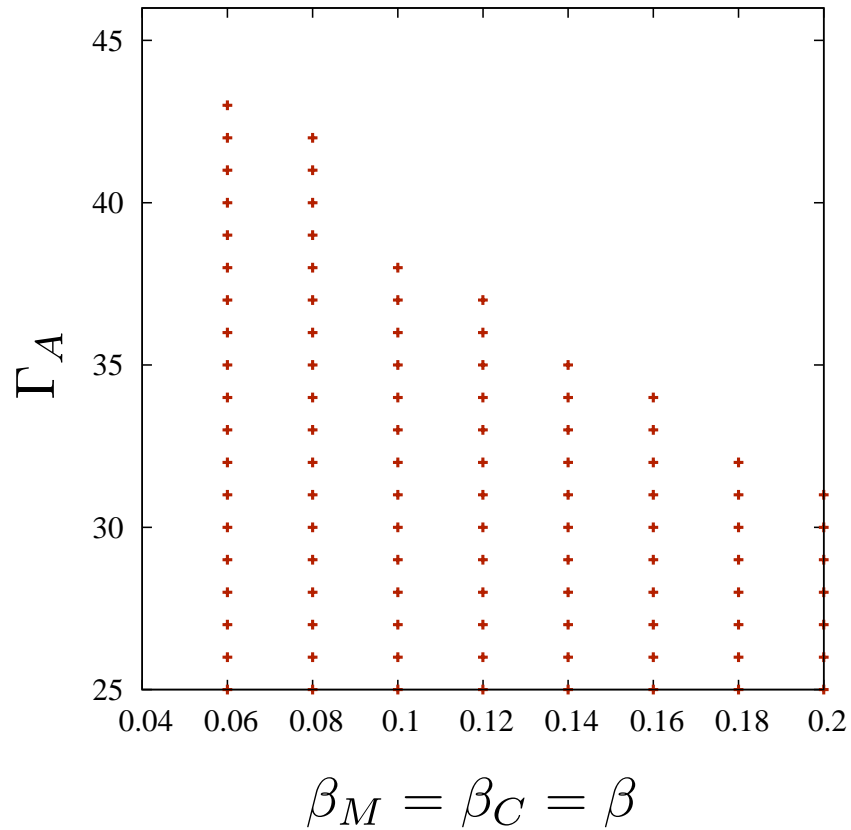


Figure 4.13: Each point represents a combination of parameters that allows bi-stability. Γ_A is varied between $30 \text{ (generation time)}^{-1}$ and $50 \text{ (generation time)}^{-1}$ while β is varied between $0.02 nM^{-1}$ and $0.2 nM^{-1}$. The rest of the parameters is set to the values shown in Appendix D. Notice that in the current parameter set, the T-dominated state exhibit a clear $T/A \gg 1$ ratio, while the other steady state is actually $T/A \simeq 1$. The area of the parameter space that shows no bistability, is monostable and T-dominated.

Chapter 5

Conclusive Remarks

This thesis is the result of three years of work that revolved around one main thread, the study of toxin-antitoxin loci in *E.coli* aimed at addressing the question of identifying their biological function. The projects described have stemmed from one another in a very natural fashion. The starting point was reproducing the dynamics of the expression of one particular TA locus in *E.coli*, *relBE*, and monitor its behavior in response to amino-acid starvation, motivated by experimental observations that suggested this system to be particularly relevant in such response. In the process, the peculiar auto-regulation mechanism of transcription of the *relBE* locus called *conditional cooperativity* caught our attention. We showed, among other results, that *conditional cooperativity* is necessary for the cell to recover after amino-acid starvation, and that it provides buffering against potentially lethal fluctuations in the level of free toxin. Intrigued by the peculiarity of this regulatory mechanism and by the fact that it appears to be a common trait for the TA loci in *E.coli*, we decided to 'abandon' the *relBE* system, to explore the potential function of *conditional regulation*, as a feedback motif, rather than in connection with the specificity of *one* locus. We concluded that the *coupling* of conditional regulation with a feedback on protein synthesis and cellular growth mediated by accumulation of free toxin, allows the activity of a TA locus to be characterized by robust bi-stability between a toxin-dominated and an antitoxin-dominated state. The toxin-dominated state is obviously either slow- or non-growing. Considering that TA systems have often been invoked in literature in connection to the phenomenon of bacterial persistence, bistability provides us with an intriguingly simple explanation for the mechanism of persister formation. However, persistence is an intrinsically stochastic phenomenon, and the dynamics of the switch between

the fast-growing and the dormant state needs to be addressed. Hence, we worked on a stochastic description of the activity of a TA locus. Furthermore, *E.coli* cells are known to be provided not with one, but eleven toxin-antitoxin loci, so we also tested the effect of considering the dynamics of the expression of multiple cross-interacting TA systems and showed that the presence of several TA loci facilitate the switch to a toxin-dominated state and stabilizes it.

As far as the mechanism of persisters formation is concerned, the work performed in this thesis can not provide a unified description of *the stochastic switch* between growth and dormancy. It only goes as far as showing that TA loci provide the cell with an effective *machinery* capable of mediating *bistability* between those two states. This is not the same as claiming that this bistability in the activity of the TA system is the sole mechanism behind persister formation. First of all, persistence might not necessarily be interpreted as corresponding to one steady state in a system that exhibit *bistable* behavior. An alternative interpretation could be, for example, to identify persisters with the occurrence of a temporary toxin-dominates state, corresponding to long-lived *fluctuations* in the proteins concentration, within a system that is, in a deterministic description, monostable. This interpretation has been discussed in very recent literature [70]. Furthermore, the natural future development of this work should be, I think, to shift the focus from the activity of TA loci to the phenomenon of persistence itself. In particular, one could embrace the idea that the stochastic activation of the *E.coli* TA loci could be only *one* component of a more intricate process involving, among other mechanisms, the coupling with fluctuations in the intracellular level of (p)ppGpp [69], as discussed in the conclusion of chapter 4.

Bibliography

- [1] P. Waage and C. Gulberg, “Studies concerning affinity,” *Journal of chemical education*, vol. 63, no. 12, p. 1044, 1986.
- [2] K. Sneppen and G. Zocchi, *Physics in molecular biology*. Cambridge University Press, 2005.
- [3] A. V. Hill *et al.*, “The possible effects of the aggregation of the molecules of haemoglobin on its dissociation curves,” *J physiol*, vol. 40, no. 4, pp. iv–vii, 1910.
- [4] L. Michaelis and M. L. Menten, “Die kinetik der invertinwirkung,” *Biochem. z*, vol. 49, no. 333-369, p. 352, 1913.
- [5] K. A. Johnson and R. S. Goody, “The original michaelis constant: translation of the 1913 michaelis–menten paper,” *Biochemistry*, vol. 50, no. 39, pp. 8264–8269, 2011.
- [6] D. T. Gillespie, “Exact stochastic simulation of coupled chemical reactions,” *The journal of physical chemistry*, vol. 81, no. 25, pp. 2340–2361, 1977.
- [7] M. G. Jørgensen, D. P. Pandey, M. Jaskolska, and K. Gerdes, “Hica of *escherichia coli* defines a novel family of translation-independent mrna interferases in bacteria and archaea,” *Journal of bacteriology*, vol. 191, no. 4, pp. 1191–1199, 2009.
- [8] D. Pandey and G. K., “Toxin-antitoxin loci are highly abundant in free-living but from host-associated prokaryotes,” *Nucleic Acids Research*, vol. 33, pp. 966–976, 2005.

- [9] E. M. Fozo, M. R. Hemm, and G. Storz, "Small toxic proteins and the anti-sense rnas that repress them," *Microbiology and Molecular Biology Reviews*, vol. 72, no. 4, pp. 579–589, 2008.
- [10] K. Gerdes and E. G. H. Wagner, "Rna antitoxins," *Current opinion in microbiology*, vol. 10, no. 2, pp. 117–124, 2007.
- [11] K. Gerdes, S. K. Christensen, and A. Løbner-Olesen, "Prokaryotic toxin-antitoxin stress response loci," *Nature Reviews Microbiology*, vol. 3, no. 5, pp. 371–382, 2005.
- [12] K. Pedersen, A. V. Zavialov, M. Y. Pavlov, J. Elf, K. Gerdes, and S. Uppsala, "The Bacterial Toxin RelE Displays Codon-Specific Cleavage of mRNAs in the Ribosomal A Site," vol. 112, pp. 131–140, 2003.
- [13] M. Christensen-Dalsgaard and K. Gerdes, "Translation affects yoeB and mazF messenger rna interferase activities by different mechanisms," *Nucleic acids research*, vol. 36, no. 20, pp. 6472–6481, 2008.
- [14] M. Christensen-Dalsgaard, M. G. Jørgensen, and K. Gerdes, "Three new re-homologous mrna interferases of escherichia coli differentially induced by environmental stresses," *Molecular microbiology*, vol. 75, no. 2, pp. 333–348, 2010.
- [15] M. H. Prysak, C. J. Mozdierz, A. M. Cook, L. Zhu, Y. Zhang, M. Inouye, and N. A. Woychik, "Bacterial toxin yafq is an endoribonuclease that associates with the ribosome and blocks translation elongation through sequence-specific and frame-dependent mrna cleavage," *Molecular microbiology*, vol. 71, no. 5, pp. 1071–1087, 2009.
- [16] O. Schmidt, V. J. Schuenemann, N. J. Hand, T. J. Silhavy, J. Martin, A. N. Lupas, and S. Djuranovic, "*prlF* and *yhav* encode a new toxin-antitoxin system in *escherichia coli*," *Journal of molecular biology*, vol. 372, no. 4, pp. 894–905, 2007.
- [17] Y. Zhang, J. Zhang, K. P. Hoefflich, M. Ikura, G. Qing, and M. Inouye, "MazF cleaves cellular mrnas specifically at aca to block protein synthesis in *escherichia coli*," *Molecular cell*, vol. 12, no. 4, pp. 913–923, 2003.

- [18] Y. Zhang, L. Zhu, J. Zhang, and M. Inouye, "Characterization of chpbk, an mrna interferase from escherichia coli," *Journal of Biological Chemistry*, vol. 280, no. 28, pp. 26080–26088, 2005.
- [19] M. A. Schumacher, K. M. Piro, W. Xu, S. Hansen, K. Lewis, and R. G. Brennan, "Molecular mechanisms of hipa-mediated multidrug tolerance and its neutralization by hipb," *Science*, vol. 323, no. 5912, pp. 396–401, 2009.
- [20] K. Gerdes and E. Maisonneuve, "Bacterial persistence and toxin-antitoxin loci," *Ann. Rev. Microbiol.*, vol. 66, pp. 103–123, 2012.
- [21] M. Overgaard, J. Borch, M. G. Jørgensen, and K. Gerdes, "Messenger RNA interferase RelE controls relBE transcription by conditional cooperativity," *Molecular microbiology*, vol. 69, pp. 841–57, Aug. 2008.
- [22] H. Afif, N. Allali, M. Couturier, and L. Van Melderen, "The ratio between ccda and ccdb modulates the transcriptional repression of the ccd poison-antidote system," *Molecular microbiology*, vol. 41, no. 1, pp. 73–82, 2001.
- [23] A. Garcia-Pino, S. Balasubramanian, L. Wyns, E. Gazit, H. D. Greve, R. Magnuson, D. Charlier, N. van Nuland, and R. Loris, "Allostery and intrinsic disorder mediate transcription regulation by conditional cooperativity," *Cell*, vol. 142, pp. 101–111, 2010.
- [24] K. S. Winther and K. Gerdes, "Regulation of enteric vapbc transcription: induction by vapc toxin dimer-breaking," *Nucleic acids research*, vol. 40, no. 10, pp. 4347–4357, 2012.
- [25] S. K. Christensen, M. Mikkelsen, K. Pedersen, and K. Gerdes, "RelE, a global inhibitor of translation, is activated during nutritional stress," *Proceedings of the National Academy of Sciences of the United States of America*, vol. 98, no. 25, 2001.
- [26] X. Wang, Y. Kim, S. H. Hong, Q. Ma, B. L. Brown, M. Pu, A. M. Tarone, M. J. Benedik, W. Peti, R. Page, *et al.*, "Antitoxin mqsa helps mediate the bacterial general stress response," *Nature chemical biology*, vol. 7, no. 6, pp. 359–366, 2011.
- [27] S. K. Christensen, K. Pedersen, F. G. Hansen, and K. Gerdes, "Toxin-antitoxin loci as stress-response-elements: Chpak/mazf and chpbk cleave

- translated rnas and are counteracted by tmrna,” *Journal of molecular biology*, vol. 332, no. 4, pp. 809–819, 2003.
- [28] J. A. Gallant, “Stringent control in E.coli,” *Annual review genetics*, vol. 13, pp. 393–415, 1979.
- [29] M. Cashel and J. Gallant, “Two Compounds implicated in the Function of RC gene,” *Nature*, vol. 221, pp. 838–841, 1969.
- [30] A. Kuroda, K. Nomura, R. Ohtomo, J. Kato, T. Ikeda, N. Takiguchi, H. Ohtake, and A. Kornberg, “Role of inorganic polyphosphate in promoting ribosomal protein degradation by the lon protease in e. coli,” *Science*, vol. 293, no. 5530, pp. 705–708, 2001.
- [31] J. W. Bigger, “The bactericidal action of penicillin on staphylococcus pyogenes,” *Irish Journal of Medical Science (1926-1967)*, vol. 19, no. 11, pp. 553–568, 1944.
- [32] N. Q. Balaban, J. Merrin, R. Chait, L. Kowalik, and L. S., “Bacterial persistence as a phenotypic switch,” *Science*, vol. 305, pp. 1622–1625, 2004.
- [33] D. Shah, Z. Zhang, A. Khodursky, N. Kaldalu, K. Kurg, and K. Lewis, “Persisters: a distinct physiological state of e. coli,” *Bmc Microbiology*, vol. 6, no. 1, p. 53, 2006.
- [34] B. R. Levin and D. E. Rozen, “Non-inherited antibiotic resistance,” *Nature Reviews Microbiology*, vol. 4, no. 7, pp. 556–562, 2006.
- [35] J. Collins and M. Richmond, “A structural similarity between n-acetylmuramic acid and penicillin as a basis for antibiotic action,” *Nature*, vol. 195, pp. 142–143, 1962.
- [36] H. S. Moyed and K. P. Bertrand, “hipa, a newly recognized gene of escherichia coli k-12 that affects frequency of persistence after inhibition of murein synthesis.,” *Journal of Bacteriology*, vol. 155, no. 2, pp. 768–775, 1983.
- [37] H. S. Moyed and S. H. Broderick, “Molecular cloning and expression of hipa, a gene of escherichia coli k-12 that affects frequency of persistence after inhibition of murein synthesis.,” *Journal of bacteriology*, vol. 166, no. 2, pp. 399–403, 1986.

- [38] O. Gefen and N. Q. Balaban, “The importance of being persistent: heterogeneity of bacterial populations under antibiotic stress,” *FEMS microbiology reviews*, vol. 33, no. 4, pp. 704–717, 2009.
- [39] E. Rotem, A. Loinger, I. Ronin, I. Levin-Reisman, C. Gabay, N. Shoresh, O. Biham, and N. Q. Balaban, “Regulation of phenotypic variability by a threshold-based mechanism underlies bacterial persistence,” *Proc. Natl. Acad. Sci. USA*, vol. 107, pp. 12541–12546, 2010.
- [40] D. S. Black, A. J. Kelly, M. Mardis, and H. Moyed, “Structure and organization of hip, an operon that affects lethality due to inhibition of peptidoglycan or dna synthesis.,” *Journal of bacteriology*, vol. 173, no. 18, pp. 5732–5739, 1991.
- [41] D. S. Black, B. Irwin, and H. S. Moyed, “Autoregulation of hip, an operon that affects lethality due to inhibition of peptidoglycan or dna synthesis.,” *Journal of bacteriology*, vol. 176, no. 13, pp. 4081–4091, 1994.
- [42] I. Keren, N. Kaldalu, A. Spoering, Y. Wang, and K. Lewis, “Persister cells and tolerance to antimicrobials,” *FEMS Microbiol. Lett.*, vol. 230, pp. 13–18, 2004.
- [43] E. Maisonneuve, L. Shakespeare, M. Jørgensen, and K. Gerdes, “Bacterial persistence by rna endonucleases,” *Proc. Natl. Acad. Sci. US*, vol. 108, pp. 13206–13211, 2011.
- [44] M. Gotfredsen and K. Gerdes, “The Escherichia coli relBE genes belong to a new toxin-antitoxin gene family,” *Molecular Microbiology*, vol. 29, pp. 1065–1076, 1998.
- [45] M. Overgaard, J. Borch, and K. Gerdes, “RelB and RelE of Escherichia coli form a tight complex that represses transcription via the ribbon-helix-helix motif in RelB.,” *Journal of molecular biology*, vol. 394, pp. 183–96, Nov. 2009.
- [46] A. Bøggild, N. Sofos, K. R. Andersen, A. Feddersen, A. D. Easter, L. a. Passmore, and D. E. Brodersen, “The crystal structure of the intact E. coli RelBE toxin-antitoxin complex provides the structural basis for conditional cooperativity.,” *Structure (London, England : 1993)*, vol. 20, pp. 1641–8, Oct. 2012.

- [47] S. Pedersen, S. Reeh, and J. D. Friesen, “Functional mrna half lives in e. coli,” *Molecular and General Genetics MGG*, vol. 166, no. 3, pp. 329–336, 1978.
- [48] S. Klumpp, Z. Zhang, and T. Hwa, “Growth rate-dependent global effects on gene expression in bacteria,” *Cell*, vol. 139, no. 7, pp. 1366–1375, 2009.
- [49] E. M. Ozbudak, M. Thattai, H. N. Lim, B. I. Shraiman, and A. Van Oudenaarden, “Multistability in the lactose utilization network of escherichia coli,” *Nature*, vol. 427, no. 6976, pp. 737–740, 2004.
- [50] M. Ptashne, “Gene regulation by proteins acting nearby and at a distance.,” *Nature*, vol. 322, no. 6081, pp. 697–701, 1985.
- [51] R. Feyter, C. Wallace, and D. Lane, “Corepression of the p1 addiction operon by phd and doc,” *Mol. Gen. Genet.*, vol. 218, pp. 81–86, 1989.
- [52] R. Magnuson and M. Yarmolinsky, “Corepression of the p1 addiction operon by phd and doc,” *J. Bacteriol.*, vol. 180, pp. 6342–6351, 1998.
- [53] N. Q. Balaban, K. Gerdes, K. Lewis, and J. D. McKinney, “A problem of persistence: still more questions than answers?,” *Nature Reviews Microbiology*, vol. 11, no. 8, pp. 587–591, 2013.
- [54] C. Lou, Z. Li, and Q. Ouyang, “A molecular model for persister in e. coli,” *J. Thor. Biol.*, vol. 225, pp. 205–209, 2008.
- [55] D. Angeli, J. E. Ferrell, and E. D. Sontag, “Detection of multistability, bifurcations, and hysteresis in a large class of biological positive-feedback systems,” *Proceedings of the National Academy of Sciences of the United States of America*, vol. 101, no. 7, pp. 1822–1827, 2004.
- [56] J. E. Ferrell, “Tripping the switch fantastic: how a protein kinase cascade can convert graded inputs into switch-like outputs,” *Trends in biochemical sciences*, vol. 21, no. 12, pp. 460–466, 1996.
- [57] J. C. J. Ray, J. J. Tabor, and O. A. Igoshin, “Non-transcriptional regulatory processes shape transcriptional network dynamics,” *Nature Reviews Microbiology*, vol. 9, no. 11, pp. 817–828, 2011.

- [58] D. Chen and A. P. Arkin, “Sequestration-based bistability enables tuning of the switching boundaries and design of a latch,” *Molecular systems biology*, vol. 8, no. 1, 2012.
- [59] C. Tan, P. Marguet, and L. You, “Emergent bistability by a growth-modulating positive feedback circuit,” *Nature Chemical Biology*, vol. 5, pp. 842–848, 2009.
- [60] I. Cataudella, A. Trusina, K. Sneppen, K. Gerdes, and N. Mitarai, “Conditional cooperativity in toxin-antitoxin regulation prevents random toxin activation and promotes fast translational recovery,” *Nucleic acids research*, vol. 40, no. 14, pp. 6424–6434, 2012.
- [61] M. Pedersen and K. Hammer, “The role of *mor* and the *ci* operator sites on the genetic switch of the temperate bacteriophage *tp901-1*,” *Journal of molecular biology*, vol. 384, no. 3, pp. 577–589, 2008.
- [62] H. Nakanishi, M. Pedersen, A. K. Alsing, and K. Sneppen, “Modeling of the genetic switch of bacteriophage *tp901-1*: a heteromer of *ci* and *mor* ensures robust bistability,” *Journal of molecular biology*, vol. 394, no. 1, pp. 15–28, 2009.
- [63] I. Cataudella, K. Sneppen, K. Gerdes, and N. Mitarai, “Conditional cooperativity of toxin-antitoxin regulation can mediate bistability between growth and dormancy,” *PLoS computational biology*, vol. 9, no. 8, p. e1003174, 2013.
- [64] M. Thattai and A. van Oudenaarden, “Intrinsic noise in gene regulatory networks,” *Proceedings of the National Academy of Sciences*, vol. 98, no. 15, pp. 8614–8619, 2001.
- [65] T. B. Kepler and T. C. Elston, “Stochasticity in transcriptional regulation: origins, consequences, and mathematical representations,” *Biophysical Journal*, vol. 81, no. 6, pp. 3116–3136, 2001.
- [66] C. H. Waddington *et al.*, *The strategy of the genes. A discussion of some aspects of theoretical biology. With an appendix by H. Kacser*. London: George Allen & Unwin, Ltd., 1957.
- [67] H. A. Kramers, “Brownian motion in a field of force and the diffusion model of chemical reactions,” *Physica*, vol. 7, no. 4, pp. 284–304, 1940.

-
- [68] M. B. Elowitz, A. J. Levine, E. D. Siggia, and P. S. Swain, “Stochastic gene expression in a single cell,” *Science*, vol. 297, no. 5584, pp. 1183–1186, 2002.
- [69] E. Maisonneuve, M. Castro-Camargo, and K. Gerdes, “(p) ppgpp controls bacterial persistence by stochastic induction of toxin-antitoxin activity,” *Cell*, vol. 154, no. 5, pp. 1140–1150, 2013.
- [70] L. Gelens, L. Hill, A. Vandervelde, J. Danckaert, and R. Loris, “A general model for toxin-antitoxin module dynamics can explain persister cell formation in e. coli,” *PLoS computational biology*, vol. 9, no. 8, p. e1003190, 2013.

Appendices

Appendix A

Estimation of Maximal Promoter Activity α_0

The value of α_0 (cfr Table 2.1) was calculated as follows, assuming a simple Michaelis-Menten kinetics for both mRNA and RelB synthesis, and assuming the steady state concentration of RelB and RelE and mRNA half-life noted in Table 2.1. The dynamics of the system is described by:

$$\frac{dm}{dt} = \frac{\alpha_0(1 + \frac{B_2E}{K_{D2}})}{1 + \frac{B_2E}{K_{D3}} + (\frac{B_2E}{K_{D2}})^2 + \frac{B_f}{K_{D1}}} - \frac{m}{\tau_m}, \quad (\text{A.1})$$

$$\frac{dB}{dt} = \text{trans}_B \cdot m - \frac{B}{\tau_B}, \quad (\text{A.2})$$

in steady state this becomes

$$\frac{\alpha_0(1 + \frac{B_2E}{K_{D2}})}{1 + \frac{B_2E}{K_{D3}} + (\frac{B_2E}{K_{D2}})^2 + \frac{B_f}{K_{D1}}} - \frac{m^{ss}}{\tau_m} = 0, \quad (\text{A.3})$$

$$m^{ss} = \frac{B^{ss}}{\text{trans}_B \tau_m}. \quad (\text{A.4})$$

The last result, together with

$$B_T = B_f + B_2E + B_2E_2 \quad (\text{A.5})$$

$$E_T = E_f + B_2E + 2 \cdot B_2E_2 \quad (\text{A.6})$$

$$(\text{A.7})$$

and the laws of mass action

$$B_2E = \frac{B_f \cdot E_f}{K_{dB_2E}} \quad (\text{A.8})$$

$$B_2E_2 = \frac{B_2E \cdot E_f}{K_{dB_2E_2}} \quad (\text{A.9})$$

allows to calculate α_0 .

Appendix B

Reference parameters in calculation of rates of persistence

<i>Parameter</i>	<i>Value</i>
σ_A	$102200 \text{ nM}(\text{generation time})^{-1}$
$\frac{\sigma_I}{\sigma_A}$	0.012
k_O	0.15325 nM
$k_T = k_{TT}$	1.8705 nM
Γ_A	$10 (\text{generation time})^{-1}$
Γ_0	$1 (\text{generation time})^{-1}$
β_M	4.0 nM^{-1}
β_C	1.0 nM^{-1}

Table B.1: Reference parameters used in the computation of $V(x, t)$ in Fig 4.1. The notation *generation time* refers to the time being measured in units of average *E.coli* generation time.

Appendix C

Reference parameters in the stochastic model of TA activity

<i>Parameter</i>	<i>Value</i>
σ_A	5000 (generation time) ⁻¹
$\frac{\sigma_T}{\sigma_A}$	$\frac{1}{30}$
k_O	10 nM
$k_T = k_{TT}$	10 nM
Γ_A	10 (generation time) ⁻¹
Γ_0	1 (generation time) ⁻¹
β_M	0.2 nM ⁻¹
β_C	0.2 nM ⁻¹

Table C.1: Reference parameters used in Fig 4.11 of section 4.2. The notation *generation time* refers to the time being measured in units of average *E.coli* generation time

Appendix D

Reference parameters in stability analysis for the multiple TA systems

<i>Parameter</i>	<i>Value</i>
σ_A	5000 (generation time) ⁻¹
$\frac{\sigma_T}{\sigma_A}$	$\frac{1}{30}$
k_O	10 nM
$k_T = k_{TT}$	1 nM
Γ_0	1 (generation time) ⁻¹

Table D.1: Reference parameters used in Fig 4.13 of conclusion of chapter 4. The notation *generation time* refers to the time being measured in units of average *E.coli* generation time

Appendix D. Reference parameters in stability analysis for the multiple TA systems

Appendix E

Reference parameters in the stochastic model for the multiple TA systems

<i>Parameter</i>	<i>Value</i>
σ_A	5000 (generation time) ⁻¹
$\frac{\sigma_T}{\sigma_A}$	$\frac{1}{30}$
k_O	10 nM
$k_T = k_{TT}$	1 nM
Γ_A	10 (generation time) ⁻¹
Γ_0	1 (generation time) ⁻¹
β_M	0.02 nM ⁻¹
β_C	0.02 nM ⁻¹

Table E.1: Reference parameters used in Fig 4.12 of section 4.3. The notation *generation time* refers to the time being measured in units of average *E.coli* generation time

Appendix E. Reference parameters in the stochastic model for the multiple TA systems

Appendix F

Derivation of Kramers escape rate

From eq 4.17 from chapter 4 we have

$$J = -D(x)\left[\frac{dV}{dx}P(x,t) + \frac{\partial P}{\partial x}\right] \quad (\text{F.1})$$

This is equivalent to

$$J = -D(x)e^{-V(x)}\frac{\partial}{\partial x}(P(x,t)e^{V(x)}) \quad (\text{F.2})$$

hence

$$J\frac{e^{V(x)}}{D(x)} = -\frac{\partial}{\partial x}(P(x,t)e^{V(x)}). \quad (\text{F.3})$$

By integrating both sides of eq. F.3 between x_{low}^{min} and x_{high}^{min} , we obtain

$$\int_{x_{low}^{min}}^{x_{high}^{min}} J\frac{e^{V(x)}}{D(x)} dx = -\int_{x_{low}^{min}}^{x_{high}^{min}} \frac{\partial}{\partial x}(P(x,t)e^{V(x)}) dx. \quad (\text{F.4})$$

The quasi-stationary approximation ($\frac{\partial P(x,t)}{\partial t} \approx 0$) implies, because of the equation of continuity in eq. 4.12 of chapter 4, that the flux J is constant ($\frac{\partial J}{\partial x} = 0$). Hence J can be taken out of the integral:

$$J \int_{x_{low}^{min}}^{x_{high}^{min}} \frac{e^{V(x)}}{D(x)} dx = -J \int_{x_{low}^{min}}^{x_{high}^{min}} \frac{\partial}{\partial x}(P(x,t)e^{V(x)}) dx = [P(x)e^{V(x)}]_{x_{low}^{min}}^{x_{high}^{min}} \quad (\text{F.5})$$

it follows

$$J = - \frac{[P(x)e^{V(x)}]_{x_{low}^{min}}^{x_{high}^{min}}}{\int_{x_{low}^{min}}^{x_{high}^{min}} \frac{e^{V(x)}}{D(x)} dx}. \quad (\text{F.6})$$

Because J is constant, and it represents the out-flux from the potential well located at x_{low}^{min} , it can be written as the product

$$J = p * r \quad (\text{F.7})$$

where p is the probability to be in the well ($p = \int_{x_{low}^{min}-\Delta}^{x_{low}^{min}+\Delta} P(x, t) dx$) and r , the rate of escape *from* the well *over* the potential barrier, is the quantity we are interested in calculating. Hence, we need to evaluate J from eq. F.6 and write it down as a function of p , to obtain r . In order to do so, we evaluate numerator and denominator of eq. F.6 separately.

Denominator

Let us first evaluate the denominator $\int_{x_{low}^{min}}^{x_{high}^{min}} \frac{e^{V(x)}}{D(x)} dx$ in eq. F.6. The largest contribution to the integral comes from the peak of $e^{V(x)}$, corresponding to the maximum x^{max} , the integral can be evaluated by Taylor expanding $V(x)$ around $x = x^{max}$, as follows:

$$V(x) \simeq V(x^{max}) + \frac{1}{2}V''(x^{max})(x - x^{max})^2 \quad (\text{F.8})$$

Integral F.8 then becomes

$$\int_{-\infty}^{\infty} \frac{e^{V(x^{max}) + \frac{1}{2}V''(x^{max})(x-x^{max})^2}}{D(x)} dx = \quad (\text{F.9})$$

$$= \frac{e^{V(x^{max})}}{D(x^{max})} \int_{-\infty}^{\infty} e^{\frac{1}{2}V''(x^{max})(x-x^{max})^2} dx \quad (\text{F.10})$$

The latter is a simple gaussian integral of the kind $\int_{-\infty}^{\infty} e^{-x^2} dx = \sqrt{\pi}$, hence

$$\int_{x_{low}^{min}}^{x_{high}^{min}} \frac{e^{V(x)}}{D(x)} dx = \frac{\sqrt{2\pi} e^{V(x^{max})}}{D(x^{max}) \sqrt{-V''(x^{max})}} \quad (\text{F.11})$$

that in turn implies that eq. F.6 becomes

$$J = - \frac{[P(x)e^{V(x)}]_{x_{low}^{min}}^{x_{high}^{min}}}{\frac{\sqrt{2\pi}e^{V(x_{max})}}{D(x_{max})\sqrt{-V''(x_{max})}}}. \quad (\text{F.12})$$

Numerator

Let us now evaluate the numerator of eq. F.6: $[P(x)e^{V(x)}]_{x_{low}^{min}}^{x_{high}^{min}}$ in order to relate it to the previously defined probability to be found in the well, p .

$$[P(x)e^{V(x)}]_{x_{low}^{min}}^{x_{high}^{min}} = P(x_{high}^{min})e^{V(x_{high}^{min})} - P(x_{low}^{min})e^{V(x_{low}^{min})}. \quad (\text{F.13})$$

Assuming that the particle is *initially* in the well, and considering the quasi-stationary approximation we obtain:

$$P(x_{high}^{min}) = P_0(x_{high}^{min}) \approx 0 \quad (\text{F.14})$$

hence

$$[P(x)e^{V(x)}]_{P(x_{low}^{min})}^{P(x_{high}^{min})} = -P(x_{low}^{min})e^{V(x_{low}^{min})}. \quad (\text{F.15})$$

Furthermore, if we assume the probability distribution around the well to be close to the local equilibrium value, for *infinitely high barrier*, namely:

$$P(x) = Ne^{-V(x)} \quad (\text{F.16})$$

one can write

$$P(x_{low}^{min}) = Ne^{-V(x_{low}^{min})} \quad (\text{F.17})$$

which implies

$$N = P(x_{low}^{min})e^{V(x_{low}^{min})} \quad (\text{F.18})$$

and hence

$$P(x) = P(x_{low}^{min})e^{-(V(x)-V(x_{low}^{min}))} \quad (\text{F.19})$$

for $|x - x_{low}^{min}| \ll |x - x^{max}|$.

The potential $V(x)$ has a minimum in x_{low}^{min} , thus we can Taylor expand it around x_{low}^{min} and obtain

$$V(x) = V(x_{low}^{min}) + \frac{1}{2}V''(x_{low}^{min})(x - x_{low}^{min})^2 \quad (\text{F.20})$$

The latter allows us to approximate the probability distribution in the neighborhood of x_{low}^{min} as follows:

$$p = \int_{x_{low}^{min}-\Delta}^{x_{low}^{min}+\Delta} P(x, t) dx \simeq P(x_{low}^{min}) \int_{-\infty}^{\infty} e^{-\frac{1}{2}V''(x_{low}^{min})(x-x_{low}^{min})^2} dx \quad (\text{F.21})$$

Considering that the latter integral is again a simple gaussian integral we obtain

$$p = P(x_{low}^{min}) \frac{\sqrt{2\pi}}{\sqrt{V''(x_{low}^{min})}} \quad (\text{F.22})$$

which implies

$$P(x_{low}^{min}) = p \frac{\sqrt{V''(x_{low}^{min})}}{\sqrt{2\pi}}. \quad (\text{F.23})$$

Finally, the numerator in eq [F.6](#) can be written as follows:

$$[P(x)e^{V(x)}]_{x_{low}^{min}}^{x_{high}^{min}} = -p \frac{\sqrt{V''(x_{low}^{min})}}{\sqrt{2\pi}} e^{V(x_{low}^{min})}. \quad (\text{F.24})$$

In conclusion from equations [F.6](#), [F.24](#), [F.12](#) we obtain:

$$J = p \cdot \frac{\frac{\sqrt{V''(x_{low}^{min})}}{\sqrt{2\pi}} e^{V(x_{low}^{min})}}{\frac{\sqrt{2\pi} e^{V(x_C)}}{D(x_C) \sqrt{-V''(x_C)}}} = p \cdot \frac{D(x^{max})}{2\pi} e^{-(V(x^{max})-V(x_{low}^{min}))} \sqrt{-V''(x^{max})} \sqrt{V''(x_{low}^{min})} \quad (\text{F.25})$$

remembering eq [F.7](#) one finally obtains the rate of escape from the potential well located in x_{low}^{min} , over the potential barrier situated in x^{max} as follows.

$$r(x_{low}^{min} \rightarrow x_{high}^{min}) = \frac{D(x^{max})}{2\pi} e^{-(V(x^{max})-V(x_{low}^{min}))} \sqrt{-V''(x^{max})} \sqrt{V''(x_{low}^{min})}. \quad (\text{F.26})$$

The latter coincides with $r_{A \rightarrow T}$ of equation [4.19](#) of chapter [4](#). The back-rate

$r_{T \rightarrow A} = r(x_{high}^{min} \rightarrow x_{low}^{min})$ can be calculated following the same procedure described so far, provided that the roles of x_{low}^{min} and x_{high}^{min} are swapped.

Appendix G

Attached article: Conditional cooperativity in toxin-antitoxin regulation prevents random toxin activation and promotes fast translational recovery

Conditional cooperativity in toxin–antitoxin regulation prevents random toxin activation and promotes fast translational recovery

Ilaria Cataudella^{1,*}, Ala Trusina¹, Kim Sneppen¹, Kenn Gerdes² and Namiko Mitarai^{1,*}

¹Center for Models of Life, Niels Bohr Institute, University of Copenhagen, Blegdamsvej 17, DK-2100 Copenhagen, Denmark and ²Centre for Bacterial Cell Biology, Institute for Cell and Molecular Biosciences, Newcastle University, Newcastle NE2 4AX, UK

Received November 7, 2011; Revised March 19, 2012; Accepted March 20, 2012

ABSTRACT

Many toxin–antitoxin (TA) loci are known to strongly repress their own transcription. This auto-inhibition is often called ‘conditional cooperativity’ as it relies on cooperative binding of TA complexes to operator DNA that occurs only when toxins are in a proper stoichiometric relationship with antitoxins. There has recently been an explosion of interest in TA systems due to their role in bacterial persistence, however the role of conditional cooperativity is still unclear. We reveal the biological function of conditional cooperativity by constructing a mathematical model of the well studied TA system, *relBE* of *Escherichia coli*. We show that the model with the *in vivo* and *in vitro* established parameters reproduces experimentally observed response to nutritional stress. We further demonstrate that conditional cooperativity stabilizes the level of antitoxin in rapidly growing cells such that random induction of *relBE* is minimized. At the same time it enables quick removal of free toxin when the starvation is terminated.

INTRODUCTION

Toxin–antitoxin (TA) loci are present in many bacteria and archaea (1). Toxin normally inhibits cell growth, whereas antitoxin neutralizes the activity of toxin by forming a tight TA complex.

One of the known functions of TA loci is to respond to nutritional stress, namely, toxins are activated upon nutritional starvation and slow down the rate of translation (2). Another significant feature of TA loci is that they contribute to persister cell formation in growing bacterial cultures

(3–5). Persisters are cells that have entered a slow-growing or dormant state in which the cells are tolerant to environmental insults such as antibiotics; thus persisters are multidrug tolerant and therefore pose a medical problem. Especially, the recent experiments by Maisonneuve *et al.* (5) demonstrated that successive deletion of 10 mRNase-encoding TA loci of *Escherichia coli* progressively reduced the level of persisters. TA loci have multiple complex levels of regulation involving both positive and negative feedbacks and sequestration through binding. The importance and role of these regulations is still an open question.

The *relBE* locus of *E. coli* is one of the best studied TA model systems. The *relBE* locus encodes for antitoxin RelB and toxin RelE. RelE is an mRNase that cleaves mRNA positioned in the ribosomal A site (6), including its own mRNA, while RelB inactivates RelE by forming a tight complex with it (7). RelB is a metabolically unstable protein whereas RelE is stable (2). However, RelB is translated at a higher rate than RelE, and in exponentially growing cells the abundant RelB molecules $\{[RelB] \approx 10[RelE] \text{ (8)}\}$ will quench RelE activity completely.

It has been shown that RelB and the RelB–RelE complex autoregulate *relBE* transcription in a complex way (9) (Figure 1): if only RelB is present then a RelB dimer ($RelB_2$) will repress *relBE* transcription. When RelE is present at a concentration such that $[RelB_2] > [RelE]$ then a $RelB_2RelE$ complex binds strongly and cooperatively to the *relBE* promoter and represses transcription (9). In contrast if RelE increases such that $[RelE] > [RelB_2]$, then the excess RelE molecules will destabilize the $RelB_2RelE$ -operator complex and thereby induce strong transcription from the *relBE* promoter (8). This sensitivity to the proper ratio between RelBE proteins is called *conditional cooperativity* (9, 10).

*To whom correspondence should be addressed. Tel: +45 353 25273. Email: cataudel@nbi.dk
Correspondence may also be addressed to Namiko Mitarai. Tel: +45 353 25402. Email: mitarai@nbi.dk

In an attempt to understand the biological role of conditional cooperativity and to analyse the TA operon transcription in general we present a mathematical model of *relBE* operon activity that takes into account the known features. We subsequently investigate the role of conditional cooperativity, and show that it provides a mechanism to stabilize the level of antitoxin in rapidly growing cells such that random induction of *relBE* is minimized. Another important prediction is that conditional cooperativity enables quick recovery from the RelE-mediated reduction of translation when the starvation is terminated.

MATERIALS AND METHODS

In our mathematical model of the *relBE* system, the transcription of the *relBE* operon (production of mRNA) and translation of *relBE* mRNA (proteins production) are taken into account as two separate processes. RelB form tight dimers, hence we can assume that RelB is always present as a dimer. In addition, RelB₂ and RelE can form complexes in the two stoichiometric forms RelB₂RelE and RelB₂RelE₂ (32).

A key goal of our model is to investigate the complex autoregulation feedback of *relBE* promoter activity. RelB₂ represses transcription. With moderate amount of RelE added, this repression become stronger because the RelB₂RelE has larger affinity to the operator. When RelE is further increased, however, the promoter is de-repressed because RelB₂RelE₂ does not bind to the operator.

RelE works as an mRNAse only in free form, by degrading the *relBE* mRNA as well as all other mRNAs in the cell. In our modeling, only the cleavage action of RelE on *relBE* mRNA is directly taken into account.

Free RelB₂ has a very short half-life since it is actively degraded by Lon protease. RelB half-life was measured to be ~3 min (9), whereas RelE is stable and its half-life is equal to the average *E. coli* doubling time (~30 min in normal growing condition). We do not model the cell division explicitly, it only enters implicitly into the RelE half-life.

Based on the fact that roughly 10 times more RelB monomers than RelE monomers are present during steady state cell growth in spite of the 10-fold difference in the half-life, we assume that the translation rate of RelB (monomers) is 100-fold higher than that of RelE.

RelB₂ in complex with RelE is known to be relatively stable (8). However, for RelE to become active, RelB in complex with RelE must be degraded at some rate. We assume RelB₂ in RelB₂RelE and RelB₂RelB₂ complexes has a half-life roughly 3-4 to fold longer than the free RelB₂ (~12 min).

The half-life of *relBE* mRNA is not known, and in our model it is set to 5 min. This is on the long side of typical *E. coli* mRNA half-life (29), which helps to keep the maximal promoter activity and the translation rate within biologically plausible values while having enough proteins.

The behavior of the system is investigated throughout three different phases.

A first phase, from time 0 to time 200 min in the plots, is what we call the 'non-starved state', where all the parameters used in the simulation refer to the exponential growth phase of the cell.

At time 200 min we switch to the nutritional stress phase (amino acid starvation). Within the framework of our model this means a sudden decrease in translation rate for both RelB and RelE by 10-fold, based on the observation that a *relBE*⁻ deletion strain shows a reduction of translation to a post-starvation level of 10%. Because the dilution by cell division does not happen in this phase, the half-life of τ_E is changed to 24h, which is much longer than the examined amino acid starvation duration (5h). We investigate whether enough free RelE can be released upon nutritional stress, since this circumstance could explain the 2-fold difference of the translation rate in starvation between wild type and *relBE*⁻ strain (2). In addition, starvation is known to significantly increase Lon activity (17), thus during starvation the half-life of the RelB₂ is reduced by a factor of 8, both in the free form and in complex.

At time 500 min, we then switch-back to the non-starved set of parameters corresponding to refeeding of the cells with amino acids and monitor the recovery of the system during the switch-back to exponential growth.

Note that the change of the parameters at the switching of the states has been done instantaneously. We discuss the effect of a time delay in the parameter change later.

We used the Gillespie algorithm (15) and performed stochastic simulations (simulation procedures given below). *relBE* mRNA, RelB₂, RelE, RelB₂RelE and RelB₂RelE₂ are the molecular players in the simulations. The concentrations are converted to number of molecules so that 1 nM corresponds to 1 molecule in a cell, which is a typical estimate based on the size of *E. coli*. Each chemical reaction event happens at a random time and it is chosen according to the reaction rates in Table 1. The possible reaction events are listed in Table 2.

In the results in the main text, we consider the presence of four chromosomes in each cell, that means four *relBE* promoters, which is an average number of chromosomes for exponentially growing *E. coli* cells. We also tried the one chromosome case, which exhibit increased noise, but the average trajectories remains similar. Each chromosome has two operators: each of them can be bound either by a RelB₂RelE complex or RelB. Since cooperativity in the interaction between RelB₂ and the *relBE* operator is not proven (9) we assume that only one RelB₂ can bind to the promoter at a given time, while either one or two RelB₂RelE can be bound to the operator (9). When the promoter is free, it shows maximal promoter activity, and $\alpha_0/4$ *relBE* mRNA {per promoter} per minute are produced. When either one RelB₂ is bound to the promoter or two RelB₂RelE bind cooperatively, the promoter is repressed and no *relBE* mRNAs are produced. In the present simulation, we did not consider the repression by one RelB₂RelE because experimentally the Hill coefficient close to 2 in repression is observed in the wide range of RelB₂RelE concentration (9).

Table 1. Set of parameters

Symbol and meaning	Description Value	Units	Reference
α_0 total promoter activity	154.665	nM min ⁻¹	See text
$[B_2]_{ss}$ steady state total concentration of RelB dimers	200	nM	See text c.f. (8)
$[E]_{ss}$ steady state total concentration of RelE	44	nM	See text c.f. (8)
τ_m mRNA half-life	7.2	min	See text c.f. (29)
τ_B RelB half-life	4.3	min	See text c.f. (8)
τ_E RelE half-life	43	min	See text
τ_c RelB ₂ half-life in complexes	17	min	See text c.f. (8)
n_H Hill's coefficient	2.3		(8)
trans _B RelB translation rate	15	min ⁻¹	See text
trans _E RelE translation rate trans _B /50	0.3	min ⁻¹	See text
k_{bind} binding on-rate $4\pi Da/V_{cell}$	3.8	min ⁻¹	(28)
K_dB2E dissociation constant for B2E complexes formation $\frac{[B_2][E]}{[B_2E]} = K_dB2E$	0.3	nM	(9)
K_dB2E2 dissociation constant for B2E2 complexes formation $\frac{[B_2][E]}{[B_2E_2]} = K_dB2E2$	0.3	nM	
k_uB2E dissociation rate for B2E $k_uB2E = k_{bind} \times K_dB2E$	1.14	nM	
k_uB2E2 dissociation rate for B2E2 $k_uB2E2 = k_{bind} \times K_dB2E2$	1.14	nM	
K_{D1} dissociation constant for B binding to DNA	10	nM	See text c.f. (16)
K_{D2} dissociation constant for second B2E bound to DNA	0.04	nM	See text c.f. (16)
K_{D3} dissociation constant for first B2E binding to DNA	30	nM	See text c.f. (16)
k_c cleavage rate	2.0	nM ⁻¹ min ⁻¹	See text c.f. (6)

Table 2. Events and rates in the simulation

Event	Rate
mRNA transcription	$\frac{\alpha_0}{4} * \text{no. of operators with two free binding sites}$
RelB dimers translation	$[mRNA] * \text{trans}_B$
RelE translation	$[mRNA] * \text{trans}_E$
relBE mRNA degradation	$\frac{[mRNA]}{\tau_m}$
RelB dimer degradation by Lon	$\frac{[RelB_2]}{\tau_B}$
RelE degradation due to cell dilution	$\frac{[RelE]}{\tau_E}$
RelB ₂ RelE formation	$k_{bind} * [RelB_2] * [RelE]$
RelB ₂ RelE ₂ formation	$k_{bind} * [RelB_2RelE] * [RelE]$
RelB ₂ RelE dissociation	$k_uB2E * [RelB_2 RelE]$
RelB ₂ RelE ₂ dissociation	$k_uB2E2 * [RelB_2RelE_2]$
degradation of RelB ₂ RelE due to cell dilution	$\frac{[RelB_2RelE]}{\tau_E}$
degradation of RelB ₂ RelE ₂ due to cell dilution	$\frac{[RelB_2RelE_2]}{\tau_E}$
degradation of RelB ₂ in RelB ₂ RelE complex	$\frac{[RelB_2RelE]}{\tau_c}$
degradation of RelB ₂ in RelB ₂ RelE ₂ complex	$\frac{[RelB_2RelE_2]}{\tau_c}$
binding of RelB ₂ to operator	$k_{bind} * [RelB_2] * \text{no. of operators with two free binding sites}$
binding of RelB ₂ RelE to operator	$k_{bind} * [RelB_2] * \text{no. of operators with at least one free binding site}$
unbinding of RelB ₂ from operator	$(K_{D1} * k_{bind}) * \text{no. of operators with 1 RelB}_2 \text{ bound}$
unbinding of one out of two RelB ₂ RelE from operator	$(K_{D2} * k_{bind}) * [RelB_2] * \text{no. of operators with two RelB}_2\text{RelE bound}$
unbinding of single RelB ₂ RelE from operator	$(K_{D3} * k_{bind}) * [RelB_2] * \text{no. of operators with a single RelB}_2\text{RelE bound}$
cleavage of relBE mRNA	$k_c * [RelE]$
stripping of RelB ₂ RelE complex bound to operator from it by RelE	$k_{bind} * [RelE] * \text{no. of operators with at least on RelB}_2\text{RelE}$

Algorithm of the Gillespie simulation

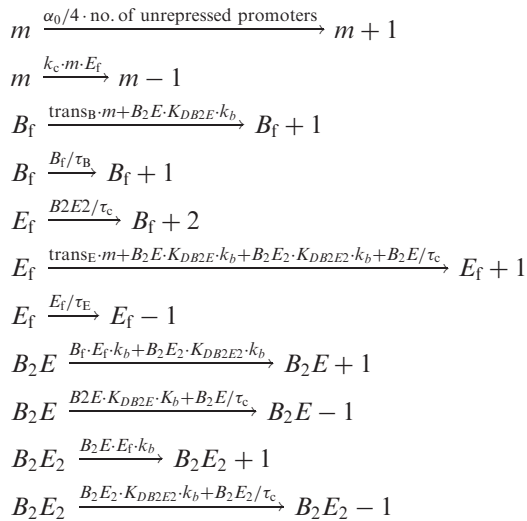
We use the Gillespie algorithm in our simulation, where the chemical reactions are treated as discrete stochastic events that happen at given rates with time interval between events drawn from the exponential distribution (15).

The state of the system at each time step is defined by the concentrations of the five molecular players, i.e. *relBE* mRNA (m), free RelE (E_f), free RelB₂ (B_f), RelB₂RelE (B_2E) and RelB₂RelE₂ (B_2E_2). The total copy number of RelB₂ (B_T) and RelE (E_T) are given by

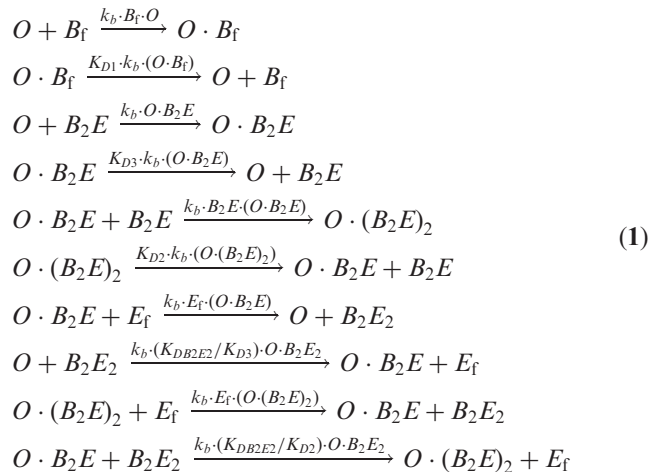
$$B_T = B_f + B_2E + B_2E_2,$$

$$E_T = E_f + B_2E + 2B_2E_2.$$

The chemical reaction with a rate specified by the parameters showed in Table 1 results in a change in the number of molecules as follows.



In addition, RelB₂ and RelB₂RelE can bind to the four operator sites. The binding happens to each operators independently, and the binding rates are given as follows (O expresses the operator):



The last four reactions are what we call ‘stripping’ (18,19), where RelE forming complex with RelB₂RelE bound on the operator and removing it, and the reverse reaction of the stripping.

Each run is from time 0 to time 600. At time $t = 200$ min the values of τ_B , τ_c , τ_E , trans_B and trans_E are changed from values that mimic fast growth conditions to values typical of amino acid starvation. At time $t = 500$ the same parameters are changed back to the fast growth value.

All the presented results refer to the averages of the concentrations over a sample of 1000 simulations, unless otherwise noted.

RESULTS

Outline of the model

The overall regulations and feedbacks in our model are summarized in Figure 1A. The mechanism of the conditional cooperativity is illustrated in Figure 1B. RelB and RelE can form two types of complexes, namely RelB₂·RelE (B_2E) and RelB₂·RelE₂ (B_2E_2). B_2 and B_2E repress the promoter activity of *relBE* operon, while B_2E_2 does not. This is a scenario proposed to reproduce the observed conditional cooperativity (9). Both RelB₂RelE complex (9, 32) and RelB₂RelE₂ complex (as heterotetramer); (32) have been observed *in vitro*.

All the molecules are exposed to either degradation by proteases or dilution by cell division, where the details are described in the next subsection. The mRNA m can be also actively degraded by the free toxin E .

Model parameters

The parameters of the model are constrained by (i) Stoichiometric data showing that when [total amount of RelE]:[total amount of RelB monomer] is in 1:2 ratio, RelB₂RelE and operator O complex, (RelB₂RelE)₂· O , is formed, while increasing the ratio of RelE further destabilizes the complex (9). This can be reproduced when the binding of RelE to RelB₂ and binding of RelE to RelB₂RelE occur with similar dissociation constants, hence when the total amount of RelE exceeds the total amount of RelB₂, RelB₂RelE are converted to RelB₂RelE₂ (See Supplementary Material A for detail).

(ii) That under normal growth in rich medium the *in vivo* concentration of RelE is about one-tenth of that of RelB (8). The actual concentration level was estimated to be 550–1100 nM for RelB while 50–100 nM for RelE (8). Here we choose parameters so that total RelB is ~500 nM and the total RelE is ~50 nM in non-starved exponential growth condition.

The *in vivo* lifetime of RelB is ~4.3 min, whereas RelE is metabolically stable but diluted by a rate set by cell division, giving it a characteristic lifetime of ~43 min in the exponential phase. This 10-fold shorter lifetime for RelB than RelE, with the 10-fold higher concentration of RelB in the exponential growing condition mentioned above gives us a translation rate of RelE ~1% of that of RelB. [Since the estimate of the RelB and RelE levels *in vivo* was difficult due to the low cellular amounts of the

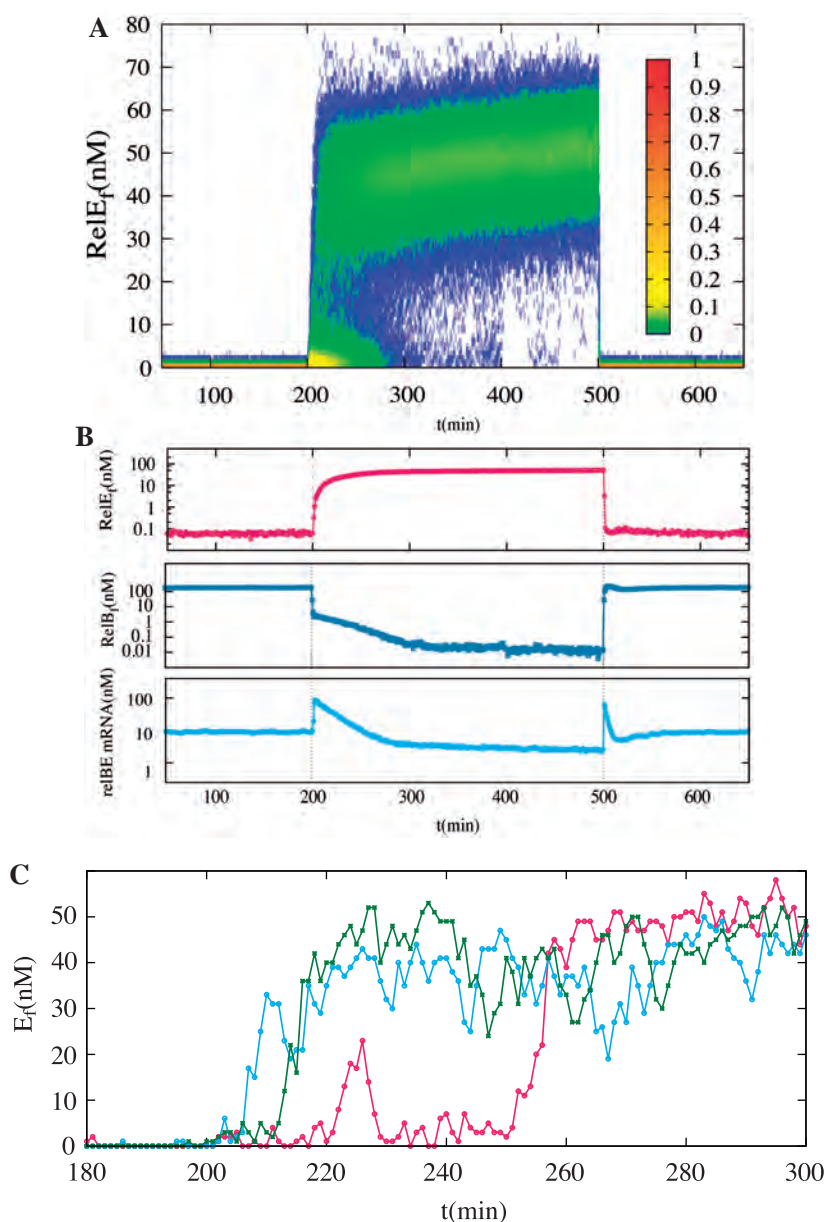


Figure 2. Response to amino acid starvation and later recovery. The system is starved for amino acids from 200 min to 500 min. (A) Probability distribution $P(E_f, t)$ of a cell having a certain concentration $[E_f]$ nM of free RelE at a given moment t . (B) Time courses averaged over 1000 cells, for free RelE, free RelB and *relBE* mRNA, illustrating how the system switches between a state of high antitoxin to a state of high free toxin. (C) The dynamics at entrance to the starvation at the single cell level. Three examples are shown, and the total amount of free RelE is plotted as function of time, from time 180 to time 300.

proteins (8), the 10-fold difference in concentration can be smaller in reality, which would indicate higher translation rate ratio (up to 10%).] (iii) That RelB_2 represses RelBE promoter by a factor 16, whereas $(\text{RelB}_2\text{RelE})_2$ represses the same promoter by a factor 800 under exponential growth in normal medium. These repression folds are about one-tenth of what was observed using *lacZ* fusion on low copy number (~ 10) plasmids (16). We adapted these repression folds mainly because they are close to the upper limit of the repression folds which can give

biologically plausible promoter strength for the *relBE* promoter and translation rate with still being able to reproduce the observed concentrations of RelB and RelE in exponential growth, where promoters are fully repressed.

In the next subsections, we demonstrate that the model with these evaluated parameter values show expected response to amino acid starvation and recovery when the starvation is over. We also investigate the robustness of the behavior against the parameter changes.

Amino acid starvation drives the switch to toxin activation

The model is examined when switching from rich medium to amino acids starvation, and subsequently exposed to refeeding after 5 h. There are three main processes taking place during starvation: (i) The overall translation rate is reduced, because of the lack of amino acids, here simulated by a 10-fold reduction. (ii) Cells stop dividing, thus dilution of RelE decreases, allowing for accumulation of this long lived protein. (iii) Lon activity is believed to be increased under starvation (17), increasing the degradation rate of RelB. We chose to make the degradation 8-fold stronger during amino acid starvation. The result presented here holds as long as the degradation of RelB in the RelB₂RelE complex is large enough during the starvation, and the 8-fold is close to the minimum fold needed.

Figure 2 shows switching from the antitoxin dominated state to the toxin dominated state elicited by amino acid starvation. Importantly, in order to make this response work we had to assume that RelB in complex with RelE must be actively degraded, at least during starvation. If such degradation was not included, then the transition to the high-RelE state cannot be achieved. Here, we assume that RelB is degraded 4-fold less effectively when in complex with RelE than when it is free (*in vitro* data supports that RelB is partly protected from degradation when it is in complex with RelE (8)). To demonstrate the necessity of this process, we compare the model with and without active degradation of RelB in the complex in the Supplementary Material B.

From Figure 2B, we also see that there is a some time-lag to enter the toxin dominated state, while the time to exit this state is very short. This time lag is due to the combined effect of ‘stripping’ and conditional cooperativity. By ‘stripping’ we mean the process where a free toxin molecules ‘invades’ the RelB₂RelE complex bound to the promoter inducing the complex to be released from operator DNA. This has been shown to occur both *in vitro* and *in vivo* (8). Note that it is possible to have conditional cooperativity without stripping, in which case excess RelE will form RelB₂RelE₂ complex in the bulk and thus sequester RelB₂RelE, but does not remove bound RelB₂RelE actively from the operator site.

The conditional cooperativity with stripping opens for an active and relatively long battle between degradation of RelB and a de-repression of the promoter with an associated rise of *relBE* mRNA (2,8) and hence increase in production of RelB. [It should be noted that in the experiment that *relBE* mRNA level was observed to rise ~30-fold just after the amino acid starvation (2,8), while in the present model we observe only ~2-fold rise (Figure 2). The height of this peak depends strongly on the cleavage rate of mRNA by free RelE, k_c , but just lowering this value delays to reach the high free toxin state at the starvation (details in Supplementary Material C). This disagreement can be in principle improved if we take into account the fact that free RelE will interact with all the mRNAs in the cell, thus it is quite likely that free RelE will be sequestered and will not cleave much of *relBE* mRNA when its concentration is very low, which should give bigger rise for *relBE* mRNA. In the present model,

however, we do not take this effect into account because of large ambiguity in detailed interactions between all mRNAs the free RelEs.] Without stripping, this rise becomes much smaller than this, and hence the delay becomes less (details in Supplementary Material D). Central in this ‘battle’ is cleavage of mRNA by free RelE, since it reduces the *relBE* mRNA for both RelE and RelB, and thereby favor the long-lived toxin RelE. The cleavage rate k_c of *relBE* mRNA by toxin is not known *in vivo*, and we use $k_c = 2/\text{min/nM}$ to obtain reasonably fast rise of the toxin upon starvation. For comparison, the *in vitro* cleavage activity per codon with empty ribosome A-site was estimated to be between 0.000042 to 2.4 /min/nM depending on the codon (6). Considering there are 79 codons for RelB, one expect 2–3 ribosomes at any time to translate the mRNA, and thus an effective cleavage rate that should not exceed 5/min/nM. Thus our assumed value is in the high end, but using for example a 10 times smaller value of k_c would delay the transition into toxin dominated state by hours, as shown in Supplementary Material E.

Single cell activation of RelE is binary

The behavior of single cells are summarized in Fig. 2A as the probability distribution $P([E_f], t)$ of a cell having a certain concentration $[E_f]$ nM of free toxin at a given moment t . We can see that the response is binary. There is a high peak at low toxin at the start of starvation (time 200), but another peak for high free toxin state (around $[E_f] \approx 45$ nM) appears already at 10 min after starvation. The low probability to take the value in between ($10 \text{ nM} < [E_f] < 30 \text{ nM}$) suggest that each cell switches from low (<10 nM) to high free toxin (>30 nM) quickly. On cell population level (Figure 2B) in contrast it takes almost 40 min for free RelE to reach 30 nM. This contrast reflects the big variation in switching time between different cells.

Figure 2C shows three representative trajectories of single cells entering starvation. At the beginning, free RelE is almost zero because RelE are bound by RelB’s, but after some time the balance switches and the concentration of free RelE rises quickly to high level. The examples show variation in switching timing over 60 min but none of them spend much time at the intermediate free toxin level. Overall this shows the significance of stochastic modeling of this type of system as well as the need for single cell measurement of the TA systems.

Amino acid starvation is terminated at $t = 500$ min in Figure 2. Compared with the entry to the starved state, the recovery from the starved state is found to be extremely quick both on average and at the single cell level. As demonstrated below the fast recovery depends on conditional cooperativity.

Conditional cooperativity primes fast exit from the toxin dominated state

To clarify the role of conditional cooperativity, we compare the system with conditional cooperativity (the same system as in Figure 2: referred as ‘cc’) and the

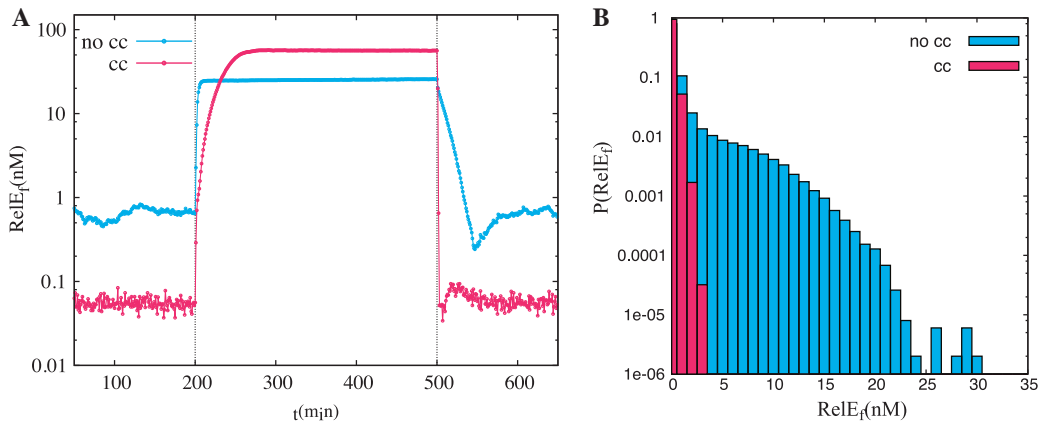


Figure 3. Role of conditional cooperativity. (A) The time evolution of free RelE level for the system with (red) and without (blue) conditional cooperativity. The system is starved for amino acid from 200 to 500 min. (B) Probability distribution of free RelE in the non-starved state without conditional cooperativity (blue) and with conditional cooperativity (red). Free RelE takes higher value without conditional cooperativity.

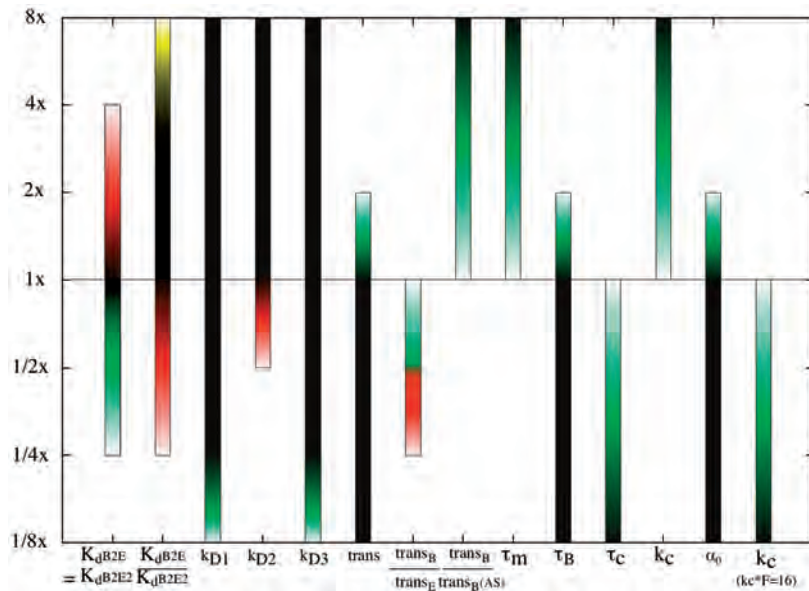


Figure 4. Summary of the model behavior against parameter changes. For each parameters (horizontal axis), fold change of the values from our reference values are tried one by one. The color gradients indicate how the model deviates from the reference behavior: yellow indicates too many free toxins in the healthy states, green indicates too slow rise of free RelE at amino acid starvation and red indicates too slow drop of toxins after the removal of amino acid starvation. In the first entry, $K_dB2E = K_dB2E2$, the ratio of the dissociation constants K_dB2E and K_dB2E2 are kept to be one, but the value itself is changed. In the second entry, the ratio K_dB2E/K_dB2E2 is changed, while keeping smaller dissociation constant to be the reference value 0.3 nM. For the entry *trans*, the translation rates for RelB and RelE are changed by the given folds, while $trans_B/trans_E$ and $trans_B/trans_B(AS)$ [$trans_B(AS)$ is the translation rate of RelB during the amino acid starvation] are kept to the reference values. For the entry $trans_B/trans_E$ and $trans_B/trans_B(AS)$ the given ratio is changed with keeping the value of the translation for RelB $trans_B$ to be 15/min. For the entry τ_B (τ_c), the lifetime of the RelB₂ (RelB's in the complexes) are changed with keeping the 1/8-fold reduction of the lifetime during the amino acid starvation. For the entry k_c (the 12th entry), the value of the cleavage rate is changed, while for the entry $k_c(k_c \times F = 16)$ (the last entry), the value of k_c and the fold-change of the RelB degradation rate F are changed, so that $k_c \times F$ is kept to the reference value 16.

system without conditional cooperativity (referred as ‘no cc’): We removed the conditional cooperativity by preventing RelB₂RelE₂ complex formation completely, while keeping the other parts of the system unchanged. Therefore, regardless of the relative concentrations of total RelE and total RelB, the only possible complex they can form is RelB₂RelE. Figure 3A illustrates that the conditional cooperativity is required for the fast recovery from the toxin dominant state under starvation

to the non-starved state. Mechanistically this reflects that formation of RelB₂RelE₂ derepresses the promoter in the high-RelE state and thereby primes the system for recovery already during starvation.

Figure 3B shows that conditional cooperativity also reduces the probability to have high free toxin in the non-starved state. In the non-starved state the excess of RelB buffers for an increase in free RelE (by the sequestration into the complex RelB₂RelE). If RelB by

fluctuations becomes low, the conditional cooperativity provides a negative feedback that secures additional RelB. This reduces free RelE by complex formation and thus the concentration of free toxin is kept low.

Robustness of the observed behaviors against the parameter changes

Finally, we study the robustness of the observed behaviors against parameter changes. This is not only to see how general our conclusion is regarding the choice of the parameter values, but also to indirectly test how the feedbacks that are not modeled in the present framework would affect the behavior. Especially, growth-rate dependences (24–27) are observed in cell physiology through for example the partitioning of the ribosomes (which affects the translation rate) or the RNAP availability (which affects the transcription rate). Such dependences will affect parameter values upon amino acid starvation. The robustness test gives idea about how significant such a feedback can be in the studied behavior.

In Figure 4, we summarize the robustness of the observed behaviors against parameter changes. We change parameters (or ratio of parameters) one by one by 2^n -fold, with $-3 \leq n \leq 3$, and we check whether the model is working with that parameter value based on the following criteria: (i) The free RelE level in the healthy state is <1 nM. (ii) The free RelE level reaches >10 nM within 20 min after the start of the amino acid starvation. (iii) The free RelE level drops <1 nM within 5 min after starvation is stopped.

The robustness analyses shows that the condition (ii) is hardest to satisfy. Most parameters are split in two sub-regions, i.e. the model is very sensitive to the change in one direction (increase or decrease) but insensitive to change in another direction. This is because our reference parameter is at borderline, i.e. just fast enough, to satisfy the criterion (ii). Even at this borderline we had to introduce the faster degradation of RelB's in complexes during starvation, to achieve fast increase in free RelE. This again support the necessity of the fast degradation of the antitoxins at amino acid starvation.

The only case where condition (i) tends to be violated is when the dissociation constant $K_d B_2 E$ for RelB₂RelE formation is very large, hence RelE are not tightly sequestered in the complex. Increasing both $K_d B_2 E$ and $K_d B_2 E_2$ has similar effect, but it affects stronger on the recovery from the free high-toxin state (iii), by freeing up toxin easier at the transient state.

In addition, the third criterion (iii) is violated when the unstable antitoxin RelB is not produced high enough, which happens when the ratio between the translation rate of RelB and RelE ($\text{trans}_B/\text{trans}_E$) is too small or the repression by RelB₂RelE (characterized by K_{D2}) is too tight. When $K_d B_2 E/K_d B_2 E_2$ is too small (1/4-fold or less), RelB₂RelE₂ is not formed as much and the conditional cooperativity becomes ineffective, which also makes the recovery slow.

The robustness of the transcription rate α_0 and the translation rate (trans) is of particular interest in the context of the growth-rate dependent feedback. We see

that the model behavior is robust 1/8- to 2-fold change of these parameters. Namely, even if there is a feedback from the growth rate to these parameters, the model behavior will not be altered as long as the change is within this fold. Especially, the transcription rate α_0 is expected to decrease upon slower growth (24), which is the direction where the model behavior is robust.

We also investigated how the time scale of the parameter changes (when the conditions are shifted to or from starvation) affect the kinetics of the transitions between two states. The relevant parameters changed are the RelB lifetime and the translation rates. Overall, we find that the time scale of parameter changes is rate-limiting for the entry into the starved state, i.e. the kinetics of the transitions is fully determined by how rapidly we change these parameters (Supplementary Material E). This is again because our reference parameters are at the borderline to reproduce the fast entry.

The recovery phase is, however, less sensitive to the time scale of the parameter changes. The translation rate has the biggest effect, but as soon as the translation rate increases by some amount, the RelB accumulate enough and free RelEs are repressed (Supplementary Material E). Furthermore, the main result regarding the conditional cooperativity is robust: the recovery is always much faster for the model with conditional cooperativity than without conditional cooperativity (Supplementary Material F).

DISCUSSION

We constructed a mathematical model of how *relBE* is regulated, with the main focus centered around the conditional cooperativity in the autoregulation of *relBE* operon. With our model we intended to capture the available experimental data, test the known and estimate the values of unknown parameters and investigate the systems dynamics when the cells are shifted between non-starved and starved states.

Our current modeling framework highlights several interesting features:

- (1) A fast entry to the high-toxin state can only be realized if antitoxin is degraded both when it is free and in complex with toxin during amino acid starvation.
- (2) The transition from the antitoxin dominated state to the toxin dominated state upon sudden amino acid starvation is not graded but binary at the level of single cells.
- (3) When amino acid starvation is terminated conditional cooperativity mediates fast recovery from the toxin dominated to the growing state.
- (4) Conditional cooperativity also reduces the occasional occurrence of high free toxin state in the non-starved condition.

In the following we discuss these four features. Active degradation of antitoxin in the TA complex during the starvation [Feature (1) above] should be closely coupled to Lon protease activation during amino acid starvation (17). More detailed understanding of Lon activity during

the starvation as well as fluctuations of Lon activity in growing cell will provide more insights about toxin activation through this pathway, which can be included in the future development of the model.

The switch-like activation of the toxin at the single cell level [Feature (2) above] comes from the positive feedback; when free toxin starts to increase, the cleavage-rate of TA mRNA increases, that in turn reduces the amount of anti-toxin and thereby forces more free toxin to accumulate (see also Figure 1). Positive feedback facilitated switches have been seen in many other systems that require decision making, for example, the lysis/lysogeny switch in temperate phage (20), sugar utilization in bacteria (21) and cell differentiation (22). In the present case, the decision that a cell needs to make is whether it should translate or shut down translation; we believe that it makes biological sense that the cells do not waste time between these two states.

Conditional cooperativity [Feature (3)] facilitates the switch to work in a robust manner, favoring the antitoxin dominated state by making the switching back dynamics fast and by reducing the probability to randomly switch to toxin dominated state without stress [Feature (4)].

Even though the present modeling relies on parameters measured for *relBE* systems, we believe that our model is relevant for the mRNase TA systems in general, where the basic framework of the regulations is believed to be similar to the one in *RelBE*. Especially, the observed switching—between low- and high-toxin states upon starvation and recovery—is interesting in relation to persisters. A current view on the persister mechanism suggest that by toxin fluctuations some cells happen to end in a toxin dominated state [cf. (4,23,24)], while the present study shows that if the TA system has the conditional cooperativity such fluctuations will be strongly suppressed (Figure 3B). The extent to which the system is subject to fluctuations, i.e., how often a cell can be in high-toxin state by chance without amino acid starvation, is an important quantity to study in the future in relation to the persister formation. It is in general an interesting theoretical and experimental problem to understand the role of TA system in persister cells formation in the light conditional cooperativity.

In order to generalize the present model, especially to the persister system, it should be noted that the several known feedbacks are not taken into account in the present model. As mentioned earlier, a number of parameters are growth-rate dependent (24–27) due to e.g. RNAP availability, stringent response via ppGpp, DksA regulation, etc. In the present level of modeling, these factors would mainly affect the transcription rate. Within the interest of the present work, the conclusions remain qualitatively the same for changing the transcription rate by 1/8- to 2-fold (Figure 4). However, the feedback where high-toxin state imposes slow growth and slow transcription which in turn favors high-toxin state opens for an interesting direction as it can have a strong effect on the stability of the persister state (24).

Finally, we propose several possible experiments based on the present results.

The direct test of the predictions of the model about the conditional cooperativity would be to construct a mutant that does not form $RelB_2RelE_2$ and yet keep other

properties of *RelB* and *RelE*, and then compare the dynamics with the wild type scenario. This, however, requires the detailed structural knowledge of the proteins.

The observation of the dynamics of the entrance to and recovery from the starved state at the single cell level will give a lot of information about the system. Especially, the binary response [Step (2)] should be confirmed experimentally, by for example visualizing the *RelE* level or *relBE* mRNA level in each cell.

The low copy number of *RelE* (~50 nM) or *relBE* mRNA (~a few molecules) makes it challenging to monitor these molecules using usual fluorescent microscopy, to overcome this challenge superresolution microscopy (e.g. STORM) has been successfully used to monitor the single cell/single molecule dynamics in bacterial cells (31). The dynamics of the recovery is also interesting to observe, especially the expected short recovery time due to the conditional cooperativity.

Another interesting experiment is to study the dependence of recovery dynamics on the duration of the amino acid starvation. The duration of typical experiments is ~5 h, and the toxin *RelE* is expected to be stable on that time scale. This is consistent with (7), where a pulse of *RelE* found to sufficient to prevent cell division for similar time scale. The limit of the stability of *RelE* in non-dividing cells, though, is not known. This factor, according to our model, can have a strong effect on the recovery behavior from high-toxin state after very long lasting amino acid starvation.

SUPPLEMENTARY DATA

Supplementary Data are available at NAR Online: Supplementary Data A–F and Supplementary References [33,34].

ACKNOWLEDGEMENTS

K.G. thanks Dagmar Iber for discussions in the initial phase of the project.

FUNDING

Center for Models of Life, Danish National Research Foundation; Steno Fellowship, The Danish Council for Independent Research. Funding for open access charge: Danish National Research Foundation.

Conflict of interest statement. None declared.

REFERENCES

1. Pandey, D. and Gerdes, K. (2005) Toxin-antitoxin loci are highly abundant in free-living but from host-associated prokaryotes. *Nucleic Acids Res.*, **33**, 966–976.
2. Christensen, S.K., Mikkelsen, M., Pedersen, K. and Gerdes, K. (2001) *RelE*, a global inhibitor of translation, is activated during nutritional stress. *Proc. Natl Acad. Sci. USA*, **98**, 14328–14333.
3. Gefen, O. and Balaban, N.Q. (2009) The importance of being persistent: heterogeneity of bacterial populations under antibiotic stress. *FEMS Microbiol. Rev.*, **33**, 704–717.

4. Rotem, E., Loinger, A., Ronin, I., Levin-Reisman, I., Gabay, C., Shoresh, N., Biham, O. and Balaban, N.Q. (2010) Regulation of phenotypic variability by a threshold-based mechanism underlies bacterial persistence. *Proc. Natl Acad. Sci. USA*, **107**, 12541–12546.
5. Maisonneuve, E., Shakespeare, L.J., Jørgensen, M. and Gerdes, K. (2011) Bacterial persistence by RNA endonucleases. *Proc. Natl Acad. Sci. USA*, **108**, 13206–13211.
6. Pedersen, K., Zavialov, A.V., Pavlov, M.Y., Elf, J., Gerdes, K. and Ehrenberg, M. (2003) The bacterial toxin RelE displays codon-specific cleavage of mRNAs in the ribosomal A site. *Cell*, **112**, 131–140.
7. Pedersen, K., Christensen, S.K. and Gerdes, K. (2002) Rapid induction and reversal of a bacteriostatic condition by controlled expression of toxins and antitoxins. *Mol. Microbiol.*, **45**, 501–510.
8. Overgaard, M., Borch, J. and Gerdes, K. (2009) RelB and RelE of *Escherichia coli* form a tight complex that represses transcription via the ribbon-helix-helix motif in RelB. *J. Mol. Biol.*, **394**, 183–196.
9. Overgaard, M., Borch, J., Jørgensen, M.G. and Gerdes, K. (2008) Messenger RNA interferase RelE controls relBE transcription by conditional cooperativity. *Mol. Microbiol.*, **69**, 841–857.
10. Garcia-Pino, A., Balasubramanian, S., Wynn, L., Gazit, E., Greve, H.D., Magnuson, R., Charlier, D., van Nuland, N. and Loris, R. (2010) Allostery and intrinsic disorder mediate transcription regulation by conditional cooperativity. *Cell*, **142**, 101–111.
11. Winther, K.S. and Gerdes, K. (2012) Regulation of enteric vapBC transcription: induction by VapC toxin dimer-breaking. *Nucleic Acid Res.*, **40**, 4347–4357.
12. Magnuson, R. and Yarmolinsky, M.B. (1998) Corepression of the *p1* addiction operon by *phd* and *doc*. *J. Bacteriol.*, **180**, 6342–6351.
13. Feyter, R., Wallace, C. and Lane, D. (1989) Autoregulation of the *ccd* operon in the F plasmid. *Mol. Gen. Genet.*, **218**, 81–86.
14. Gerdes, K., Christensen, S.K. and Lobner-Olesen, A. (2005) Prokaryotic toxin-antitoxin stress response loci. *Nat. Rev. Microbiol.*, **3**, 371–382.
15. Gillespie, D.T. (1977) Exact stochastic simulation of coupled chemical reactions. *J. Phys. Chem.*, **81**, 2340–2361.
16. Gottfredsen, M. and Gerdes, K. (1998) *Escherichia coli* relBE genes belong to a new toxin-antitoxin gene family. *Mol. Microbiol.*, **29**, 1065–1076.
17. Kuroda, A., Nomura, K., Ohtomo, R., Kato, J., Ikeda, T., Takiguchi, N., Ohtake, H. and Kornberg, A. (2001) Role of inorganic polyphosphate in promoting ribosomal protein degradation by the Lon protease in *E. coli*. *Science*, **293**, 705–708.
18. Bergqvist, S., Alverdi, V., Mengel, M., Hoffmann, A., Ghosh, G. and Komives, E.A. (2009) Kinetic enhancement of NF- κ B · dna dissociation by I κ B α . *Proc. Natl Acad. Sci. USA*, **106**, 19328–19333.
19. Zabel, U. and Baeuerle, P.A. (1990) Purified human I κ B can rapidly dissociate the complex of the NF- κ B transcription factor with its cognate DNA. *Cell*, **2**, 255–265.
20. Ptashne, M. (1986) Gene regulation by proteins acting nearby and at a distance. *Nature*, **322**, 697–701.
21. Ozbudak, E., Thattai, M., Lim, H., Shraiman, B. and Oudenaarden, A.V. (2004) Multistability in the lactose utilization network of *Escherichia coli*. *Nature*, **427**, 737–740.
22. Becskei, A., Seraphin, B. and Serrano, L. (2001) Positive feedback in eukaryotic gene networks: cell differentiation by graded to binary response conversion. *EMBO J.*, **20**, 2528–2535.
23. Lou, C., Li, Z. and Ouyang, Q. (2008) A molecular model for persistence in *E. coli*. *J. Theor. Biol.*, **255**, 205–209.
24. Klumpp, S., Zhang, Z. and Hwa, T. (2009) Growth rate-dependent global effects on gene expression in bacteria. *Cell*, **139**, 1366–1375.
25. Klumpp, S. and Hwa, T. (2008) Growth-rate-dependent partitioning of RNA polymerases in bacteria. *Proc. Natl Acad. Sci. USA*, **105**, 20245–20250.
26. Scott, M., Gunderson, C.W., Mateescu, E.M., Zhang, A. and Hwa, T. (2010) Inter-dependence of cell growth and gene expression: origins and consequences. *Science*, **330**, 1099–1102.
27. Zaslaver, A., Kaplan, S., Bren, A., Jinich, A., Mayo, A., Dekel, E. and Uri, A. (2009) S. Itzkovitz Invariant distribution of promoter activities in *Escherichia coli*. *PLoS Comp. Biol.*, **5**, e1000545.
28. Sneppen, K. and Zocchi, G. (2005) *Physics in Molecular Biology*. Cambridge University Press, Cambridge, UK.
29. Pedersen, S. and Reeh, S. (1978) Functional mRNA half lives in *E. coli*. *Mol. Gen. Genet.*, **166**, 329–336.
30. Takagi, H., Kakuta, Y., Okada, T., Yao, M., Tanaka, I. and Kimura, M. (2005) Crystal structure of archaeal toxin antitoxin RelE/RelB complex with implications for toxin activity and antitoxin effects. *Nat. Struct. Mol. Biol.*, **12**, 327–331.
31. Elf, J., Li, G.W. and Xie, X.S. (2007) Probing transcription factor dynamics at the single molecule level a living cell. *Science*, **316**, 1191–1194.
32. Li, G.-Y., Zhang, Y., Inouye, M. and Ikura, M. (2008) Structural mechanism of transcriptional autorepression of the *Escherichia coli* RelB/RelE antitoxin/toxin module. *J. Mol. Biol.*, **380**, 107–119.
33. Slutsky, M., Kardar, M. and Mirny, L.A. (2004) Diffusion in correlated random potentials with applications to DNA. *Phys. Rev.*, **69**, 061903.
34. Elf, J., Li, G.W. and Xie, X.S. (2007) Probing transcription factor dynamics at the single molecular level in a living cell. *Science*, **316**, 1191–1194.

Supplementary material for "Conditional Cooperativity in Toxin-Antitoxin Regulation Prevents Random Toxin Activation and Promotes Fast Translational Recovery" by Ilaria Cataudella, Ala Trusina, Kim Sneppen, Kenn Gerdes, and Namiko Mitarai

Supplement A: Parameter constraint for dissociation constants to reproduce the conditional cooperativity

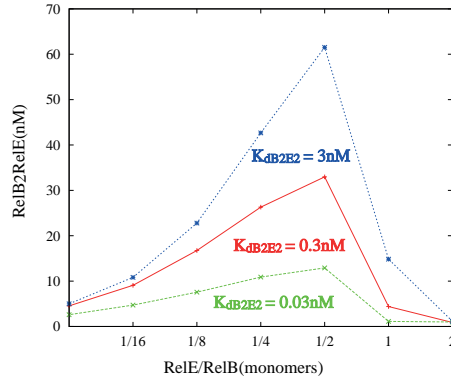


Figure 5: Concentration of RelB₂RelE as a function of (total RelE)/(total RelB monomer) calculated according to law of mass action. The amount of total RelB monomer is fixed to 200 nM. K_{B_2E} is set to 0.3 nM, and the cases where $K_{B_2E_2}$ =0.03nM, 0.3nM, 3nM are shown.

In the in-vitro experiment on the conditional cooperativity by Overgaard et al. [9], it has been shown that the formation of the operator-(RelB₂RelE)₂ complex depends on the RelE/RelE molar ratio. Especially, in Fig.2C in [9], the amount of RelB monomer is fixed to 200nM, and the amount of RelE is changed from (total RelB monomer):(total RelE)=16:1 to 1:4, and it has been found that the amount of operator-(RelB₂RelE)₂ complex gradually increases upto 2:1 ratio, and suddenly drops to almost zero at 1:1 ratio and beyond.

Inspired by this experiment, we calculated the the amount of RelB₂RelE complex according to the law of mass action

$$[B_2E] = \frac{[B_2][E]}{K_{B_2E}}, \quad (2)$$

$$[B_2E_2] = \frac{[B_2E_2][E]}{K_{B_2E_2}} \quad (3)$$

$$[B_{2T}] = [B_2] + [B_2E] + [B_2E_2], \quad (4)$$

$$[E_T] = [E] + [B_2E] + 2[B_2E_2]. \quad (5)$$

$$(6)$$

with keeping $[B_{2T}]$ =100 nM (therefore relB monomer concentration is 200 nM).

K_{B_2E} is fixed to 0.3nM, and the cases with $K_{B_2E_2} = 0.03$ nM, 0.3 nM (the reference parameter value), 3nM are shown. With the reference parameter, $K_{B_2E_2} = 0.3$ nM, a clear peak of RelB₂RelE is found at 2:1 ratio, while at 1:1 ratio it drops lower than the level at 16:1 ratio. When $K_{B_2E_2} = 3$ nM, the drop at 1:1 ratio is not as strong. When $K_{B_2E_2} = 0.03$ nM, the peak of RelB₂RelE is not as high. Therefore, we conclude that the conditional cooperativity is the best reproduced when K_{B_2E} and $K_{B_2E_2}$ are at similar value.

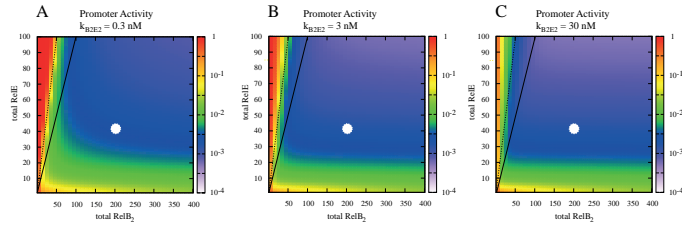


Figure 6: A,B,C: The repression fold of the *relBE* promoter for various total amount of RelB and RelE, with changing the dissociation constant of RelB₂RelE₂ formation $K_{B_2E_2}$. The white point shows the total amount of RelE and RelB in the non-starved state. For all the figure, the dissociation constant of RelB₂RelE formation is fixed to be $K_{B_2E} = 0.3$ nM. A: $K_{B_2E_2} = 0.3$ nM, which is the value used in the paper. B: $K_{B_2E_2} = 3$ nM. C: $K_{B_2E_2} = 30$ nM. The solid line in the figure shows the line where the amount of total RelE is equal to that of total RelB₂ (i.e., RelE_t: RelB_t = 1:2), while the dashed line shows the line where the amount of total RelE is equal to the double amount of total RelB₂ (i.e., RelE_t: RelB_t = 1:1).

Furthermore, Figs. 6 show the the repression fold of the *relBE* promoter for various total amount of RelB and RelE, keeping $K_{B_2E} = 0.3$ nM but changing $K_{B_2E_2}$. In 6A with $K_{B_2E_2} = 0.3$ nM, we can see that when RelB_t: RelE_t = 1:2 (here RelB_t is total concentration in monomer) the system stay repressed since there are many RelB₂RelE, while almost complete de-repression happens when total RelE exceed the RelE_t: RelB_t = 1:1 line because most of the RelB₂RelE is converted to RelB₂RelE₂. However, as we increase $K_{B_2E_2}$, this sharp de-repression gets blurred.

Supplement B: Switch to high RelE require degradation of RelB in complex

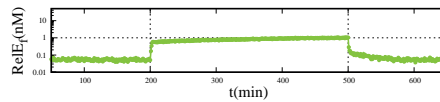


Figure 7: Development of free RelE in case that there is no active degradation of RelB in complexes, thus RelB in complex the same half-life as τ_E . Free RelE is seen to remain low, in contrast to behavior of standard model (Fig2B) where RelB in complex is degraded a factor 4 times slower than in complex but still degraded much faster than RelE.

The response to starvation in Fig2 depends on the possible ways that RelB can be degraded. In particular, the starved state depends critically on our assumption of increased degradation of RelB during starvation, and also on the assumption that RelB can be degraded in the $RelB_2RelE$ complex. Fig7 shows that the toxin dominated state is not reached when RelB is completely protected in complex, thus having the same life time as RelE in complex. In summary, the necessary feature to obtain toxin activation is a high degradation-rate of RelB not only in the free state but also in the complex with RelE.

Supplement C: Effect of the cleavage rate of mRNA by toxin

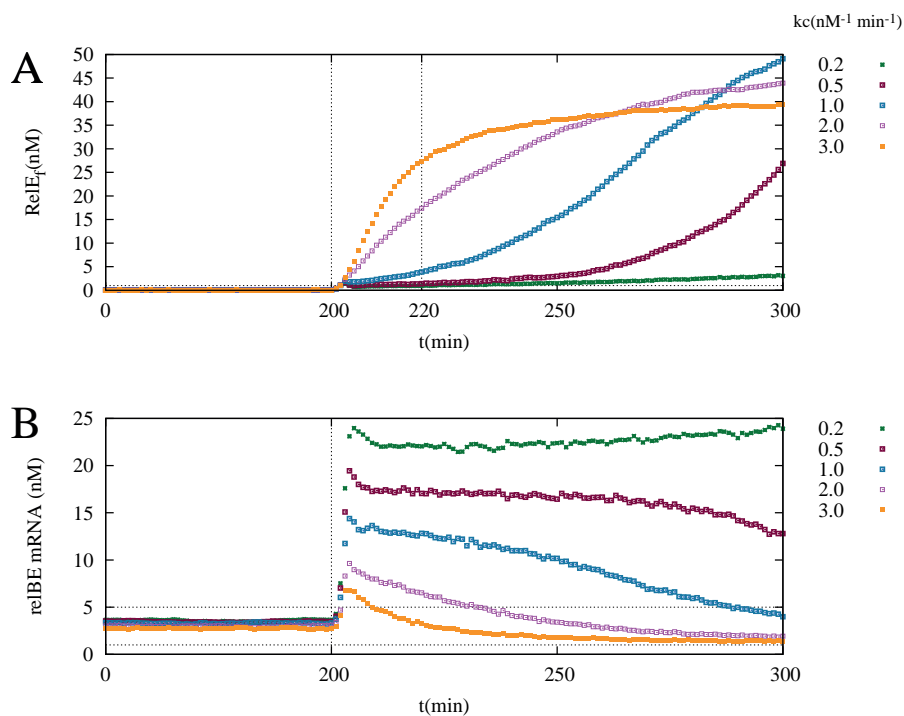


Figure 8: Effect of changing the k_c value on evolution of free RelE and *relBE* mRNA. At time $t = 200$ minutes the system is switched to amino acid starvation.

A: Concentration of free RelE over time. The higher the value of k_c the sooner a substantial raise in the concentration is recorded. In order for free *RelE* to raise above $1 nM$ within 20 minutes k_c needs to be higher than $1 nM^{-1} min^{-1}$. A slower raise also results in higher accumulation of RelE on the long period. This is a direct consequence of the higher concentration of $RelB_2RelE$ complexes due to higher RelB level, that act as a reservoir for free toxin once the antitoxin starts getting degraded.

B: Concentration of *relBE* mRNA over time. Lower values of the cleavage rate k_c result in a higher increase in the amount of mRNA at the onset of starvation, allowing an effective production of antitoxin RelB that slows down the raise in the concentration of RelE shown above.

Fig8 shows how lower values of k_c allow a stronger increase in *relBE* mRNA at the onset of starvation, enhancing RelB's ability to fight back, and thus slowing down the raise in free RelE.

Supplement D: Stripping delays entry into high free toxin state

We now investigate the effect of only removing the possibility for $\text{RelB}_2\text{RelE}_2$ complex formation when this is bound to the operator, in other word we investigate the role of the assumed reaction where free RelE directly “strips” [18] the operator and thereby derepresses it. If RelB_2RelE and the operator as well as the complex formations by RelB's and RelE's were characterized by a fast on and off dynamics, the effect of such a stripping would be small. This is because the speed of the reaction determines the relaxation time to the thermal equilibrium, where the stripping and the reverse reaction satisfies the detailed balance and hence cancels out. However, when the unbinding rate of $(\text{RelB}_2\text{RelE})_2$ bound to the operator is estimated to be low, stripping modifies the temporal behavior significantly. For example, it has been suggested that the stripping plays a crucial role in quickly deactivating human NF- κ B [19, 18]. In the RelBE case, with a diffusion limited on-rate of about 0.06/sec/molecule, and a repression factor of 800 in the non-starved conditions, the residence for the complex $(\text{RelB}_2\text{RelE})_2$ on the operator is estimated to be long (~ 6 min), and the effect of stripping can be substantial.

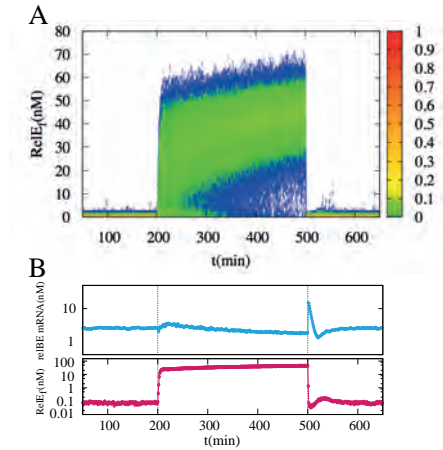


Figure 9: The model behavior without stripping. A: Time development of the probability distribution of free RelE, sampled over 1000 cells. B: Average trajectory of *relBE* mRNA and free RelE without stripping. Compared to in Fig. 2B, entry into the toxin dominated state is faster.

Fig. 9 shows the behavior of the system without stripping, demonstrating that absence of stripping results in faster transition into the RelE dominated

state, and increases fluctuations of RelE during starvation (compare it with Fig. 2). That is, without stripping, it takes more time before the operator is de-repressed when RelE becomes dominant, because the system needs to wait until bound $\text{RelB}_2\cdot\text{RelE}$ leaves from the operator. In this scenario, the system cannot “fight back” by strong de-repression and hence strong production of RelB does not occur as fast as in the case with stripping. Thus, without stripping the toxin is much more prone to be activated.

Note that our assumption of a diffusion limited on-rate may be incorrect: On the one hand, DNA facilitated search increases the on-rate *in vitro* [20], but *in vivo* unspecific bindings of RelB_2RelE typically slow down the search [21]. If the on-rate of $(\text{RelB}_2\text{RelE})_2$ is lower than assumed here, the effect of stripping becomes even more pronounced than illustrated in the figure.

Supplement E: Effect of time delay in the change of parameters at transitions between the starved and the non-starved states

In the main text the switching from one level of nutrients to another (amino-acid starvation to rich medium and vice versa) was achieved by changing some key parameters, namely, the free RelB half-life τ_B , the half-life of RelB in complexes τ_c , the translation rate for *RelB* (and consequently the translation rate for *RelE*), and the half-life of free *RelE*. The changes in the parameters were treated as happening instantaneously for simplicity of the model.

Here we investigate the effect of varying the life time of RelB and the translation rate slower (linearly over time) at the transition to understand the role of these time scales.³

³The change of the life time of free RelE τ_E does not have significant effect in the transition because τ_E is at shortest 43 min, much longer than the systems dynamics at the transitions.

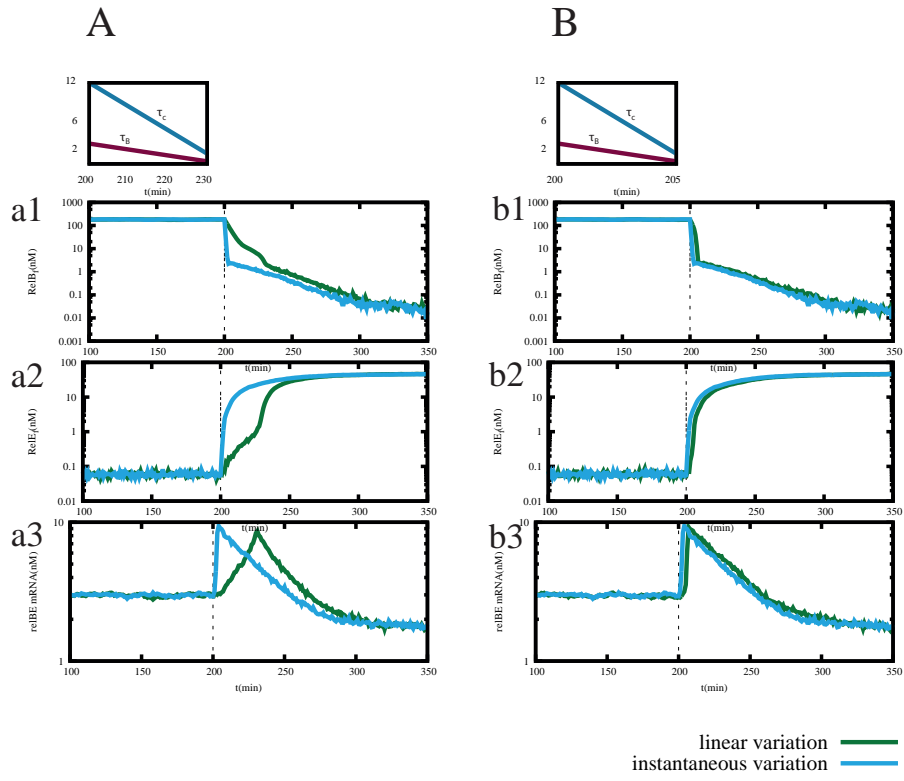


Figure 10: Effect of changing the half-life of free RelB (τ_B) and RelB in complexes (τ_c) from fast grow conditions levels ($\tau_B = 3min$ and $\tau_c = 12min$) to amino-acid starvation estimated level ($\tau_B = 0.375min$ and $\tau_c = 1.5min$) linearly over time in two different cases: over a time interval of 30 min (A) and 5 min (B)

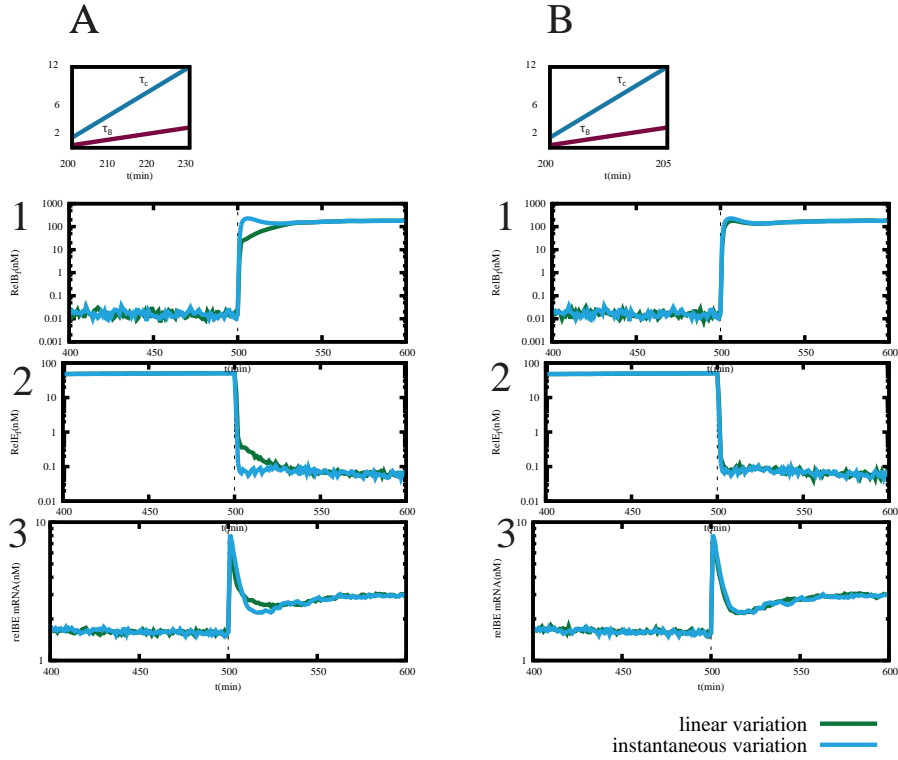


Figure 11: Effect of changing the half-life of free RelB (τ_B) and RelB in complexes (τ_c) from amino-acid starvation estimated levels ($\tau_B = 0.375min$ and $\tau_c = 1.5min$) to fast growth conditions level ($\tau_B = 3min$ and $\tau_c = 12min$) linearly over time in two different cases : over a time interval of 30 min (A) and 5 min (B)

Effect of the RelB degradation. Figure 10 shows the effect of varying τ_B and τ_c over 30 min (A) and 5 min (B) at the transition from fast growth conditions to amino-acid starvation. The time scale of the change is directly reflected to the time for free RelE to rise (a2). This is expected from the fact that this change was required to have the fast enough entrance to the high-toxin state at the starvation. In order to reproduce the experimental observation that the effect of RelE seen on the protein level about 10 min after the amino acid starvation, we predict that the effect of activation of Lon on τ_B and τ_c should be significant after 10 min.

On the other hand, as can be seen in fig. 11, the dynamics of recovery from starved state is little affected the time scale of change of τ_B and τ_C . We conclude that recovery behavior is robust with respect to a slower change of τ_B and τ_c .

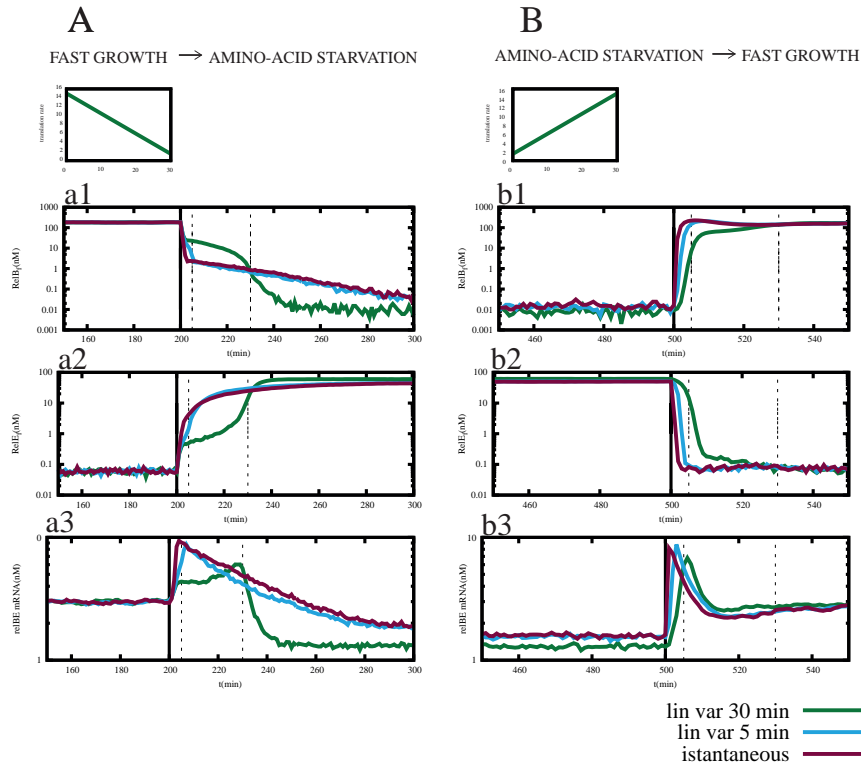


Figure 12: Effect of continuous variation of the translation rate for RelB and RelE continuously over time on the dynamics of the transitions from fast growth conditions to amino-acid starvation and vice-versa. Panel A) Behaviour over time of free RelB (a1), free RelE (a2) and relBE mRNA (a3) at the transition from fast growth conditions to amino-acid starvation in three different cases : translation rate is changed abruptly at the switching time from fast growth level (15 nM/mRNA/min) to amino-acid starvation level (1.5 nM/mRNA/min)(red line), translation rate is changed linearly over a time span of 5 minutes (blue line), translation rate is changed linearly over a time span of 30 minutes (green line). Panel B) Behaviour over time of free RelB (b1), free RelE (b2) and relBE mRNA (b3) at the transition from amino-acid starvation to fast growth conditions in three different cases : translation rate is changed abruptly at the switching time from fast growth level (15 nM/mRNA/min) to amino-acid starvation level (1.5 nM/mRNA/min)(red line), translation rate is changed linearly over a time span of 5 minutes (blue line), translation rate is changed linearly over a time span of 30 minutes (green line).

Effect of the translation rate. We explore the effects of changing the value of the translation rate at the two switching point (fast growth to amino-acid starvation and vice-versa) linearly over time instead of abruptly as it was done in the main text. We took into account two extreme cases, in one case the change in translation rate happens over a time span of 5 minutes (blue lines in fig. 12) and in the other case the time span is 30 minutes.

In the case of transition to amino-acid starvation (fig. 12 A) the activation of free RelE is delayed by almost the same amount as the time interval over which

the translation rate is changed. This is natural because the high translation rate gives RelB to fight back against the rise of RelE.

In the case of transition to recovery phase (fig. 12 B), even though also in this case we see a noticeable delay in the fall of free RelE, the free RelE falls to low level much faster than the introduced time delay. This is because the system need enough number of RelBs produced to repress RelE, and this can be realized even before the translation happens at full speed.

Supplement F: Conditional cooperativity gives faster recovery from amino-acid starvation induced growth-arrest than without conditional cooperativity independent of the delay in the recovery of the translation rate

As it has been shown in supplement E, the time scale over which the translation rate increases after starvation phase affect the time scale of the fall of the free RelE. Here we confirm that the conditional cooperativity will still give faster recovery than without consitional cooperativity even if the translation rate increase slower.

Figure 13 compare without conditional cooperativity case (top) and with conditional cooperativity case (bottom), when the translation rate changes instantaneously (circles) or over 30 min. In both cases we see that the case without conditional cooperativity is much slower in recovery. We conclude that our qualitative conclusion of importance of conditional cooperativity for recovery from the high-toxin phase is robust against the detail of the time scale of parameter change.

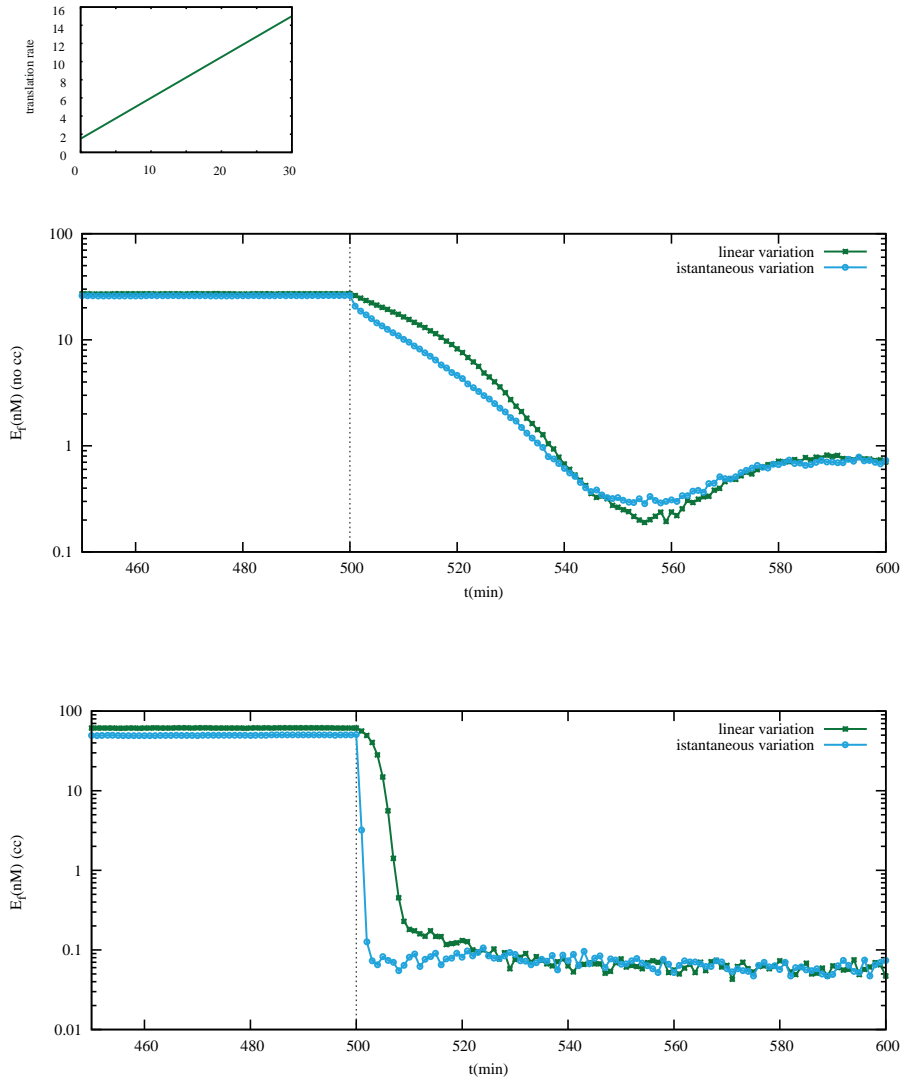


Figure 13: Comparison between time-scale over which recovery takes place without (A) and with (B) conditional cooperativity, in the case where translation rate is changed abruptly from amino-acid starvation value to fast-growth value (blue line) and in the case where it's changed linearly with time over an interval of 30 minutes.

Appendix H

Attached article: Conditional
Cooperativity of Toxin-Antitoxin
Regulation Can Mediate
Bistability between Growth and
Dormancy

Conditional Cooperativity of Toxin - Antitoxin Regulation Can Mediate Bistability between Growth and Dormancy

Ilaria Cataudella¹, Kim Sneppen¹, Kenn Gerdes², Namiko Mitarai^{1*}

1 Niels Bohr Institute/CMOL, University of Copenhagen, Copenhagen, Denmark, **2** Centre for Bacterial Cell Biology, Institute for Cell and Molecular Biosciences, Newcastle University, Newcastle, United Kingdom

Abstract

Many toxin-antitoxin operons are regulated by the toxin/antitoxin ratio by mechanisms collectively coined “conditional cooperativity”. Toxin and antitoxin form heteromers with different stoichiometric ratios, and the complex with the intermediate ratio works best as a transcription repressor. This allows transcription at low toxin level, strong repression at intermediate toxin level, and then again transcription at high toxin level. Such regulation has two interesting features; firstly, it provides a non-monotonous response to the concentration of one of the proteins, and secondly, it opens for ultrasensitivity mediated by the sequestration of the functioning heteromers. We explore possible functions of conditional regulation in simple feedback motifs, and show that it can provide bistability for a wide range of parameters. We then demonstrate that the conditional cooperativity in toxin-antitoxin systems combined with the growth-inhibition activity of free toxin can mediate bistability between a growing state and a dormant state.

Citation: Cataudella I, Sneppen K, Gerdes K, Mitarai N (2013) Conditional Cooperativity of Toxin - Antitoxin Regulation Can Mediate Bistability between Growth and Dormancy. *PLoS Comput Biol* 9(8): e1003174. doi:10.1371/journal.pcbi.1003174

Editor: Jeffrey J. Saucerman, University of Virginia, United States of America

Received: December 19, 2012; **Accepted:** June 26, 2013; **Published:** August 29, 2013

Copyright: © 2013 Cataudella et al. This is an open-access article distributed under the terms of the Creative Commons Attribution License, which permits unrestricted use, distribution, and reproduction in any medium, provided the original author and source are credited.

Funding: This study was supported by the Danish National Research Foundation through the Center for Models of Life. The funders had no role in study design, data collection and analysis, decision to publish, or preparation of the manuscript.

Competing Interests: The authors have declared that no competing interests exist.

* E-mail: mitarai@nbi.dk

Introduction

Many bacteria and archaea have multiple Toxin-Antitoxin (TA) loci [1], where the toxin normally inhibits cell growth, while the antitoxin neutralizes the activity of the toxin by forming a tight TA complex. One of the known functions of TA loci is to respond to nutritional stress [2], namely, toxins are activated upon nutritional starvation and slow down the rate of translation. When cells are under normal fast growth conditions, on the other hand, the majority of the cells will be in the antitoxin-dominated state, such that toxin activity is fully inhibited.

It has been found that many bacterial TA loci are auto-regulated at the transcriptional level by a mechanism called “Conditional Cooperativity” (CC) [3], where the transcription factor can bind cooperatively to the operator only if the concentrations of two different proteins satisfy a certain stoichiometric ratio. CC was quantitatively studied in one of the *Escherichia coli* TA loci, *relBE* [3–6]. Here the two proteins, the toxin (mRNase) RelE and the antitoxin RelB, are encoded by the same operon, which is negatively auto-regulated. The tight dimer RelB₂ is a weak transcriptional auto-repressor, but this repression is strongly enhanced by the presence of RelE and becomes strongest at RelB₂:RelE ratio 1:1. Over-expression of RelE above twice of RelB₂, though, will result in an abrupt de-repression of the promoter. This unique behavior is a consequence of formation of alternative hetero-complexes of RelB and RelE; RelB₂RelE and RelB₂RelE₂. Two RelB₂RelEs bind to the promoter site cooperatively to repress the promoter strongly, while RelB₂RelE₂ does not bind to the promoter.

Interestingly, all plasmid and chromosome-encoded TA loci investigated are found to be regulated by CC so far, including *relBE* of *E. coli* [3,4], *vapBC* of *Salmonella enterica* [7], *phd/doc* of plasmid P1 [8,9] and *ccdA/ccdB* of plasmid F [10]. This suggests that CC is a common feature for TA loci.

In our previous work, we have explored the function of CC in the starvation response of the RelBE system, and showed that CC prevents random toxin activation and promotes fast translational recovery when starvation conditions terminate. However, to reproduce the full dynamics of the starvation response, we took into account details of the RelBE system, which made the model rather specific to it. The primary purpose of this paper is to construct a simple mathematical model that demonstrates the functions of CC in a more general perspective.

TA loci have been suggested to be involved in persister formation [11–16]. When an antibiotic is applied to a growing bacterial population, the majority of the bacteria are killed. However, a very small fraction of them survives and re-grows after the antibiotic is removed. If the progeny of the bacteria is again sensitive to the same antibiotic, they are called persisters, in contrast to the resistant bacteria that have acquired resistance to antibiotic by mutation. Persisters are genetically identical to the sensitive cells, but believed to be in a non- or slow-growing, dormant state. Since the majority of antibiotics interferes with the cell growth and division process, cells can survive if they grow slowly or not at all.

The exact molecular mechanism underlying persistence is not fully understood. However, it has been found that mutations in *hipAB* genes severely increase the level of persisters formation. Interestingly *hipAB* is one of the TA loci in *E. coli* [11,13,14]. In

Author Summary

The effectiveness of antibiotics on many pathogenic bacteria is compromised by multidrug tolerance. This is caused by a small sub-population of bacteria that happen to be in a dormant, non-dividing state when antibiotics are applied and thus are protected from being killed. These bacteria are called persisters. Unraveling the basic mechanism underlying this phenomenon is a necessary first step to overcome persistent and recurring infections. Experiments have shown a connection between persister formation and the battle between a toxin and its antitoxin inside an *E. coli* cell. Toxin inhibits the cell growth but is neutralized by the antitoxin by forming a complex. The proteins also regulate their own production through this complex, thereby forming a feedback system that controls the growth of the bacterium. In this work we provide mathematical modeling of the feedback module and explore its abilities. We find that the auto-regulation with reduced growth associated with free toxins allows the cell to be bistable between two states: an antitoxin-dominated, normal growing one, or a dormant one caused by the activity of the toxin. The latter can be the simplest description of persister state. The toxin-antitoxin system presents a powerful example of mixed feedback design, which can support epigenetics.

addition, recent experiments [15] showed that removal of 10 mRNase-encoding TA loci reduced the persister fraction significantly. These observations strongly suggest that TA loci are important factors for persister formation.

One of the possible explanations is that stochastic activation of the toxin will slow down cell growth, resulting in a dormant state. This will be possible if the TA locus dynamics exhibits bistability, where a cell can be either in the antitoxin-dominated state that ensures the growth or in the toxin-dominated state that inhibits the growth. This viewpoint is also consistent with the observation that the persister state can be described as a metastable state with a constant stochastic switching rate to and from normal growing state [12].

This idea was theoretically pursued by Lou et al. [17] with a simple mathematical model that did not take CC into account. They concluded that, for bistability to be achieved, high cooperativity (Hill-coefficients ~ 4) is necessary, both in transcriptional auto-regulation of the TA operon and in the free toxin activity.

In this paper, we explore the basic features of CC as a regulation mechanism mediated by heteromer formation. We demonstrate that CC provides bistability in a simple feedback motif in a wide range of the parameters. We then construct a simplified model of TA system regulation and demonstrate that CC with growth rate-mediated feedback via toxin activity can provide the bistable alternatives between the antitoxin-dominated and the toxin-dominated states.

Results

Conditional regulation

Complex formation. We examine a simplified system, where protein A and T can form two kinds of heteromers, AT and ATT (Fig.1A):



Here, we assume that AT is the active molecule that act as a

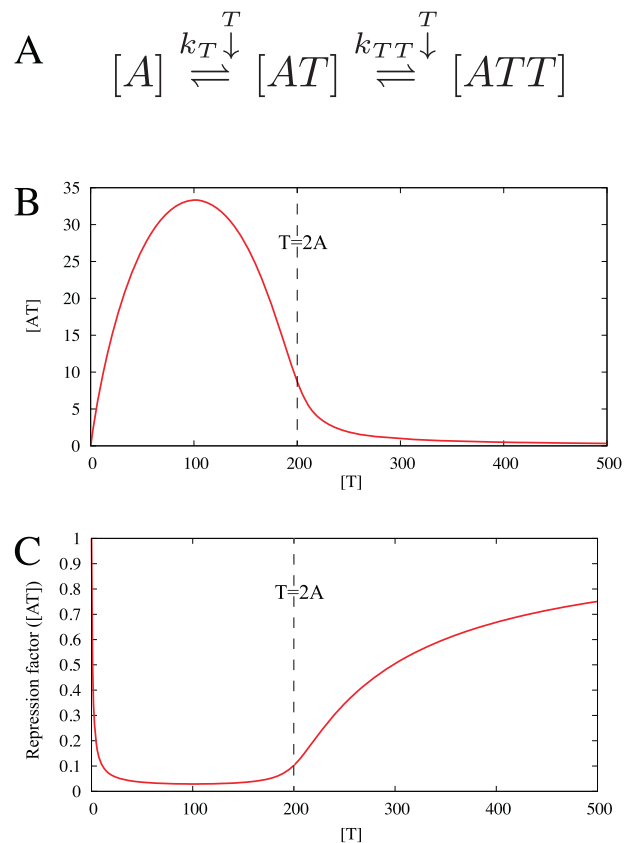


Figure 1. Heterocomplex formation in a TA system. (A) Reaction scheme of the heterocomplex formations, implying that the active complex [AT] is constrained by through $A=[A_f]+[AT]+[ATT]$ and $T=[T_f]+[AT]+2[ATT]$ with complex concentrations expressed by eq. (2). (B) Concentration of AT heteromers for a fixed value of $A=100$ as a function of T with $K_T=K_{TT}=1$. Note that it has a peak at $A=T$. In the strong binding limit of $K_T \rightarrow \infty$ with $K_{TT}=rK_T$ (r kept constant), $[AT]$ for $T < 2A$ is given by $\frac{1}{4-r}(-rA + \sqrt{r^2A^2 + (4-r)rT(2A-T)})$ for $r \neq 4$ and $T(2A-T)/(2A)$ for $r=4$, where $[AT]$ always has a peak at $A=T$. In this limit, $[AT]=0$ for $T \geq 2A$. (C) The behavior of $[AT]$ shown in (B) is reflected in the behavior of the repression factor $1/(1+[AT]/K_O)$ as a function of T , calculated for fixed $A=100$, and dissociation constant for AT-DNA binding $K_O=1$. doi:10.1371/journal.pcbi.1003174.g001

transcriptional repressor, whereas free A, free T, and ATT are not active in transcriptional control. This is a simplification of the transcriptional regulation by RelBE, where RelB₂ corresponds to one A, while RelE corresponds to one T.

The amount of active molecule $[AT]$ shown in Fig. 1 is determined from total A and T distributed among complexes $[AT]$ and $[ATT]$ according to

$$[AT] = \frac{[A_f][T_f]}{K_T}, \tag{2}$$

$$[ATT] = \frac{[T_f][AT]}{K_{TT}}, \tag{3}$$

Here K_T and K_{TT} are the dissociation constants for AT and ATT, respectively, whereas the concentration of free A (T) is denoted $[A_f]$ ($[T_f]$).

Fig. 1B shows $[AT]$ as a function of T for fixed A , pinpointing that when $T < A$, T is limiting the amount of AT, while $T > A$ implies that a substantial fraction of A is sequestered in the ATT complex. For $T > 2A$, ATT formation sequesters nearly all AT and $[AT]$ drops sharply to a value close to zero. This last transition can be ultrasensitive, provided that the binding between AT and ATT is strong, $K_{TT} \ll A$. For RelB-E system the binding is indeed very strong, with a measured K_{TT} in the nanomolar regime [6]. A sequestration-mediated ultra-sensitivity is also known in small RNA regulation [18–21] as well as in transcription factors [22–25]. In the present case, just a factor two difference in T around $T \approx 2A$ can change $[AT]$ dramatically.

This ultra-sensitivity is reflected in the promoter activity behavior, that shows a sharp de-repression occurring at $T \approx 2A$ (Fig. 1C), where $[AT]$ drops. Another unique feature of CC is its non-monotonicity, and an associated derepression for small T because $[AT]$ is small, see Fig. 1B,C.

Note that Fig. 1C does not include possible cooperativity in AT-DNA binding. The unique characteristics of CC, ultra-sensitivity by sequestration and non-monotonicity, do not require this cooperativity. For simplicity, therefore, we focus on regulation by AT without cooperativity, and we call it “conditional regulation” (CR), rather than CC. Of course, adding cooperativity will make the response even sharper, and the following results hold for the cooperative case, too.

Bistability in a simple feedback motif. We now study production of T repressed by AT, while A is fixed. The regulatory circuit is described by

$$\frac{dT}{dt} = \frac{\sigma}{1 + \frac{[AT]}{K_O}} - T, \quad (4)$$

where σ is the maximum production rate of T, and K_O is the dissociation constant of AT molecule to DNA. We assume that total A can be controlled and maintained at a steady state by a AT independent promoter. In this subsection, we take the lifetime of T to be the time unit and set $K_T = K_{TT} = 1$ for the dissociation constants, thus measuring concentrations of AT and ATT in units of their mutual binding strength. Further, focusing on CR, we assume that there is no cooperativity in binding of AT to promoter.

Fig. 2(A) shows the production term of eq.(4) as a function of T , for three different values of A with each of them two different values of K_O . The repression is always strongest at $T = A$, and sharp de-repression happens at $T > 2A$ for all the cases. The higher A , the more $[AT]$ will present when $A = T$, resulting in stronger repression at $A = T$ for larger A . The AT-DNA dissociation constant K_O also contribute to the repression strength.

The thick black line represents the degradation term in eq. (4), and the intersection between this and the production gives the steady state values of T . For small A ($=20$) with $K_O = 1$, there is only one crossing, happening at a relatively high value of T (≈ 900). At intermediate A ($=100$), there are two stable fixed points and one unstable fixed point in between ($T \approx 200$), reflecting a bistable system. At high A ($=400$), the high T fixed point vanishes and the system settles at a monostable state with low T . We have also analyzed the systems systematically for weaker repression, i.e. higher values of K_O , and again found bistability provided that A (and thus T) is increased accordingly.

In addition, the non-monotonicity of the CR has a striking implication in regulation at low T values: It guarantees that the low (uninduced) T steady state value has finite amount of T that

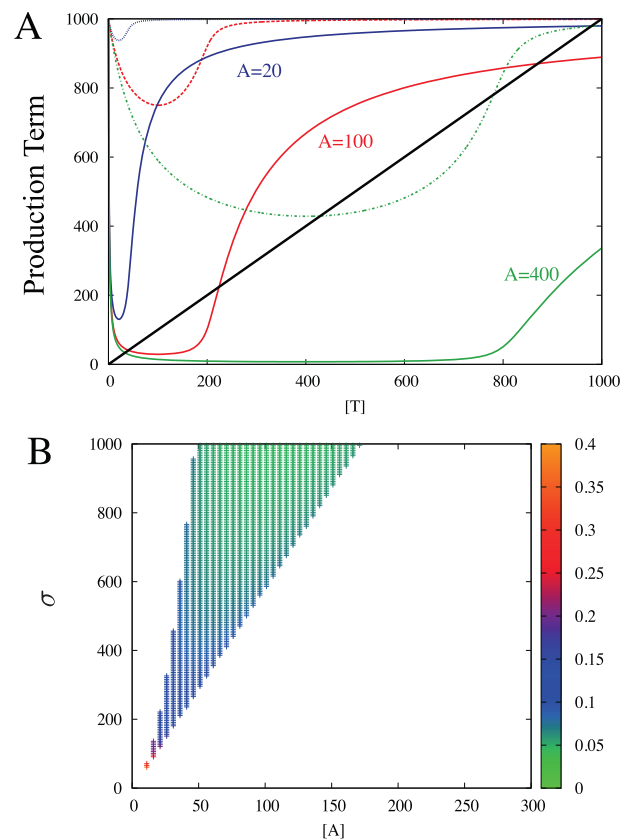


Figure 2. Conditional regulation of T with fixed A concentration. (A) Production term of eq. (4) as a function of T for $\sigma = 1000$, for $A = 20$ (blue line), 100 (red line), and 400 (green line). The solid lines represent $K_O = 1$ case, and the dashed lines represent $K_O = 100$ case, where K_O is the dissociation constant for the binding of AT-DNA. (B) Region in the parameter space (A , σ) that shows bistability for $K_O = 1$. The color of each bistable point represents the ratio between the low- T fixed point and the high- T fixed point. doi:10.1371/journal.pcbi.1003174.g002

is maintained at a level nearly independent of A (Fig. 2A, compare $A = 100$ and 400 with $K_O = 1$). This is an important feature for TA system in terms of the starvation response, as discussed later.

Remarkably, the system exhibits bistability without cooperative binding to DNA. In the TA system the cooperativity is instead provided by the ultrasensitive de-repression at $T = 2A$ that is facilitated by a very strong protein-protein binding [22–25]. This bistability is seen in a wide range of A and σ values as shown in Fig. 2(B). The larger σ and A , the high- T steady state value increase proportionally, while the low- T steady state value remains practically unchanged. Thus, as externally imposed A is increased, the model predict a larger contrast between the two steady states. If the binding to DNA is cooperative, the de-repression at ATT formation becomes even sharper, thereby favouring bistability.

We have also studied other possible motifs, where either T or A is repressed or activated by AT complex (data not shown). For example we found that if AT activate A while T is kept constant, one can obtain bistability between a high A state and a low A state in a wide range of parameters. This bistability is again supported by the ultrasensitivity of AT sequestration, as $[AT]$ increase sharply with increasing A around $\sim T/2$.

Simple model of persister formation

In this section, we construct a simple model of TA activity control with CR, a model aimed at capturing the central features of persister formation. We use the RelBE system as a reference because the molecular interactions and parameters are best known here. The reference parameters are listed in Materials and Methods.

In RelBE [6], the antitoxin RelB and the toxin RelE are encoded by the same operon, and transcriptionally auto-regulated by CC. RelE is metabolically stable, and its concentration decreases only by dilution due to cell division (generation time ~ 30 min in log phase growth in rich medium). On the other hand, RelB is actively degraded by protease Lon, resulting in its very short half-life of ~ 3 min. In spite of this, the RelB concentration in a normally growing cell is about 10 times of that of RelE [4], suggesting that the RelB mRNA is translated about 100 times more often than RelE mRNA [6].

This situation is depicted in Fig. 3A1. Since both toxin T and antitoxin A are regulated by the same promoter, the corresponding equations apply:

$$\frac{dT}{dt} = \frac{\sigma_T}{1 + \frac{[AT]}{K_O}} - T \quad \text{and} \quad \frac{dA}{dt} = \frac{\sigma_A}{1 + \frac{[AT]}{K_O}} - \Gamma_A \cdot A, \quad (5)$$

where σ_T and σ_A are the maximal production rate for T and for A, respectively. The dilution rate of T is given by cell division,

and is taken as a unit rate, while Γ_A is the active degradation rate of A.

This motif, however, cannot exhibit bistability. Fig. 3A2 shows example null-clines, which have only one stable fixed point at the antitoxin dominated state. We performed parameter scan spanning from 1/8 to 8 fold relative to the values used for Fig. 3A2, but did not find any combination of parameters that gives bistability, even if we allow cooperative binding of AT to DNA with Hill coefficient 2 (data not shown). This absence of bistability is due to A being regulated identically to T. Accordingly, the de-repression of the promoter around $T \approx 2A$ increases not only the toxin production but also the antitoxin production, and the latter is so large that the system remains in the antitoxin-dominated state.

When we include the activity of free toxin on cell growth, however, the model system can show bistability. This is because the toxin-induced arrest of cell growth prolong lifetime of T, while leaving A being degraded by Lon at a high rate. The mathematical formulation of this extended model is

$$\frac{dT}{dt} = \frac{\sigma_T}{\left(1 + \frac{[AT]}{K_O}\right)(1 + \beta_M T_f)} - \frac{1}{1 + \beta_C [T_f]} \cdot T \quad (6)$$

$$\frac{dA}{dt} = \frac{\sigma_A}{\left(1 + \frac{[AT]}{K_O}\right)(1 + \beta_M [T_f])} - \Gamma_A \cdot A. \quad (7)$$

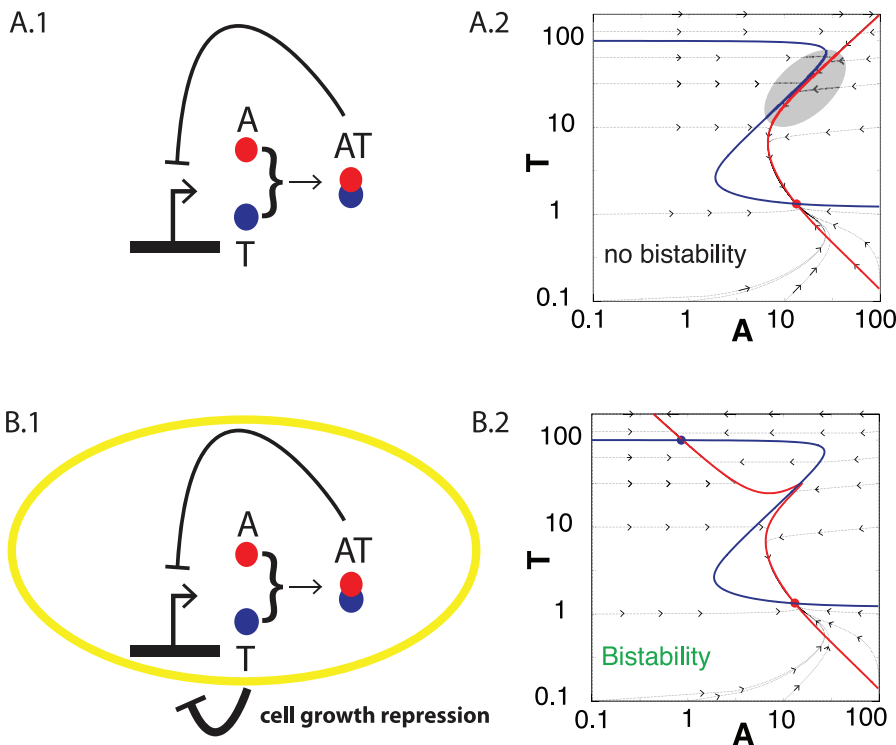


Figure 3. TA system with CR without and with feedback through free toxin activity. (A.1) Schematic representation of the genetic circuit described by eq. (5) for TA system with CR, without considering toxic activity of free T. (A.2) Null-clines for eq. (5). Blue line represents $\frac{dT}{dt} = 0$, and red line represents $\frac{dA}{dt} = 0$. For comparable values of A and T the two null clines become parallel and does not cross, as shown in the area highlighted in grey, i.e. the system does not show bistability. The parameters used are listed in Table 1 in Materials and Methods. Dashed lines with arrows show the flow to the fixed point. (B.1) Schematic representation of the genetic circuit described by the model (6) and (7) with $\beta_M = \beta_C \approx 11$. (B.2) Null-clines for the system of eqs. (6) and (7) with $\beta_M = \beta_C \approx 11$. Blue line $\frac{dT}{dt} = 0$, Red line $\frac{dA}{dt} = 0$. Dashed lines with arrows show the flow to the stable fixed points. doi:10.1371/journal.pcbi.1003174.g003

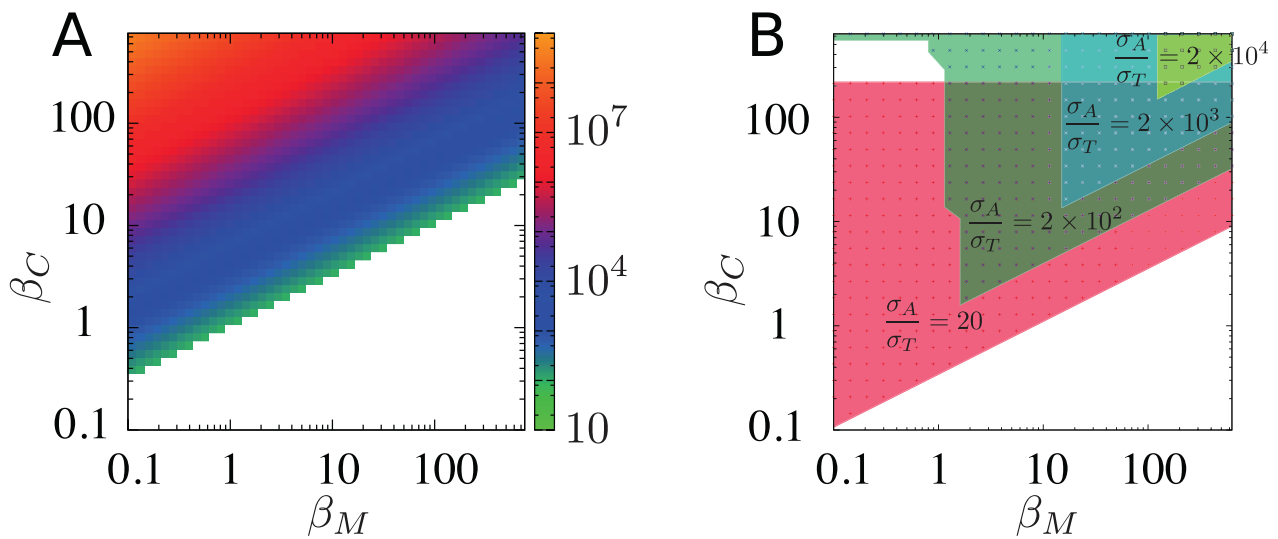


Figure 4. The state diagram of the bistability. Colored region represents the combinations of (β_M, β_C) that makes the system bistable. (A) Reference parameters in table 1 are used except for β_M and β_C . The color code represents ratio between T dilution rate calculated upon the low- T steady state and the high- T steady state, $[1 + \beta_c T_f(\text{high})]/[1 + \beta_c T_f(\text{low})]$. (B) Bistable region for various values of $\frac{\sigma_A}{\sigma_T}$, with $\sigma_T = 100$. The remaining 6 parameters are fixed to the reference values. The shaded regions represent the areas in the 2D parameters space β_M, β_C that show bistable behavior. doi:10.1371/journal.pcbi.1003174.g004

expressing that $[T_f]$ reduces all protein production, and accordingly also decreases the dilution by cell growth. β_M represents the reduction of protein expression per free toxin (T_f) molecule, and β_C represents the growth inhibition per free toxin molecule. Notice that $[T_f]$ does not influence degradation of A, because it is anyway so unstable that cell division hardly affects its concentration.

These terms correspond to the growth-rate dependent feedback [17,26,27]. The reduction of the protein production (β_M term) can account for both direct activity of free toxin to TA locus and the global slowdown of the transcription rate due to change of physiological conditions [26]. Comparison of the present model with the steady state growth data in Ref.[26] is given in Text S1. We expect $\beta_M \approx \beta_C$ because the slowing down of the growth rate is due to the global slowing down of the protein production. At the same time, there can be some quantitative difference because β_M may include the effect specific to the TA locus.

The growth-rate reduction mediated by T constitutes a positive feedback [17,26,27] on T accumulation, which is essential for bistability and persister formation. The term with β_M reduces the production of both antitoxin and toxin, and thus overall weaken the ability to maintain the bistability. Note that β_M primarily influences the transition state from A to T dominated state, because the reduction of production targets the short lived A protein first.

Fig. 3B1 examines eqs. (6)–(7) with parameters extracted from the RelBE system [6] (see the figure caption of Fig. 3). The nullclines in Fig. 3B2 are from the $\beta_M = \beta_C \approx 11$ case, exhibiting two stable fixed point, one at the antitoxin-dominated state (the low- T state, $A \approx 10$, $T \approx 1$) and another at the toxin dominated state (the high- T state, $A \approx 1$, $T \approx 100$). Note that the antitoxin dominated state has almost the same concentrations as the stable fixed point in Fig. 3A2 with $\beta_M = \beta_C = 0$. The antitoxin dominated state scarcely depends on β_M and β_C , since there is almost no free toxin ($[T_f] \approx 0$) in the antitoxin dominated state.

Figure 4A shows the ratio between the T dilution rates at the low and high T steady state, $[1 + \beta_c T_f(\text{high})]/[1 + \beta_c T_f(\text{low})]$.

The figure illustrates that our model predicts bistability for a wide range of parameters, and further that this bistability is indeed governed by the increase in cell generation parameterized by the β_C term. For too large β_M the bistability is counteracted because the toxin production is reduced too much by free toxin to accumulate enough for the stable high toxin state. Remarkably, for proportional reduction of protein production and increased cell generation, $\beta_M = \beta_C$, the model predicts bistability for all $\beta_M = \beta_C > 1$.

We also studied the robustness of the bistability against parameter change. One of the most crucial parameters for the bistability is the ratio σ_A/σ_T , because this determines the difference of the concentration of A and T. We therefore varied σ_A/σ_T with keeping σ_T constant, and searched for the bistable regime in (β_M, β_C) space. The rest of the parameters are kept same as those used in Fig. 4A. Only $\sigma_A/\sigma_T > 10$ is considered, because lower ratios prevent antitoxin domination due to its 10 times higher degradation rate. For rather small $\sigma_A/\sigma_T (\approx 20)$, too large β_C makes the anti-toxin dominated state unstable, because very small amount of free toxin is enough to activate the positive feedback to toxin via the growth rate. With even larger σ_A/σ_T , stronger feedback is needed to stabilize toxin-dominated state, reflected in larger values of β_C and β_M .

We further performed scanning of other parameters. We fixed one parameter at a time and sampled the rest of the parameters randomly to test 1000 samples in logarithmic scale within the range between 1/8 to 8 fold of the reference values. We then systematically changed the fixed parameters between 1/8 to 8 fold and repeated the procedure, to see the effect of the parameter. We found that 20% to 80% of the samples showed bistability. The detailed results are given in Text S2. We also explored the effect of the dissociation constant K_T and K_{TT} more intensively, by changing $K_T = K_{TT}$ from the reference value to 64 fold, since they describe the sharpness of the CR and this is expected to influence the bistability. We find that the number of bistability parameter sets decreases gradually with the fold change of K_T and K_{TT} . Details are given in Fig. S4.

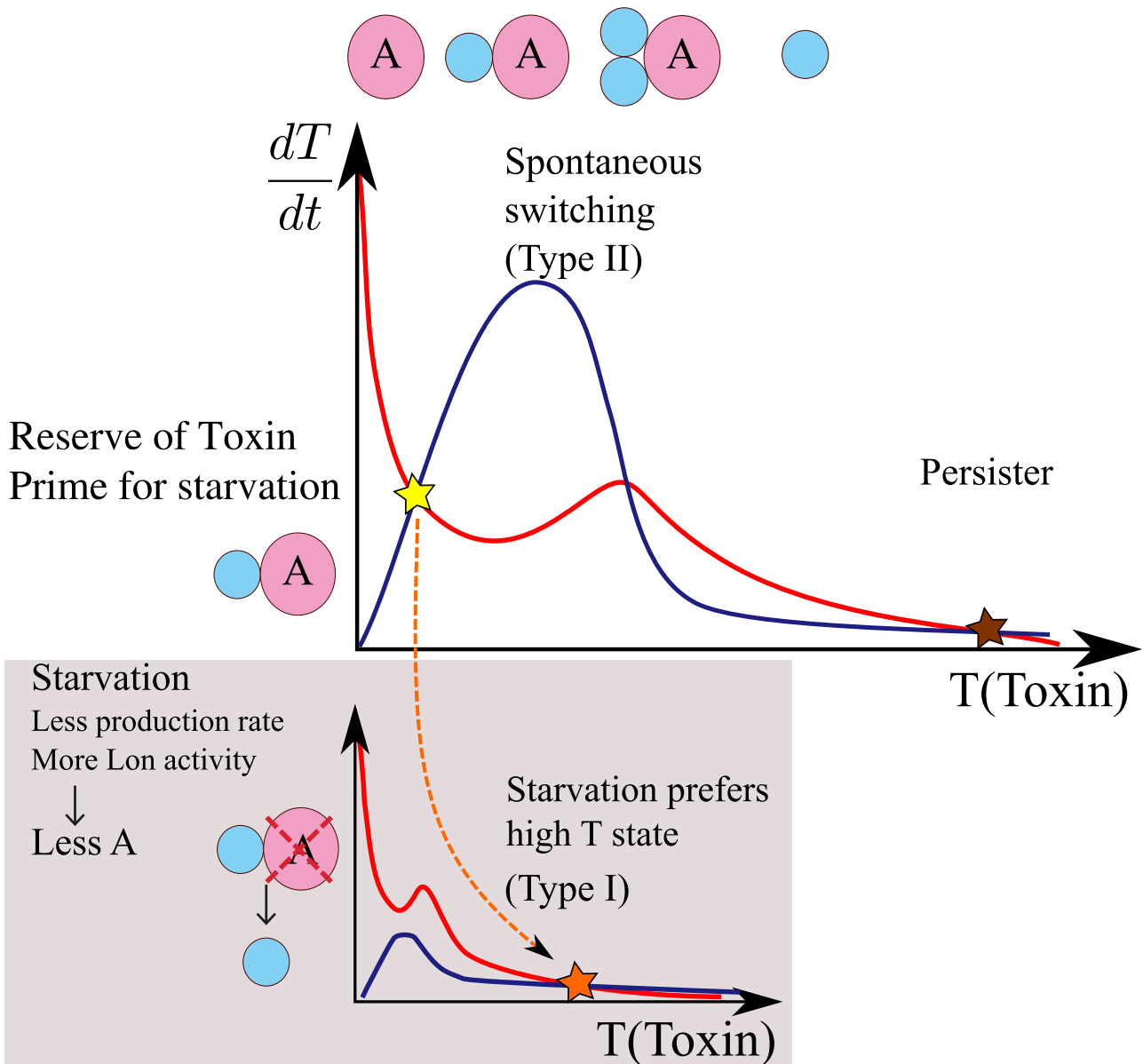


Figure 5. Schematic summary of the role of conditional regulation in persister formation. The red curves show the toxin production rate and the blue lines give the degradation rate, both from eq. (6). Both terms depend on A , and here we make approximation that A is always in steady state (eq. 7 with $dA/dt=0$) for given T , because dynamics of A is much faster than T due to high production and degradation rate. Since production term of A and T are proportional to each other and A is degraded at a constant rate, resulting A concentration is proportional to the production term of T (red curves). The scales of curves are modified from actual functional forms so that the characteristic behaviours can be grasped easily. The ultra-sensitivity mediated by protein-protein binding combined with feedback from free toxin activity is reflected in the peak of the production rate and drop of the degradation rate, resulting in bistability of the system. This accounts for the type II persister where a cell can spontaneously switch to and out of the persister state. The non-monotonicity of the conditional regulation secures that some toxins are stored in antitoxin dominated state, helping the transition to the stress-induced activation of toxin [6], which becomes the base for type I persister formation. doi:10.1371/journal.pcbi.1003174.g005

Discussion

Using known parameters for the RelBE system in *E. coli*, we constructed a minimal model for TA activity, combining conditional regulation with a feedback from free toxin to the cell growth. It was demonstrated that this model shows bistability for a wide range of parameters, with a stable state corresponding to the antitoxin-dominated, normal growing state, and another metastable state corresponding the toxin

dominated state, potentially corresponding to the persister state.

Noticeably, the model eqs. (6)–(7) did not rely on details of the molecular mechanisms of how the toxin works, and therefore the model is not limited to the RelBE system. The important assumptions are: (i) The TA system is conditionally regulated, (ii) toxins are stable and diluted mainly by cell division, while antitoxins are metabolically unstable, and (iii) free toxins reduce the productions of proteins and hence cell growth. All the

Table 1. Reference parameter values.

	$X[6]$	\rightarrow	\rightarrow	\bar{X}
σ_T	$166.28nMmin^{-1}$	$\frac{\sigma_T \cdot \tau_u}{C_u}$	$\frac{166.28nMmin^{-1} \cdot 43min}{71.5nM}$	100
K_O	1 nM	$\frac{K_O}{C_u}$	$\frac{1nM}{71.5nM}$	0.015
K_T	0.3 nM	$\frac{K_T}{C_u}$	$\frac{0.3nM}{71.5nM}$	0.004
K_{TT}	0.3 nM	$\frac{K_{TT}}{C_u}$	$\frac{0.3nM}{71.5nM}$	0.004
Γ_A	$0.2min^{-1}$	$\Gamma_A \cdot \tau_u$	$0.2min^{-1} \cdot 43min$	10
Γ_T	$0.02min^{-1}$	$\Gamma_T \cdot \tau_u$	$0.02min^{-1} \cdot 43min$	1
β_C	$0.16nM^{-1}$	$\beta_c \cdot C_u$	$0.16nM^{-1} \cdot 71.5nM$	11
β_M	$0.16nM^{-1}$	$\beta_c \cdot C_u$	$0.16nM^{-1} \cdot 71.5nM$	11

doi:10.1371/journal.pcbi.1003174.t001

conditions are satisfied in the TA loci that are confirmed to be regulated by conditional cooperativity [3,4,7–10].

Our simple model pinpoints minimal ingredients for obtaining a persister state, but did not include stochastic production and/or degradation, and therefore cannot address the switching rates. In order to understand stochastic persister formation in *E. coli*, just performing stochastic simulation of the present motif is not enough, because the frequency of persisters depends on multiple parallel TA systems. In *E. coli*, 11 simultaneously interfering TA systems maintain a probability of persisters to be about 0.01%, while this probability is changed substantially first when about 50% of the TA systems is removed [15]. This clearly suggests that the interference of parallel systems has a strong influence to the switching behavior. Furthermore, comparing the stochastic simulations with the experimentally observed frequency of persisters requires a knowledge of the underlying distribution of the T expression levels and corresponding growth rates in the cell population. It is not a simple task when the single cell growth rate depends on T expression levels, because it feeds back to the frequency of the cells as pointed out by Nevzhay et al. in [28]. In addition, it has been suggested that there is a strong link between the activation of the protease Lon and the TA-mediated persister formation, through the increase of the antitoxin degradation rate [15,16]. The fluctuation of the Lon activity may be particularly important in determining switching rates, because it can provide coherent noise that favours simultaneous switching of many TAs to the persister state. It should also be noted that the Lon activity is activated by polyphosphate, which is regulated by the stringent response signalling molecule (p)ppGpp [16]. We plan to extend the present model to include these features and study the switching behavior in near future.

It is still interesting to think about possible implication of the observed switching rate to the present model. The fact that the persister formation is a rare event may indicate that the actual parameter value in the real system is located close to the boundary between the bistable region and the monostable region of the antitoxin-dominated state. Such parameter values can be chosen through selection process in a fluctuating environment, where slow growth of the persister pays off as a risk hedging strategy; the switching rate is expected to reflect the time scale of the temporal fluctuation of the environment [29].

Conditional regulation is an example of mixed feedback motifs [30], where protein-protein interactions and transcriptional repression are combined. In natural systems, protein-protein interaction mediated bistable switch was previously found for example in the

epigenetic switch of the TP901 phage [23,25] and in the sigma-factor/antisigma-factor system [24]. Conditional cooperativity in TA systems opens for a toolbox of regulatory units that can exhibit sufficient bistability to support also epigenetics. When removing the toxic ability of toxin, which has been done for RelE [3], and separating antitoxin from the operon to allow independent control, the strong binding between RelE and RelB should provide extreme ultrasensitivity, and thus very well separated metastable states. This conditional cooperativity-mediated bistability is the base for the bistability in full TA systems, and thus for the type II persister formation [12,13], where a cell can spontaneously switch between the dormant state and the growing state (Fig. 5).

While simple protein-protein heteromers could produce ultrasensitivity, the non-monotonicity of the conditional cooperativity also secure that the antitoxin dominated state has a substantial amount of toxins present (Fig. 5). These toxins' activity is normally inhibited by short lived antitoxins, but the stored toxins can be used for faster switching to a dormant state if overall protein productions are externally inhibited, for example by starvation (Fig. 5). Therefore, the non-monotonicity may enhance the transition to type I persister formation [12,13], where environmental stress triggers persister formation.

The importance of the protein-protein interaction mediated ultrasensitivity [22–25] and the growth rate-mediated feedback [17,26–28] to bistable systems have been discussed as independent regulatory features in recent literature [31]. The uniqueness of the bistability in the TA system is that *it combines both of these mechanisms*. The need for combining these two mechanisms is closely associated with the fact that T and A are produced from the same operon, and thus are exposed to identical transcription regulation. Though it is difficult to get bistability with only one of the mechanisms [17], the TA system realizes a persister state by regulating the products of one operon through a combination of growth modulation and hetero-complex formation.

Materials and Methods

Numerical solutions of the model equations

All the numerical analyses are done using C++ codes developed by the authors. When necessary, $[AT]$ was calculated by solving algebraic equations (2) and (3) with conservation of mass for a given amount of (A, T) by Newton's method [32]. The bistable solutions in Fig. 2 B (Fig. 4) were obtained by finding the fixed points for $dT/dt=0$ with eq. (4) ($dT/dt=0$ and $dA/dt=0$ with

eqs. 6 and 7) by Newton's method and then evaluating the stability based on the Jacobian. The trajectories that constitute the flux in Figs. 3A2 and 3B2 were calculated by the 4th-order Runge-Kutta method [32].

Reference parameters

The values of the parameters used in the ODEs correspond to a conversion to dimensionless numbers of the parameters relative to the *RelBE* system we studied in [6].

In particular we used the lifetime of *RelE* in exponential growth conditions ($\frac{1}{\Gamma_0}$) as time-unit (τ_u) and the maximal amount of *A* proteins produced in the unit time as concentration unit (C_u). In the *RelBE* system $\frac{\sigma_A}{\Gamma_0} \simeq 715000$ nM thus fixing $\sigma_A = 10000$ we obtain $C_u = 71.5$ nM, while $\tau_u = \frac{\sigma_A}{\Gamma_0} = 43$ min. The value of β_M in the starved condition [6] was evaluated to be around 1000 in this units. However, it is expected to be smaller in the normal condition, since *RelE* cleaves mRNA at the ribosomal A-site, which is expected to be more accessible at the starvation. Therefore, we mostly explore β_M values smaller than 1000.

The reference parameters are shown in table 1.

Supporting Information

Figure S1 Fit of the free toxin activity parameters to the grown-rate dependent global transcription rate. Left: Red points: Global transcription rate $\alpha_m(\Gamma)$ from Klumpp et al. [26]. Green Line: normalised production rate $\alpha(\Gamma)$ from our model with $\beta = 0.4$. Right: Red points: Normalized global transcription rate multiplied by gene copy number, $\alpha_m(\Gamma)g(\Gamma)/g(1)$ from Klumpp et al. [26]. Green Line: normalised production rate $\alpha(\Gamma)$ from our model with $\beta = 1.2$.
(EPS)

Figure S2 β_M/β_C fitted to the global transcription rate lies in the bistable region. Each green dot in the plot represents a combination of β_M and β_C that give bistable results. The red line represents $\beta_M/\beta_C = 0.4$, and the black line $\beta_M/\beta_C = 1.2$.
(EPS)

Figure S3 The robustness of the bistability against parameter change. We fix $\sigma_T = 100$ and $\Gamma_0 = 1$, and vary rest

References

- Pandey D, Gerdes K (2005) Toxin-antitoxin loci are highly abundant in free-living but from host-associated prokaryotes. *Nucleic Acids Research* 33: 966–976.
- Christensen SK, Mikkelsen M, Pedersen K, Gerdes K (2001) *RelE*, a global inhibitor of translation, is activated during nutritional stress. *Proc Natl Acad Sci USA* 98: 14328–14333.
- Overgaard M, Borch J, Jørgensen M, Gerdes K (2008) Messenger RNA interferase *RelE* controls *relBE* transcription by conditional cooperativity. *Mol Microbiol* 69: 841–857.
- Overgaard M, Borch J, Gerdes K (2009) *RelB* and *RelE* of *Escherichia coli* form a tight complex that represses transcription via the ribbon-helix-helix motif in *RelB*. *J Mol Biol* 394: 183–196.
- Bøggild A, Sofos N, Andersen K, Feddersen A, Easter A, et al. (2012) Messenger RNA interferase *RelE* controls *relBE* transcription by conditional cooperativity. *Structure* 20: 1641–1648.
- Cataudella I, Trusina A, Snekpen K, Gerdes K, Mitarai N (2012) Conditional cooperativity in toxinantitoxin regulation prevents random toxin activation and promotes fast translational recovery. *Nucleic Acid Res* 40: 6424–6434.
- Winther K, K G (2012) Regulation of enteric *valbc* transcription: induction by vapc toxin dimer breaking. *Nucleic Acid Res* 40: 4347–43576.
- Magnuson R, Yarmolinsky M (1998) Corepression of the p1 addiction operon by phd and doc. *J Bacteriol* 180: 6342–6351.

of the parameters. In (a) β_M is changed systematically between $\frac{1}{8}$ and 8 fold of the value used in the main text $\beta_M^0 = 11.4475$; we change it between $\frac{1}{8} \cdot \beta_M^0 = 1.4309$ and $8 \cdot \beta_M^0 = 91.58$ with a pace given by $2^n \cdot \beta_M^0$ with an integer $n \in [-3, 3]$. For each value of β_M , we sample rest of the parameters randomly and independently of each other, and they can take any values from the set $2^n \cdot$ (the reference value) with $n \in [-3, 3]$. The reference values are given in Table 1. We collect a sample of 1000 points in the parameter space. The bars in the histogram represent the fraction of this sample of points in the parameter space that still shows bistable behavior. The same procedure is then carried out for β_C (b), Γ_B (c), K_T (d), K_{TT} (e), K_O (f) and σ_A (g).
(EPS)

Figure S4 The robustness of the bistability against the change of the dissociation constants K_T and K_{TT} . We set $K_T = K_{TT}$, and increase them systematically from the reference value (0.004) to 64 fold of the reference value. Since the dissociation constants set the concentration of *A* and *T* at which *AT* and *ATT* formation is significant, we fix $\sigma_A = 10000$ and $\Gamma_A = 10$ in addition to fixing $\sigma_T = 100$ and $\Gamma_0 = 1$. We then sample the rest of the parameters randomly in the base 2 logarithmic scale, within 1/8 to 8 fold of the reference value. We tried 1000 parameter sets for each values of $K_T = K_{TT}$. The plot shows the fraction of the parameter set that shows the bistability. We see that the number of bistability parameter sets decrease gradually with fold increase of the dissociation constants.
(EPS)

Text S1 Correspondence of parameters with the growth rate dependence data of protein production rate in the steady state growth.
(PDF)

Text S2 Parameter scan by Monte Carlo sampling to test the robustness of bistability.
(PDF)

Author Contributions

Wrote the paper: IC KS KG NM. Model building and model analysis: IC KS KG NM.

19. Levine E, Zhang Z, Kuhlman T, Hwa T (2007) Quantitative characteristics of gene regulation by small rna. *PLoS Comp Biol* 5: e229.
20. Mitarai N, Andersson A, Krishna S, Semsey S, Sneppen K (2007) Efficient degradation and expression prioritization with small rnas. *Physical Biology* 4: 164171.
21. Mitarai N, Benjamin J, Krishna S, Semsey S, Csiszovszki Z, et al. (2009) Dynamic features of gene expression control by small regulatory rnas. *Proc Natl Acad Sci USA* 106: 10655–10659.
22. Buchler N, Cross F (2009) Protein sequestration generates a flexible ultrasensitive response in a genetic network. *Molecular Systems Biology* 5: 272.
23. Nakanishi H, Pedersen M, Alsing A, Sneppen K (2009) Modeling of the genetic switch of bacteriophage ϕ 901-1: A heteromer of *ci* and *mor* ensures robust bistability. *J Mol Biol* 394: 15–28.
24. Chen D, Arkin A (2012) Sequestration-based bistability enables tuning of the switching boundaries and design of a latch. *Mol Syst Biol* 8: 620.
25. Pedersen M, Hammer K (2008) The role of *mor* and the *ci* operator sites on the genetic switch of the temperate bacteriophage ϕ 901-1. *J Mol Biol* 384: 577–589.
26. Klumpp S, Zhang Z, Hwa T (2009) Growth rate-dependent global effects on gene expression in bacteria. *Cell* 139: 1366–1375.
27. Tan C, Marguet P, You L (2009) Emergent bistability by a growth-modulating positive feedback circuit. *Nature Chemical Biology* 5: 842–848.
28. Nevozhay D, Adams R, Van Itallie E, Bennet M, Balazsi G (2012) Mapping the environmental fitness landscape of a synthetic gene circuit. *PLoS Comput Biol* 8: e1002480.
29. Krussel E, Kishony R, Balaban N, Leibler S (2005) Bacterial persistence: A model of survival in changing environment. *Genetics* 169: 1807–1814.
30. Francois P, Hakim V (2004) Design of genetic networks with specified functions by evolution in silico. *Proc Natl Acad Sci USA* 102: 580–585.
31. Ray J, Tabor J, Igoshin O (2011) Non-transcriptional regulatory processes shape transcriptional network dynamics. *Nature Reviews Microbiology* 9: 817–828.
32. Press A, Teukolsky W, Vetterling W, Flannery B (2007) *Numerical recipes 3rd edition: The art of scientific computing*. Cambridge University Press.

Text S1: Correspondence of parameters with the growth rate dependence data of protein production rate in the steady state growth

Klumpp et al. [1] reported that a decrease in cellular growth rate results in a global slow down of transcription, and provided the relative change of the transcription rate for steady state growth.

In our model equations,

$$\frac{dT}{dt} = \frac{\sigma_T}{\left(1 + \frac{[AT]}{K_O}\right) (1 + \beta_M [T_f])} - \frac{\Gamma_0}{1 + \beta_C [T_f]} \cdot T \quad (1)$$

$$\frac{dA}{dt} = \frac{\sigma_A}{\left(1 + \frac{[AT]}{K_O}\right) (1 + \beta_M [T_f])} - \Gamma_A \cdot A. \quad (2)$$

the growth rate slows down due to the free toxin, characterised by β_C , while the protein production rate is reduced at the same time, which is characterised by β_M . We can reproduce the relation in [1] when β_C and β_M satisfy a certain relation as follows.

In our model, the term $\Gamma \equiv \frac{\Gamma_0}{1 + \beta_C [T_f]}$ in equation is the division rate. In ref. [1], cell division rate is measured in terms of doubling per hour, while our Γ_0 is estimated to be 30 minutes doubling time [2]. Namely, we have

$$\Gamma = \frac{2 \text{dbl}/\text{hour}}{1 + \beta_C [T_f]}, \quad (3)$$

and we get the amount of free toxin as a function of Γ [dbl/hour]:

$$[T_f] = \frac{2 - \Gamma}{\beta_C \cdot \Gamma}. \quad (4)$$

This gives the growth-rate dependent protein production change in our model to be

$$\tilde{\alpha}(\Gamma) = \frac{1}{1 + \beta_M [T_f]} = \frac{\Gamma/(2\beta)}{1 + \frac{1-\beta}{2\beta} \Gamma},$$

where $\beta \equiv \beta_M/\beta_C$.

In ref. [1], the growth-rate dependent change of the transcription rate $\alpha_m(\Gamma)$ normalised by the value at $\Gamma = 1$ and the gene copy number $g(\Gamma)$ is given. In Fig. S1 left, we plotted $\alpha_m(\Gamma)$ and fitted β so that normalised growth-dependent production rate

$$\alpha(\Gamma) = \frac{\tilde{\alpha}(\Gamma)}{\tilde{\alpha}(1)} = \frac{\frac{1+\beta}{2\beta} \cdot \Gamma}{1 + \frac{1-\beta}{2\beta} \cdot \Gamma} \quad (5)$$

agrees best with the data. With $\beta \approx 0.4$, we get a good fit to the data.

If we also take into account the change in the gene copy number, we should compare $\alpha_m(\Gamma)$ with $\alpha_m(\Gamma)g(\Gamma)/g(1)$, which is shown in Fig. S1 right. In this case, we get $\beta \approx 1.2$.

In fig S2, we plotted the lines $\beta = \frac{\beta_M}{\beta_C} = 0.4$ and $\beta = \frac{\beta_M}{\beta_C} = 1.2$ in the phase diagram for the bistability with reference parameters, which demonstrate that we can get bistability with satisfying the relation from [1].

It should be noted that the growth-rate change in [1] is obtained by the steady state exponential growth, and the relation may not be the same if the growth rate is changed dynamically by the overproduction of toxin.

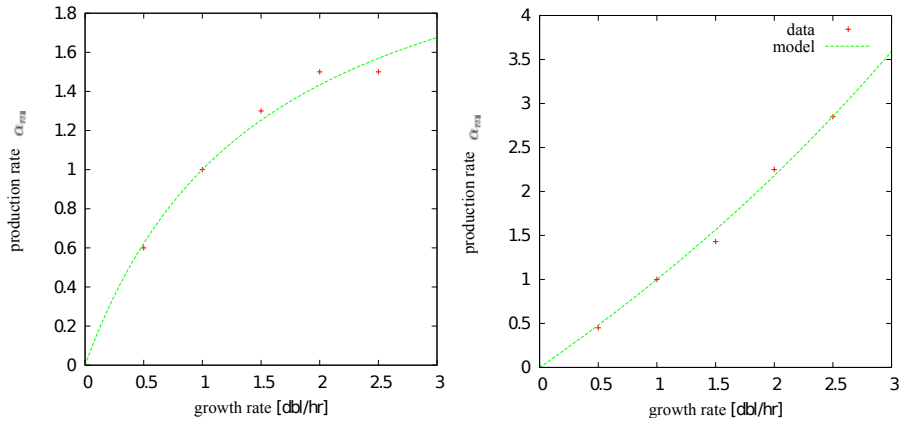


Figure S1: **Fit of the free toxin activity parameters to the growth-rate dependent global transcription rate.** Left: Red points: Global transcription rate $\alpha_m(\Gamma)$ from Klumpp et al. [1]. Green Line: normalised production rate $\alpha(\Gamma)$ from our model with $\beta = 0.4$. Right: Red points: Normalized global transcription rate multiplied by gene copy number, $\alpha_m(\Gamma)g(\Gamma)/g(1)$ from Klumpp et al. [1]. Green Line: normalised production rate $\alpha(\Gamma)$ from our model with $\beta = 1.2$.

References

- [1] S. Klumpp, Z. Zhang, T. Hwa "Growth-rate dependent global effects on gene expression in bacteria" *Cell* **139(7)** 1366-1375 (2009)
- [2] I. Cataudella, A. Trusina, K. Sneppen, K. Gerdes and N. Mitarai "Conditional cooperativity in toxin antitoxin regulation prevents random toxin activation and promotes fast translational recovery" *Nucleic Acids Res.* **40** 6424-6434 (2012).

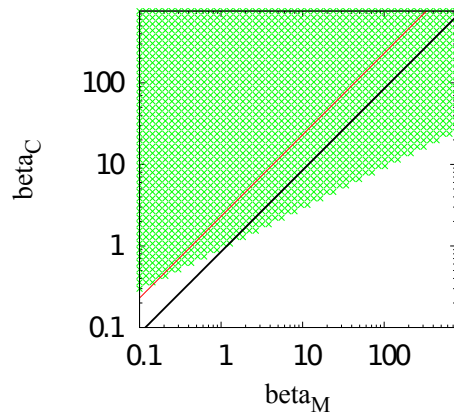


Figure S2: β_M/β_C fitted to the global transcription rate lies in the **bistable region**. Each green dot in the plot represents a combination of β_M and β_C that give bistable results. The red line represents $\beta_M/\beta_C = 0.4$, and the black line $\beta_M/\beta_C = 1.2$.

Supplement: Conditional cooperativity of Toxin - Antitoxin regulation can mediate bistability between growth and dormancy

Ilaria Cataudella, Kim Sneppen, Kenn Gerdes, and Namiko Mitarai

Text S2: Parameter scan by Monte Carlo sampling to test the robustness of bistability.

We tested the robustness of the bistability against parameter change by using the Monte-Carlo sampling. We fixed σ_T and Γ_0 , which define the units, and scanned β_M , β_C , Γ_A , K_T , K_{TT} , K_O , and σ_A . In order to understand the systematic dependence on the parameter, if any, we change one of the parameters systematically, and sample the rest of the parameters randomly in the base 2 logarithmic scale, with in 1/8 to 8 fold of the reference value. We summarise the result in this section.

In fig S3 a) the effects of changing the value of β_M are investigated. The value used in the main text is $\beta_M^0 = 11.4475$ and we change it between $\frac{1}{8}\beta_M^0 = 1.4309$ and $8 \cdot \beta_M^0 = 91.58$. β_M quantifies the entity of the negative feedback on production of both A and T due to the increase in the concentration of T_f . The fraction of the sample of parameter sets that shows bistability decreases with increasing β_M . For high values of β_M bistability is lost because the high T fixed point tends to disappear. This is because an increase in T_f will result in a strong inhibition in production of both A and T , but T maximal production rate is , in the best case scenario, 10 times less than A 's, thus the effect of the inhibition will be stronger on T , the rise in T_f will be counterbalanced and achieving a high T fixed point becomes harder.

Analogous reasoning can be carried out when looking at the effects of changing β_C in fig.S3 b). Again, $\beta_C^0 = 11.4475$ and is varied between $\frac{1}{8}\beta_C^0 = 1.4309$ and $8 \cdot \beta_C^0 = 91.58$. β_C quantifies the positive feedback on accumulation of T provided by increasing T_f (that slows down translation reducing frequency of cell division and thus degradation of T). Here the fraction of the sample of parameter sets that exhibits bistability tends to increase with increasing β_C , it peaks for $\beta_C \simeq 2 - 4 \cdot \beta_C^0$ and goes slightly down again at $8 \cdot \beta_C^0$. The reason for this behavior is the following: for low values of β_C an increase in T_f will not be sufficient to inhibit cell division enough to sustain the increase in T , thus it's hard to obtain a high T fixed point. As β_C increases it becomes easier and easier to achieve a high T fixed point, but if β_C becomes too high, a very small increase in T_f can be amplified to the point that it becomes harder and harder to sustain a low T fixed point, thus bistability is lost again for a higher fraction of parameter sets.

In Fig S3 c) the effect of changing the degradation rate for A is explored. The value of Γ_A used in the main text is $\Gamma_A^0 = 10$ and hereby we change it between $\frac{1}{8}\Gamma_A^0 = 1.25$ and $8 \cdot \Gamma_A^0 = 80$. The highest fraction of bistable set of

parameters is detected for the value of Γ_A used in the main text. Both for lower and higher values the bistability fraction decreases. In fact, for high values of Γ_A it becomes hard to obtain high A dominated fixed points. The toxin is degraded at the rate 1, so if Γ_A is low, considering the fact that A produced more than T , the system will in most cases (parameter sets) end up in a monostable high A state.

In Fig. S3 d) and e) the effect of changing respectively K_T and K_{TT} between $\frac{1}{8}K_{T(T)}^0 = 0.0005$ and $8 \cdot K_{T(T)}^0 = 0.032$ ($K_{T(T)}^0 = 0.004$) is investigated. The effect of changing K_T is practically irrelevant in this range, because the reference parameter is already in very strong binding limit for AT formation. Higher values of K_{TT} , on the other hand, results in a slightly lower fraction of bistable sets of parameters. As stated in the main text one of the key ingredient for achieving bistability is the protein sequestration mechanism, and in particular, the resulting ultrasensitive behavior. High values of K_{TT} (weak binding) will weaken ultrasensitivity, resulting in a decrease in the bistable fraction.

In Fig S3 f) we study the effect of changing the binding constant of the repression factor AT to the operator. The value used in the main text for K_O^0 is 0.015. Thus we explore the behavior of the system for values of K_O ranging between $\frac{1}{8}K_{T(T)}^0 = 0.001875$ and $8 \cdot K_{T(T)}^0 = 0.12$. The fraction of bistable parameter set increases with increasing K_O . This is because if the binding of AT complexes to the operon region is very tight, a low concentration of AT is enough to keep the promoter repressed all the time, making the A dominated state, which requires high production of A due to high degradation rate, difficult to maintain.

Finally we investigate the robustness against change of the value of σ_A . As in can be seen in fig S3 (g), the consequences are not dramatic within this range, but it is evident that for low values of σ_A , the production advantage with respect to T becomes insufficient to compensate for high degradation rate for A , thus for many parameter combinations it is hard to obtain a high A fixed point. In the main text, we show systematic dependence on σ_A/σ_T for wider range.

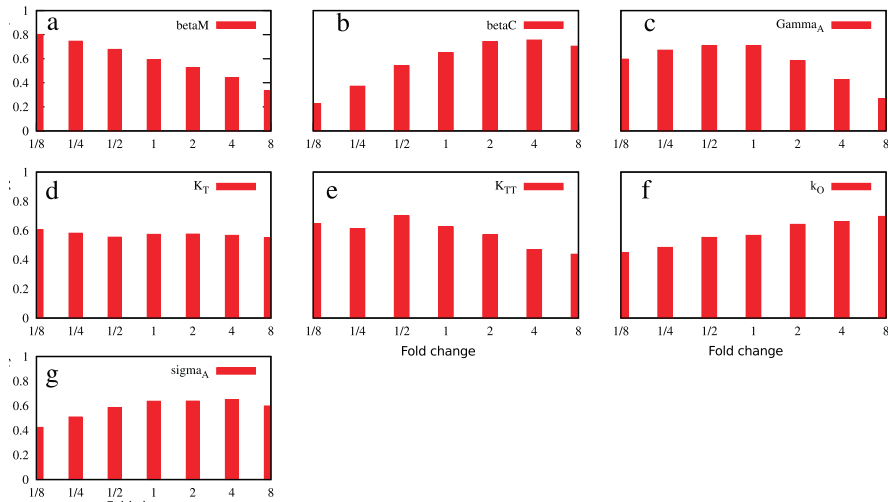


Figure S3: **The robustness of the bistability against parameter change.** We fix $\sigma_T = 100$ and $\Gamma_0 = 1$, and vary rest of the parameters. In (a) β_M is changed systematically between $\frac{1}{8}$ and 8 fold of the value used in the main text $\beta_M^0 = 11.4475$; we change it between $\frac{1}{8} \cdot \beta_M^0 = 1.4309$ and $8 \cdot \beta_M^0 = 91.58$ with a pace given by $2^n \cdot \beta_M^0$ with an integer $n \in [-3, 3]$. For each value of β_M , we sample rest of the parameters randomly and independently of each other, and they can take any values from the set $2^n \cdot (\text{the reference value})$ with $n \in [-3, 3]$. The reference values are given in Table ???. We collect a sample of 1000 points in the parameter space. The bars in the histogram represent the fraction of this sample of points in the parameter space that still shows bistable behavior. The same procedure is then carried out for β_C (b), Γ_B (c), K_T (d), K_{TT} (e), K_O (f) and σ_A (g).

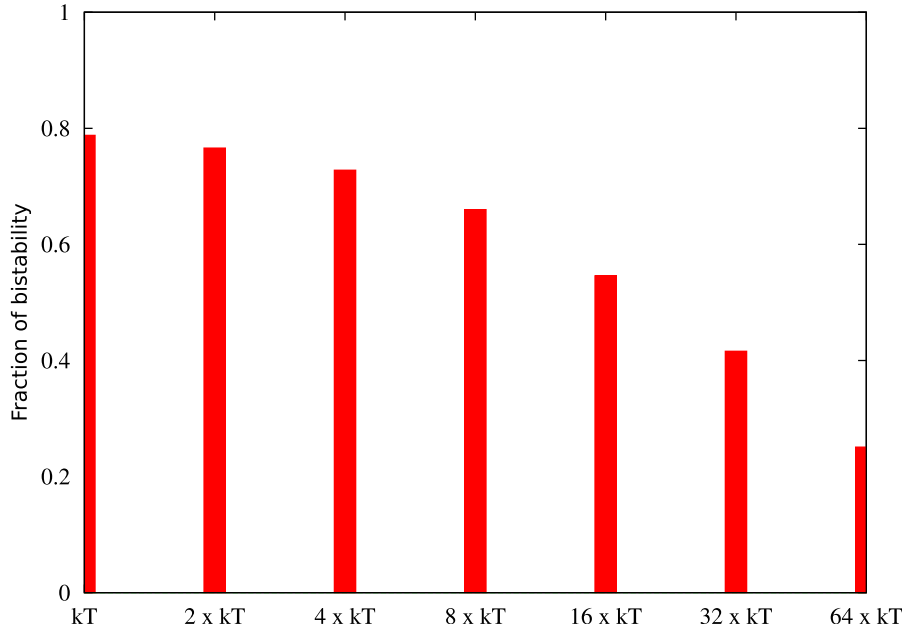


Figure S4: **The robustness of the bistability against the change of the dissociation constants K_T and K_{TT} .** We set $K_T = K_{TT}$, and increase them systematically from the reference value (0.004) to 64 fold of the reference value. Since the dissociation constants set the concentration of A and T at which AT and ATT formation is significant, we fix $\sigma_A = 10000$ and $\Gamma_A = 10$ in addition to fixing $\sigma_T = 100$ and $\Gamma_0 = 1$. We then sample the rest of the parameters randomly in the base 2 logarithmic scale, within 1/8 to 8 fold of the reference value. We tried 1000 parameter sets for each values of $K_T = K_{TT}$. The plot shows the fraction of the parameter set that shows the bistability. We see that the number of bistability parameter sets decrease gradually with fold increase of the dissociation constants.